

การตรวจวัดแคทีคอลเอมีนด้วยเซ็นเซอร์ที่สังเคราะห์ขึ้น โดยฟลูออเรสเซนส์สเปกโทรโฟโตเมตรี

นางสาวณัฐศา สงวนทรัพย์

วิทยานิพนธ์นี้เป็นส่วนหนึ่งของการศึกษาตามหลักสูตรปริญญาวิทยาศาสตรมหาบัณฑิต

สาขาวิชาเคมี ภาควิชาเคมี

คณะวิทยาศาสตร์ จุฬาลงกรณ์มหาวิทยาลัย

ปีการศึกษา 2556

ลิขสิทธิ์ของจุฬาลงกรณ์มหาวิทยาลัย

CATECHOLAMINE DETECTION BY ARTIFICIAL SENSORS UNDER  
FLUORESCENCE SPECTROPHOTOMETRY

Miss Yanisa Sanguansap

A Thesis Submitted in Partial Fulfillment of the Requirements  
for the Degree of Master of Science Program in Chemistry

Department of Chemistry

Faculty of Science

Chulalongkorn University

Academic Year 2013

Copyright of Chulalongkorn University

Thesis Title                    CATECHOLAMINE DETECTION BY ARTIFICIAL  
    SENSORS UNDER FLUORESCENCE  
    SPECTROPHOTOMETRY  
By                                    Miss Yanisa Sanguansap  
Field of Study                    Chemistry  
Thesis Advisor                    Assistant Professor Boosayarat Tomapatanaget, Ph. D.

---

Accepted by the Faculty of Science, Chulalongkorn University in  
Partial Fulfillment of the Requirements for the Master's Degree

.....Dean of the Faculty of Science  
(Professor Supot Hannongbua, Dr.rer.nat.)

THESIS COMMITTEE

..... Chairman  
(Assistant Professor Warinthorn Chavasiri, Ph. D.)

..... Thesis Advisor  
(Assistant Professor Boosayarat Tomapatanaget, Ph. D.)

..... Examiner  
(Numpon Insin, Ph. D.)

..... External Examiner  
(Assistant Professor Nantanit Wanichacheva, Ph. D.)

ญาณิศา สงวนทรัพย์ : การตรวจวัดแคทีคอลเอมีนด้วยเซ็นเซอร์ที่สังเคราะห์ขึ้นโดยฟลูออเรสเซนส์สเปกโทรโฟโตเมตรี. (CATECHOLAMINE DETECTION BY ARTIFICIAL SENSORS UNDER FLUORESCENCE SPECTROPHOTOMETRY) อ. ที่ปริกษาวิทยานิพนธ์หลัก: ผศ.ดร. บุญยรัตน์ ธรรมพัฒน์กิจ, 133 หน้า.

เป้าหมายของงานวิจัยนี้คือการสังเคราะห์เซ็นเซอร์เคมี NB ที่ประกอบด้วยหมู่แนฟทาลิไมด์และกรดโบโรนิก และเซ็นเซอร์เคมี CC ประกอบด้วยส่วนของคูมารินและควาอีเทอร์เพื่อใช้ตรวจวัดสารสื่อประสาทในกลุ่มแคทีคอลเอมีน ในขั้นต้นได้นำเซ็นเซอร์ NB มาศึกษาสมบัติการเกิดสารประกอบเชิงซ้อนกับสารกลุ่มเอมีนทางชีวภาพชนิดต่างๆ ในตัวทำละลายผสมของไดเมทิลซัลฟอกไซด์กับฟอสเฟตบัฟเฟอร์ที่ pH 7.4 ในอัตราส่วน 1:9 โดยใช้เทคนิคฟลูออเรสเซนส์สเปกโทรโฟโตเมตรี พบว่าเมื่อเติม DA และ NE ลงในเซ็นเซอร์ NB ทำให้เกิดการลดลงของสัญญาณฟลูออเรสเซนส์ที่ความยาวคลื่น 384 นาโนเมตร โดยเกิดกระบวนการ PET และเมื่อเติม EPI ทำให้เกิดสัญญาณฟลูออเรสเซนส์เพิ่มขึ้นและเคลื่อนที่ไปทางความยาวคลื่นมากขึ้นที่ความยาวคลื่น 475 นาโนเมตร เนื่องจากเกิดกระบวนการ PCT จากนั้นหาค่าคงที่การเกิดสารประกอบเชิงซ้อนด้วยเทคนิคฟลูออเรสเซนส์ไทเทรชันระหว่างเซ็นเซอร์ NB กับสารแคทีคอลเอมีนทั้งสามชนิดคือ DA, NE และ EPI ได้ค่าคงที่การจับ ( $\log K_s$ ) เท่ากับ 4.01, 4.08 และ 3.00 ตามลำดับ และสามารถคำนวณขีดจำกัดต่ำสุดในการตรวจวัดสารแคทีคอลเอมีนได้ในช่วงความเข้มข้นที่ต่ำระดับไมโคร โมลาร์ นอกจากนี้การใช้เซ็นเซอร์ NB และ CC ร่วมกันในการตรวจวัดสารสามารถแยกสาร DA และ NE ออกจากกันได้ด้วย 2 ความยาวคลื่นของการคายพลังงานที่ต่างกันภายใต้กระบวนการ PET และสิ่งที่น่าสนใจคือสามารถคำนวณหาอัตราส่วนความเข้มแสงที่  $I_{475}/I_{384}$  ของสารประกอบเชิงซ้อน NB-DA-CC มีค่าเท่ากับ 4.84 ซึ่งมากกว่าค่าอัตราส่วนของสารประกอบเชิงซ้อน NB-DA-CC ที่มีค่าเท่ากับ 4.28 เพียงเล็กน้อย ดังนั้นจึงใช้เทคนิค PCA เพื่อเพิ่มประสิทธิภาพการแยก DA และ NE พบว่าการใช้เซ็นเซอร์ NB ผสมกับเซ็นเซอร์ CC สามารถแยก DA ออกจาก NE ได้อย่างชัดเจนซึ่งดีกว่าการใช้เซ็นเซอร์เพียงชนิดเดียว นอกจากนี้ผู้วิจัยได้นำเซ็นเซอร์ NB มาศึกษาการตรวจวัด EPI ในปัสสาวะมนุษย์ และคำนวณหาร้อยละของสารที่ได้กลับมาในช่วง 100.14 % ถึง 101.06%

ภาควิชา.....เคมี..... ลายมือชื่อนิสิต.....  
 สาขาวิชา.....เคมี..... ลายมือชื่อ อ.ที่ปริกษาวิทยานิพนธ์หลัก.....  
 ปีการศึกษา.....2556.....

# # 5372234023: MAJOR CHEMISTRY

KEYWORDS: CATECHOLAMINE / FLUORESCENCE SENSOR / BORONIC  
NAPHTHALIMIDE / COUMARIN CROWN ETHER

YANISA SANGUANSAP: CATECHOLAMINE DETECTION BY  
ARTIFICIAL SENSORS UNDER FLUORESCENCE SPECTROPHOTO  
METRY. ADVISOR: ASST. PROF. BOOSAYARAT TOMAPATANA  
GET, Ph. D., 133 pp.

A goal of this research is to synthesize the chemosensors **NB** containing a naphthalimide and boronic acid group and **CC** consisting coumarin and 18-crown-6 moieties for detection of catecholamine neurotransmitters. Initially, the complexation properties of sensor **NB** with biogenic amines in DMSO: phosphate buffer pH 7.4 (1:9) were investigated by fluorescence spectrophotometry. It was found that sensor **NB** exhibited a fluorescence quenching at 384 nm in the presence of **DA** and **NE** under PET process and a large red shift along with the fluorescent enhancement at 475 nm by PCT mechanism for **EPI** binding. Then, the log  $K_s$  values evaluated by fluorescence titration of sensor **NB** with three catecholamines including **DA**, **NE** and **EPI** were 4.01, 4.08 and 3.00, respectively. The detection limit of sensor **NB** serves as the catecholamines sensing in a low concentration of micromolar range. Moreover, the combination of two sensing elements **NB** and **CC** is capable of classification of **DA** and **NE** with dual emission bands under PET mechanism. Interestingly, the dual emission ratio ( $I_{475}/I_{384}$ ) of **NB-DA-CC** complex of 4.84 showed a slight larger value than that of **NB-NE-CC** complex showing 4.28. The PCA analysis was applied to address the effective differentiation of **DA** and **NE**. The PCA score plot of both sensors **NB** and **CC** toward biogenic amines obviously separated **DA** and **NE** in the different quadrant better than a single sensing element in the case of excluding **EPI** sensing. We have utilized the sensor **NB** to detect **EPI** in real biological system of human urine samples. The % recovery for **EPI** exhibits in the range of 100.14% to 101.06%.

Department : .....Chemistry..... Student's Signature .....

Field of Study : .....Chemistry..... Advisor's Signature .....

Academic Year : .....2013.....

## ACKNOWLEDGEMENTS

I wish to express my deepest appreciation to my advisor, Assistant Professor Dr. Boosayarat Tomapatanaget for guidance, sincere kindnesses, valuable suggestions and constant encouragement both course work and research throughout my undergraduate and master studying for 4 years. I also would like to acknowledge to Assistant Professor Dr. Warinthorn Chavasiri, Dr. Numpon Insin and Assistant Professor Dr. Nantanit Wanichacheva for their valuable comments, useful suggestions as thesis committee and thesis examiner.

Absolutely, I would like to thank the financial support for my study from National Center of Excellence for Petroleum, Petrochemical, and Advanced Materials (NCE-PPAM). I gratefully acknowledge the Thailand Research Fund, Commission on Higher Education and Chulalongkorn University (RSA5680015 and RTA5300083), The Higher Education Research Promotion and National Research University Project of Thailand, Office of the Higher Education Commission (AM1006A-55) and The 90<sup>th</sup> Anniversary of Chulalongkorn University Fund (Ratchadaphiseksomphot Endowment Fund) for research grants.

In addition, this accomplishment could not occur without the support from Chulalongkorn University. Special thanks are due to Professor Dr. Thawatchai Tuntulani for financial support, beneficial suggestions and helpful from all members of the Supramolecular Chemistry Research Unit at Department of Chemistry, Chulalongkorn University for their giving consultant, encouragement throughout my research.

Eventually, I wish to express my deepest gratitude to my parents for their greatest love, important moral support and comprehension throughout my life.

## CONTENTS

	<b>Page</b>
ABSTRACTS IN THAI.....	iv
ABSTRACTS IN ENGLISH.....	v
ACKNOWLEDGEMENTS.....	vi
CONTENTS.....	vii
LIST OF TABLES.....	xii
LIST OF FIGURES.....	xiv
LIST OF SCHEMES.....	xxii
LIST OF ABBREVIATIONS.....	xxiii
<b>CHAPTER I INTRODUCTION.....</b>	<b>1</b>
1.1 Supramolecular chemistry concept.....	1
1.2 Molecular recognition.....	1
1.3 Chemical sensor.....	2
1.4 Phenomena of fluorescence.....	2
1.4.1 Photoinduced electron transfer (PET).....	4
1.4.2 Photoinduced charge transfer (PCT).....	4
1.4.3 Fluorescence resonance energy transfer (FRET).....	5
1.5 Formation of 1:1 complex.....	7
1.6 Determination of stoichiometry of a complex by the method of continuous variation (Job's method).....	8
1.7 Limit of detection.....	9
1.8 Principal component analysis (PCA).....	10
<b>CHAPTER II LITERATURE REVIEWS.....</b>	<b>12</b>
2.1 Literature reviews.....	12
2.1.1 Determination of catecholamine by electrochemical technique..	12
2.1.2 Determination of catecholamine by NMR & mass spectroscopy.....	17

	<b>Page</b>
2.1.3 Determination of catecholamine by fluorescence spectrophotometry.....	20
2.1.4 Ratiometric sensors under FRET mechanism.....	28
2.2 Objectives and scope of this research.....	33
<b>CHAPTER III EXPERIMENTAL.....</b>	<b>34</b>
3.1 General procedures.....	34
3.1.1 Analytical instrument.....	34
3.1.2 Materials.....	34
3.2 Synthesis.....	35
3.2.1 Synthesis of boronic/naphthalimide based sensor.....	35
3.2.1.1 Preparation of <i>N</i> -(1,8-Naphthaloyl)-3-aminophenylboronic acid ( <b>NB</b> ).....	35
3.2.2 Synthesis of diazacrown ether/dansyl based sensor.....	36
3.2.2.1 Preparation of 2,2'-(ethane-1,2-diylbis(oxy)) bis(ethane-2,1-diyl) bis(4-methylbenzenesulfonate) ( <b>1</b> ).....	36
3.2.2.2 Preparation of 1,4,10,13-tetraoxa-7,16-diazacyclooctadecane ( <b>2</b> ).....	37
3.2.2.3 Preparation of Dansyl azacrown ( <b>DC</b> ).....	38
3.2.3 Synthesis of boronic/amino phenyl based sensor.....	39
3.2.3.1 Preparation of 3-((phenylamino)methyl)phenylboronic acid ( <b>m-BA</b> ).....	39
3.2.4 Synthesis of picolyl amine/pyrene based sensor.....	40
3.2.4.1 Preparation of sensor <b>L2-Zn</b> .....	40
3.2.5 Synthesis of boronic/anthraquinone based sensor.....	41
3.2.5.1 Preparation of 2-(5,5-dimethyl-1,3,2-dioxaborinan-2-yl)benzaldehyde ( <b>3</b> ).....	41
3.2.5.2 Preparation of 2-(2-(5,5-dimethyl-1,3,2-dioxaborinan-2-yl)phenyl)-1H-anthra[1,2-d]imidazole-6,11-dione ( <b>4</b> ).....	42



	<b>Page</b>
3.2.5.3 Preparation of 2-(6,11-dioxo-6,11-dihydro-1H-anthra[1,2-d]imidazol-2-yl)phenylboronic acid ( <b><i>o</i>-AB</b> ).....	43
3.2.6 Synthesis of crown ether/coumarin based sensor.....	44
3.2.6.1 Preparation of 7-diethylamino-2-oxo-2H-chromen-3-carboxylic acid ( <b>5</b> ).....	44
3.2.6.2 Preparation of 7-diethylamino-2-oxo-2H-chromen-3-carboxylic chloride ( <b>6</b> ).....	45
3.2.6.3 Preparation of (1,4,7,10,13,16-hexaoxacyclooctadecan-2-yl)methyl 7-(diethylamino)-2-oxo-4a,8a-dihydro-2H-chromene-3-carboxylate ( <b>CC</b> ).....	46
3.3 Complexation studies.....	48
3.3.1 Complexation studies of sensor <b>NB</b> and sensor <b>DC</b> with <b>DA</b> by fluorescence spectrophotometry technique.....	48
3.3.2 Complexation studies of sensor <b><i>m</i>-BA</b> and sensor <b>L2-Zn</b> with <b>DA</b> by fluorescence spectrophotometry technique.....	48
3.3.3 Complexation studies of sensor <b>L2-Zn</b> and sensor <b><i>o</i>-AB</b> with <b>DA</b> by fluorescence spectrophotometry technique.....	49
3.3.4 Complexation studies of sensor <b>NB</b> with various guests by fluorescence spectrophotometry technique.....	50
3.3.5 Fluorescence image of sensor <b>NB</b> with various guests.....	52
3.3.6 Job's plot studies of sensor <b>NB</b> with <b>DA</b> , <b>NE</b> and <b>EPI</b> .....	53
3.3.7 Complexation studies of sensor <b>NB</b> with <b>DA</b> , <b>NE</b> and <b>EPI</b> by fluorescence spectrophotometric titration technique.....	54
3.3.8 Determination of detection limit of sensor <b>NB</b> with <b>DA</b> , <b>NE</b> and <b>EPI</b> by fluorescence spectrophotometry.....	60
3.3.9 Complexation studies of sensor <b>CC</b> with various guests by fluorescence spectrophotometry technique.....	61
3.3.10 Complexation studies of sensor <b>NB</b> and sensor <b>CC</b> with various guests by fluorescence spectrophotometry technique.....	62

	<b>Page</b>
3.3.11 Principal component analysis (PCA) method for analysis of complexation.....	63
3.3.11.1 PCA method for complexation of sensor <b>NB</b> with various guests.....	63
3.3.11.2 PCA method for complexation of sensor <b>CC</b> with various guests.....	64
3.3.11.3 PCA method for complexation of sensor <b>NB</b> and sensor <b>CC</b> with various guests.....	64
3.3.12 Complexation study of sensor <b>NB</b> with <b>EPI</b> in human urine sample.....	64
3.3.13 Complexation study of sensor <b>NB</b> and sensor <b>CC</b> with <b>NE</b> by mass spectroscopy.....	66
<b>CHAPTER IV RESULTS AND DISCUSSION.....</b>	<b>67</b>
4.1 Design and synthesis of boronic acid based sensors.....	67
4.2 Synthesis.....	70
4.2.1 Preparation of sensor <b>NB</b> .....	70
4.2.2 Preparation of sensor <b>DC</b> .....	71
4.2.3 Preparation of sensor <b>m-BA</b> .....	72
4.2.4 Preparation of sensor <b>o-AB</b> .....	73
4.2.5 Preparation of sensor <b>CC</b> .....	75
4.3 Complexation studies.....	76
4.3.1 Complexation studies of sensor <b>NB</b> and sensor <b>DC</b> with dopamine ( <b>DA</b> ) by fluorescence spectrophotometry technique.....	76
4.3.2 Complexation studies of sensors <b>m-BA</b> and sensor <b>L2-Zn</b> with <b>DA</b> by fluorescence spectrophotometry technique.....	79
4.3.3 Complexation studies of sensor <b>L2-Zn</b> and sensor <b>o-AB</b> with <b>DA</b> by fluorescence spectrophotometry technique.....	82
4.3.4 Complexation studies of sensor <b>NB</b> with various guests by fluorescence spectrophotometry technique.....	84

	<b>Page</b>
4.3.5 Job's plot study of sensor <b>NB</b> with <b>DA</b> , <b>NE</b> and <b>EPI</b> .....	88
4.3.6 Complexation studies of sensor <b>NB</b> with <b>DA</b> , <b>NE</b> and <b>EPI</b> by fluorescence spectrophotometric titration technique.....	90
4.3.7 Determination of detection limit of sensor <b>NB</b> with <b>DA</b> , <b>NE</b> and <b>EPI</b> by fluorescence spectrophotometry.....	94
4.3.8 Complexation studies of sensors <b>NB</b> and sensor <b>CC</b> with various guests by fluorescence spectrophotometry technique.....	97
4.3.9 Complexation studies of sensor <b>CC</b> with various guests by fluorescence spectrophotometry technique.....	100
4.3.10 Principle component analysis (PCA) method for analysis of complexation.....	101
4.3.11 Complexation study of sensor <b>NB</b> with <b>EPI</b> in human urine sample.....	106
4.3.12 Complexation study of sensor <b>NB</b> and sensor <b>CC</b> with <b>NE</b> by mass spectroscopy.....	108
<b>CHAPTER V CONCLUSION</b> .....	109
5.1 Conclusion.....	109
5.2 Future work.....	110
<b>REFERENCES</b> .....	111
<b>APPENDICES</b> .....	119
<b>VITAE</b> .....	133

## LIST OF TABLES

		Page
Table 2.1	Transport rates for catecholamines, glucosides, and uridine in the presence and absence of carrier <b>1</b> .....	17
Table 2.2	Association constants obtained for complexation of receptor <b>2</b> toward various organoammonium ions in D <sub>2</sub> O by <sup>1</sup> H-NMR titrations.....	19
Table 3.1	Amounts of guests used for studies of fluorescence spectrophotometry technique.....	50
Table 3.2	Amounts of guests used for studies of fluorescence spectrophotometry technique.....	51
Table 3.3	The amount ratio of guest and sensor <b>NB</b> used for study the fluorescence image.....	52
Table 3.4	Mole fraction and volume of sensor <b>NB</b> (1 x 10 <sup>-5</sup> M) and catecholamine guests (1 x 10 <sup>-5</sup> M) for Job's plot experiment.....	53
Table 3.5	The concentration of <b>DA</b> used for complexation studies with sensor <b>NB</b> and the ratios of <b>NB:DA</b> .....	55
Table 3.6	The concentration of <b>NE</b> used for complexation studies with sensor <b>NB</b> and the ratios of <b>NB:NE</b> .....	57
Table 3.7	The concentration of <b>EPI</b> used for complexation studies with sensor <b>NB</b> and the ratios of <b>NB:EPI</b> .....	59
Table 3.8	Amounts of guests used for studies fluorescence spectrophotometry technique.....	61
Table 3.9	Amounts of guests used for studies fluorescence spectrophotometry technique.....	63
Table 3.10	Composition of synthetic urine.....	65
Table 4.1	The FRET donor and FRET acceptor used for study of the complexation.....	68
Table 4.2	The Binding constant (log K <sub>s</sub> ) of sensor <b>NB</b> with <b>DA</b> , <b>NE</b> and <b>EPI</b> .....	94
Table 4.3	The fluorescence intensity of sensor <b>NB</b> at 384 nm.....	94

		<b>Page</b>
Table 4.4	The detection limits of sensor <b>NB</b> with <b>DA</b> , <b>NE</b> and <b>EPI</b> .....	96
Table 4.5	Results for the determination of <b>EPI</b> in Human urine samples.....	107

## LIST OF FIGURES

		Page
Figure 1.1	Schematic presentation of interaction of chemosensor with guest analyte.....	2
Figure 1.2	Perrin-Jablonski diagram and illustration of the relative positions of absorption, fluorescence and phosphorescence spectra.....	3
Figure 1.3	a) Schematic and b) energy level representations of an ON-OFF sensor. The dashed line in the energy level representation of the acceptor-analyte shows the energy level prior to binding of analyte.....	4
Figure 1.4	PCT system of interaction with a) the donor group and b) the acceptor group.....	5
Figure 1.5	The integral overlap between the emission spectrum of the donor and the absorption of the acceptor.....	6
Figure 1.6	The schematic diagram of the fluorescence resonance energy transfer.....	6
Figure 1.7	Job's plots for a 1:1 complex.....	9
Figure 1.8	Principal of the PCA.....	10
Figure 1.9	PCA as a form of variable reduction.....	11
Figure 1.10	Graphical representation of samples in the original data space (left) and the position of samples in PC spaces (right).....	11
Figure 2.1	Proposed mechanism of dopamine oxidation on the surface of DMS/(ensal) <sub>2</sub> Cu/C electrode.....	13
Figure 2.2	Amperometric response of <b>DA</b> , each step corresponds to the increment of 10 $\mu\text{mol L}^{-1}$ <b>DA</b> containing 200 $\mu\text{mol L}^{-1}$ of $\text{H}_2\text{O}_2$ and inset shows the analytical curve.....	13
Figure 2.3	Cyclicvoltammograms obtained a) DMS/C electrode modified with (ensal) <sub>2</sub> Cu and b) unmodified DMS/C electrode. Scan rate 10 $\text{mVs}^{-1}$ , 0.04 $\text{mol L}^{-1}$ BRB at pH 7.0 containing 1 $\text{mol L}^{-1}$ KCl..	14

	<b>Page</b>	
Figure 2.4	Amperometric response of the addition of concentration in $\mu\text{mol L}^{-1}$ of [NADH] = (a) 10, (d) 20, [AA] = (b) 10, (e) 20 and [DA] = (c) 10, (f) 20 into the electrochemical cell.....	14
Figure 2.5	The inclusion complex formation between $\beta$ -cyclodextrin and <b>5-HT/DA</b> as guest molecules.....	15
Figure 2.6	Cyclic voltammograms of 100 $\mu\text{M}$ <b>5-HT</b> and <b>DA</b> in 0.05 M of phosphate buffer pH 7.4 on the bare (a, dashed), MWNT modified (b, dash-dotted), <b>CD/PNAANI</b> modified (c, solid) and <b>CD/PNAANI/CNT</b> modified (d, round-dotted) CPE (background currents are substrated for simplicity).....	16
Figure 2.7	The structure of carrier <b>1</b> and complexation of carrier <b>1</b> with dopamine.....	18
Figure 2.8	Proposed interactions of designed receptor <b>2</b> with dopamine•HCl in water and CPK view of an inclusion complex between <b>2</b> and dopamine ammonium ion.....	18
Figure 2.9	$^1\text{H-NMR}$ spectral changes at proton $\text{H}_f$ of <b>2</b> (40 mM) at upon addition of dopamine hydrochloride (0 to 16.5 equiv.) in water....	20
Figure 2.10	a) Structure of sensor <b>3</b> and b) proposed binding mode of sensor <b>4</b> with dopamine.....	20
Figure 2.11	Fluorescence spectra of a) sensor <b>4</b> (3 $\mu\text{M}$ ) upon the addition of dopamine in MeOH (excitation at 397 nm) b) sensor <b>3</b> (3 $\mu\text{M}$ ) upon the addition of dopamine in 50% MeOH/0.05M HEPES buffer at pH 7.4 (excitation at 367 nm).....	21
Figure 2.12	The complexation of sensor <b>5</b> with <b>L-DOPA</b> in buffer solution...	22
Figure 2.13	Fluorescence spectra of 5 $\mu\text{M}$ chemosensor <b>5</b> in the presence of gradual increasing of <b>L-DOPA</b> concentrations in 0.1 M MOPS buffer pH 7.2 and excitation at 430 nm.....	22
Figure 2.14	Normalized peak emission intensity of <b>5</b> toward catechol, <b>L-DOPA</b> and other amino acid in buffered aqueous solution (0.1 M MOPS, pH 7.2) and excitation wavelength at 430 nm.....	23

	<b>Page</b>
Figure 2.15	The complexation of fluorescence probe of 2,7-diazapyrenium dication modified on silica particles toward dopamine..... 24
Figure 2.16	Relative emission intensity of fluorescent particles (0.3 mg/mL, sodium phosphate buffer, pH = 7.0, 32°C, $\lambda_{em} = 432$ nm) in the presence of various concentrations of catechol, dopamine or propylamine..... 24
Figure 2.17	a) Structure of receptor-noradrenaline complexes b) schematic structure of the receptor/phospholipid/PDA assemblies. Blue: PDA. Black: phospholipids. Green: host. Red: ligand..... 25
Figure 2.18	Fluorescence emissions (560 nm, excitation 490 nm) were induced by ligand addition to host/DMPC/PDA vesicles. The values shown (calculated as percentage intensities compared to host/DMPC/PDA) vesicle..... 26
Figure 2.19	a) The fluorescence response of the BSA-AuNCs with <b>DA</b> . b) Schematic representation of peroxidase-like catalytic color reaction for sensitive sensing of <b>DA</b> ..... 27
Figure 2.20	a) The fluorescence responses of the BSA-AuNCs in the presence of 100 $\mu$ M <b>DA</b> or other analytes. b) Photographs of BSA-AuNCs solutions in the presence of 1 mM <b>DA</b> or other analytes under UV light..... 28
Figure 2.21	The complexation of sensor <b>9</b> toward $Cu^{2+}$ under inhibition of FRET process..... 29
Figure 2.22	a) The fluorescent titration spectra of sensor <b>1</b> with $Cu^{2+}$ ion and b) relative emission intensity change of sensor <b>1</b> toward various metal ions in 20% acetonitrile containing 2 mM of neutral micelle TX-100 and excitation wavelength at 339 nm..... 30
Figure 2.23	FRET process between dendrimer-QD and Alexa Fluor 488-labeled..... 30



Figure 2.24	ELISA data of FRET mechanism of polyamidoamine (PAMAM) dendrimer (G5)-CdS with AlexaFluor 488-conjugated antibody: (a) dendrimer-QD and AlexaFluor 488 antibody conjugation, (b) dendrimer-QD secondary antibody and primary antibody conjugation and (c) the effect of 10 mM of anti-dopamine-dopamine conjugation on time period shows (30 min – 12 h), Inset shows change of fluorescence intensity at 520 nm.....	31
Figure 2.25	Fluorescent intensity change under FRET process between dendrimer-QD and AlexaFluor 488-conjugated antibody: (a) 0, (b) 1, (c) 2, (d) 5, and (e) 10 mM, Inset shows the change of emission intensity of dendrimer-QD with various dopamine concentration at 520 nm.....	32
Figure 2.26	Structure of fluorescence chemosensors <b>NB</b> and <b>CC</b> .....	33
Figure 4.1	The <sup>1</sup> H-NMR spectrum of sensor <b>NB</b> in DMSO- <i>d</i> <sub>6</sub> at 400 MHz...	70
Figure 4.2	The <sup>1</sup> H-NMR spectrum of sensor <b>DC</b> in CDCl <sub>3</sub> at 400 MHz.....	72
Figure 4.3	The <sup>1</sup> H-NMR spectrum of sensor <b><i>m</i>-BA</b> in CD <sub>3</sub> OD at 400 MHz..	73
Figure 4.4	The <sup>1</sup> H-NMR spectrum of sensor <b><i>o</i>-AB</b> in DMSO- <i>d</i> <sub>6</sub> at 400 MHz	74
Figure 4.5	The <sup>1</sup> H-NMR spectrum of sensor <b>CC</b> in CDCl <sub>3</sub> at 400 MHz.....	76
Figure 4.6	The conceptually proposed structure and mechanism of <b>NB-DA-DC</b> complex under FRET mechanism.....	77
Figure 4.7	Fluorescence spectra of sensor <b>NB</b> (1 x 10 <sup>-5</sup> M) and sensor <b>DC</b> (1 x 10 <sup>-6</sup> M) in the presenst of excess dopamine in 10% DMSO:phosphate buffer (0.01 M, pH 7.4) vary time (λ <sub>ex</sub> = 353 nm).....	78
Figure 4.8	Fluorescence spectra of sensor <b>DC</b> (1 x 10 <sup>-5</sup> M) in 10% DMSO:phosphate buffer (0.01 M, pH 7.4) vary time (λ <sub>ex</sub> = 353 nm).....	79
Figure 4.9	The conceptually proposed structure and mechanism of <b>(<i>m</i>-BA)-DA-(L2-Zn)</b> complex under FRET mechanism.....	80

	<b>Page</b>	
Figure 4.10	Fluorescence spectra of sensor <b>L2-Zn</b> and sensor <b>m-BA</b> ( $1 \times 10^{-5}$ M) in 50% MeOH:phosphate buffer (0.01 M, pH 8.0) in the presence of <b>DA</b> 50 equiv. ( $\lambda_{\text{ex}} = 290$ nm).....	81
Figure 4.11	Fluorescence spectra of solvent and <b>DA</b> (50 equiv.) in 50% MeOH:phosphate buffer (0.01 M, pH 8.0) with excitation at 290 nm.....	82
Figure 4.12	The conceptually proposed structure and mechanism of ( <b>L2-Zn</b> )- <b>DA</b> -( <b>o-AB</b> ) complex under FRET mechanism.....	83
Figure 4.13	Fluorescence spectra of sensor <b>L2-Zn</b> ( $1 \times 10^{-5}$ M) and sensor <b>o-AB</b> ( $1 \times 10^{-5}$ M) in 10% DMSO:phosphate buffer (0.01 M, pH 7.4) with varying the amount of <b>DA</b> ( $\lambda_{\text{ex}} = 345$ nm).....	83
Figure 4.14	The structures of various biogenic amines.....	84
Figure 4.15	Fluorescence spectra of sensor <b>NB</b> ( $1 \times 10^{-5}$ M) in 10% DMSO:phosphate buffer (0.01 M, pH 7.4) in the presence of various guests at 100 equiv. and inset shows the fluorescence spectra of sensor <b>NB</b> and <b>EPI</b> .....	86
Figure 4.16	Fluorescence color change of sensor <b>NB</b> ( $1 \times 10^{-5}$ M) in 10% DMSO:phosphate buffer (0.01 M, pH 7.4) in the present of the various guests 100 equiv. ....	87
Figure 4.17	Fluorescence images of a) sensor <b>NB</b> and b) sensor <b>NB</b> dipped with <b>EPI</b> on a filter paper in word “ <b>EPI</b> ” under the black light.....	87
Figure 4.18	Job’s plots for 1:1 complex of sensor <b>NB</b> with a) <b>DA</b> b) <b>NE</b> and c) <b>EPI</b> at pH 7.4 ( $1 \times 10^{-5}$ M in 10% DMSO: phosphate buffer)...	89
Figure 4.19	The fluorescence titration spectra of sensor <b>NB</b> ( $1 \times 10^{-5}$ M) upon gradual addition a) <b>DA</b> , c) <b>NE</b> and e) <b>EPI</b> and fluorescence responses ( $I-I_0/I_0$ ) in the presence of 0-80 equiv. of b) <b>DA</b> , d) <b>NE</b> and f) <b>EPI</b> in 10% DMSO:phosphate buffer (0.01 M, pH 7.4).....	91

	<b>Page</b>
Figure 4.20	Benesi-Hidebrand plots of sensor <b>NB</b> ( $1 \times 10^{-5}$ M) toward 0-80 equiv. of a) <b>DA</b> b) <b>NE</b> and c) <b>EPI</b> in 10% DMSO:phosphate buffer (0.01 M, pH 7.4) for calculation of binding constant ( $K_s$ )... 93
Figure 4.21	Linear plot of fluorescence intensity between sensor <b>NB</b> with a) <b>DA</b> b) <b>NE</b> c) <b>EPI</b> complexes and concentration of catecholamine guests..... 96
Figure 4.22	The conceptually proposed structure and mechanism of <b>NB</b> -guest- <b>CC</b> complex under FRET mechanism. .... 97
Figure 4.23	Fluorescence spectra of sensor <b>NB</b> ( $1 \times 10^{-5}$ M) and sensor <b>CC</b> ( $5 \times 10^{-5}$ M) in 10% DMSO:phosphate buffer (0.1 M, pH 7.4) in the presence of <b>DA</b> or <b>NE</b> 100 equiv. ( $\lambda_{ex} = 340$ nm)..... 98
Figure 4.24	The conceptually proposed structure and mechanism of <b>NB</b> -guest- <b>CC</b> complex under PET process. .... 99
Figure 4.25	Fluorescence spectra of sensor <b>NB</b> ( $1 \times 10^{-5}$ M) and sensor <b>CC</b> ( $5 \times 10^{-5}$ M) in 10% DMSO:phosphate buffer (0.1 M, pH 7.4) in the presence of various guest 100 equiv. ( $\lambda_{ex} = 340$ nm)..... 100
Figure 4.26	Fluorescence spectra of sensor <b>CC</b> ( $5 \times 10^{-5}$ M) in 10% DMSO:phosphate buffer (0.1 M, pH 7.4) in the present of various guest 100 equiv. ( $\lambda_{ex} = 340$ nm)..... 101
Figure 4.27	PCA score plot of a) sensor <b>NB</b> b) sensor <b>CC</b> and c) the mixture sensors <b>NB</b> and <b>CC</b> upon addition of various guests (100 equiv.) in 10% DMSO:phosphate buffer. PCA score plot shows clustering for all 9 samples. .... 104
Figure 4.28	PCA score plots of a) sensor <b>NB</b> b) sensor <b>CC</b> and c) sensors <b>NB</b> and <b>CC</b> upon addition of various guests (100 equiv.) in 10% DMSO:phosphate buffer and excluding fluorescence data of <b>EPI</b> for determining of PCA analysis..... 106
Figure 4.29	Calibration curve of sensor <b>NB</b> with the spiked <b>EPI</b> in the synthetic urine..... 107

	<b>Page</b>
Figure 4.30 MALDI-TOF mass spectrum of 1:1:1 complex of <b>NB-NE-CC</b> in 5% D <sub>2</sub> O:DMSO and 5 mM NaOH. ....	108
Figure A1 The <sup>13</sup> C-NMR spectrum of sensor <b>NB</b> in DMSO- <i>d</i> <sub>6</sub> at 400 MHz	120
Figure A2 MALDI-TOF mass spectrum of sensor <b>NB</b> shown at 317.379 m/z.....	120
Figure A3 The <sup>1</sup> H-NMR spectrum of <b>1</b> in CDCl <sub>3</sub> at 400 MHz.....	121
Figure A4 The <sup>13</sup> C-NMR spectrum of <b>1</b> in CDCl <sub>3</sub> at 400 MHz.....	121
Figure A5 The <sup>1</sup> H-NMR spectrum of <b>2</b> in CDCl <sub>3</sub> at 400 MHz.....	122
Figure A6 The <sup>13</sup> C-NMR spectrum of <b>2</b> in CDCl <sub>3</sub> at 400 MHz.....	122
Figure A7 The <sup>13</sup> C-NMR spectrum of sensor <b>DC</b> in CDCl <sub>3</sub> at 400 MHz.....	123
Figure A8 MALDI-TOF mass spectrum of sensor <b>DC</b> shown at 729.335 m/z.....	123
Figure A9 The <sup>13</sup> C-NMR spectrum of sensor <b><i>m</i>-BA</b> in CD <sub>3</sub> OD at 400 MHz	124
Figure A10 MALDI-TOF mass spectrum of sensor <b><i>m</i>-BA</b> shown at 227.285m/z.....	124
Figure A11 The <sup>1</sup> H-NMR spectrum of <b>3</b> in CDCl <sub>3</sub> at 400 MHz.....	125
Figure A12 The <sup>13</sup> C-NMR spectrum of <b>3</b> in CDCl <sub>3</sub> at 400 MHz.....	125
Figure A13 The <sup>1</sup> H-NMR spectrum of <b>4</b> in DMSO- <i>d</i> <sub>6</sub> at 400 MHz.....	126
Figure A14 The <sup>13</sup> C-NMR spectrum of <b>4</b> in DMSO- <i>d</i> <sub>6</sub> at 400 MHz.....	126
Figure A15 MALDI-TOF mass spectrum of <b>4</b> shown at 436.48 m/z.....	127
Figure A16 The <sup>13</sup> C-NMR spectrum of sensor <b><i>o</i>-AB</b> in DMSO- <i>d</i> <sub>6</sub> at 400 MHz.....	127
Figure A17 The <sup>13</sup> C-NMR spectrum of sensor <b><i>o</i>-AB</b> in DMSO- <i>d</i> <sub>6</sub> at 400 MHz.....	128
Figure A18 The <sup>1</sup> H-NMR spectrum of <b>5</b> in CDCl <sub>3</sub> at 400 MHz.....	128
Figure A19 The <sup>13</sup> C-NMR spectrum of <b>5</b> in CDCl <sub>3</sub> at 400 MHz.....	129
Figure A20 MALDI-TOF mass spectrum of <b>5</b> shown at 261.322 m/z.....	129
Figure A21 The <sup>1</sup> H-NMR spectrum of <b>6</b> in CDCl <sub>3</sub> at 400 MHz.....	130
Figure A22 The <sup>13</sup> C-NMR spectrum of sensor <b>CC</b> in CDCl <sub>3</sub> at 400 MHz.....	130

	Page
Figure A23 MALDI-TOF mass spectrum of sensor <b>CC</b> shown at 537.887 m/z.....	131
Figure A24 The ESI-High Resolution Mass spectrum of sensor <b>CC</b> .....	131
Figure A25 IR spectrum of sensor <b>CC</b> .....	132

**LIST OF SCHEMES**

	<b>Page</b>
Scheme 4.1 Conceptual hypothesis under FRET mechanism.....	68
Scheme 4.2 Synthesis pathway of sensor <b>NB</b> .....	70
Scheme 4.3 Synthesis pathway of sensor <b>DC</b> .....	71
Scheme 4.4 Synthesis pathway of sensor <i>m</i> - <b>BA</b> .....	72
Scheme 4.5 Synthesis pathway of sensor <i>o</i> - <b>AB</b> .....	73
Scheme 4.6 Synthesis pathway of sensor <b>CC</b> .....	75
Scheme 4.7 The condensation reaction of sensor <b>NB</b> with <b>DA</b> in 10% DMSO: phosphate buffer (0.01 M, pH 7.4).....	84
Scheme 4.8 Principal of photoinduced charge transfer (PCT) system.....	86

**LIST OF ABBREVIATIONS**

Anal. Calcd.	Analysis calculated
ATR-IR	Attenuated Total Reflectance-Infrared
°A	Angstrom
$\delta$	Chemical shift
$^{13}\text{C}$ -NMR	Carbon-13 nuclear magnetic resonance
°C	Degree Celsius (centigrade)
$\text{CH}_2\text{Cl}_2$	Dichloromethane
DA	Dopamine
DMSO	Dimethyl sulfoxide
EA	Elemental Analysis
EPI	Epinephrine
ESI-HRMS	Electrospray Ionization High Resolution Mass Spectroscopy
EtOAc	Ethyl acetate
EtOH	Ethanol
equiv.	Equivalent
g	Gram
Glu	Glutamic acid
$\text{g mol}^{-1}$	Gram per mole
$^1\text{H}$ -NMR	Proton nuclear magnetic resonance
h	Hour
His	Histidine
Hist	Histamine
Hz	Hertz
<i>J</i>	Coupling constant
Lys	L-lysine
m/z	Mass per charge ratio
$\mu\text{L}$	Microliter
$\mu\text{M}$	Micromolar

M	Molar
MeOH	Methanol
mg	milligram
min	Minute
mL	Milliliter
mmol	Millimole
MOPS	3-(N-morpholino)propanesulfonic acid
NE	Norepinephrine
%	Percentage
RT	Room temperature
s, d, t, m	Splitting patterns of $^1\text{H-NMR}$ (singlet, doublet, triplet, multiplet)
THF	Tetrahydrofuran
TY	Tyramine



# CHAPTER I

## INTRODUCTION

### 1.1 Supramolecular chemistry concept

The definition of supramolecular chemistry or host guest chemistry has been introduced by Prof. Lehn in 1978 [1] as a development and generalization of anterior works. He created the word. A supramolecule is an organized of complex entity which ensue on the association of two or more chemical species held together by intermolecular forces. The cooperative interactions including hydrogen bonding, coordination and hydrophobic interaction between the small molecules are form into supramolecule structures.

Widely known, Supramolecular chemistry is a multidisciplinary field of chemistry such as the area of organic and inorganic chemistry, needed to synthesize the substrates for supramolecule and physical chemistry, to study complex supramolecule behavior and property of supramolecular system. [2] Nowadays, Ariga [3] classified the supramolecular chemistry into three types: (i) molecular recognition; (ii) translocation and (iii) transformation. Furthermore, we will describe the most fundamental of supramolecular chemistry by initially explaining the molecular recognition.

### 1.2 Molecular recognition

Molecular recognition is a process involved interactions between hosts and guests which do not define only binding event but this process requires the selectivity between the host and the guest. In physiological system, the perfect recognition of a receptor results from the complementary match of many factors such as electronic, geometry and polar of host and guest. [1, 4-5] Considering on the signaling unit, optical signals based on the change of absorbance or fluorescence properties are the most frequently employed because of their simple applications using inexpensive

instruments. On the other hand, the alternation changes of optical properties, particularly of color or emissions, can immediately reveal the recognition event. Especially fluorescence emissions allow sensors to have very high sensitivity. [6, 7]

### 1.3 Chemical sensor

A chemosensor is the molecule of abiotic origin that is able to bind selectively and reversibility toward analyte with a concurrent change in one or more properties of the system, for example a colorimetric, redox potentials and fluorescence changes. [8-12] Hence, the chemosensor generally comprises two molecular units that are a binding unit for selective interaction with analytes including cation, anion and neutral molecule and signaling unit for responsibility after complexation between sensor and analyte [13] as shown in Fig. 1.1.

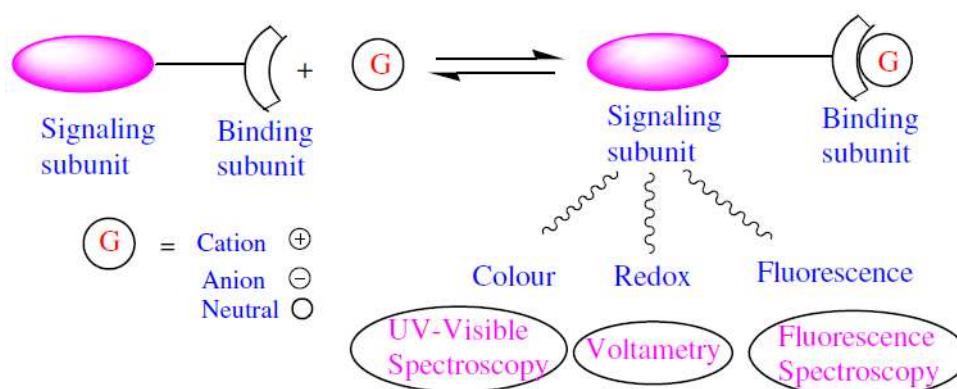


**Figure 1.1** Schematic presentation of interaction of a chemosensor with a guest analyte [14]

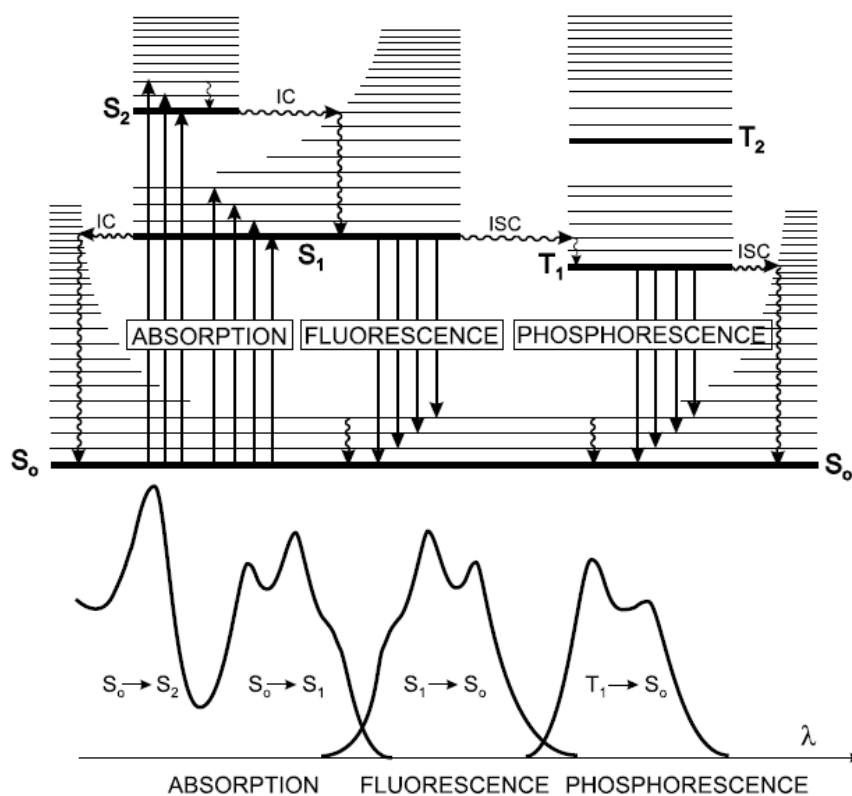
### 1.4 Phenomena of fluorescence

In 1888, Eilhardt Wiedmann [7] introduced the term “luminescence” that is the emission of light from any molecules and occurs from electronically excited state. Officially, luminescence is divided into two kinds, the phosphorescence and the fluorescence according to the excited state.

Phosphorescence is an emission light when the transition of electron from triplet excited state ( $T_1$ ) to the ground state ( $S_0$ ) is forbidden. Thus, the life time of phosphorescence is too long in the range of milliseconds to seconds.

Fluorescence is a light emission of an allowed electronic transition between singlet excited state ( $S_1$ ) and singlet ground state ( $S_0$ ) at the same multiplicity. Hence, the fluorescence life time is shorter approximately nanosecond. [15]

The processes of phosphorescence and fluorescence are described by the Jablonski diagrams as illustrated in Fig. 1.2.



#### CHARACTERISTIC TIMES

absorption	$10^{-15}$ s	
vibrational relaxation	$10^{-12} - 10^{-10}$ s	
lifetime of the excited state $S_1$	$10^{-10} - 10^{-7}$ s	→ fluorescence
intersystem crossing	$10^{-10} - 10^{-8}$ s	
internal conversion	$10^{-11} - 10^{-9}$ s	
lifetime of the excited state $T_1$	$10^{-6} - 1$ s	→ phosphorescence

**Figure 1.2** Perrin-Jablonski diagram and illustration of the relative positions of absorption, fluorescence and phosphorescence spectra [7]

### 1.4.1 Photoinduced electron transfer (PET)

The molecule sensor consists of a fluorophore linked to a receptor unit. Generally, the fluorescence emission of the sensor is a consequence of emitted radiation after an excited electron on the lowest unoccupied molecule orbital (LUMO) return to the ground state or the highest occupied molecule orbital (HOMO). [17]

After the binding between sensor and guest, an electron of the HOMO is promoted to the LUMO by excitation at fluorophore of the complexation. Then, the PET from HOMO of donor to the fluorophore appeared, leading to a decrease in emission intensity or quenching of fluorescence [17-21] as displayed in Fig. 1.3.

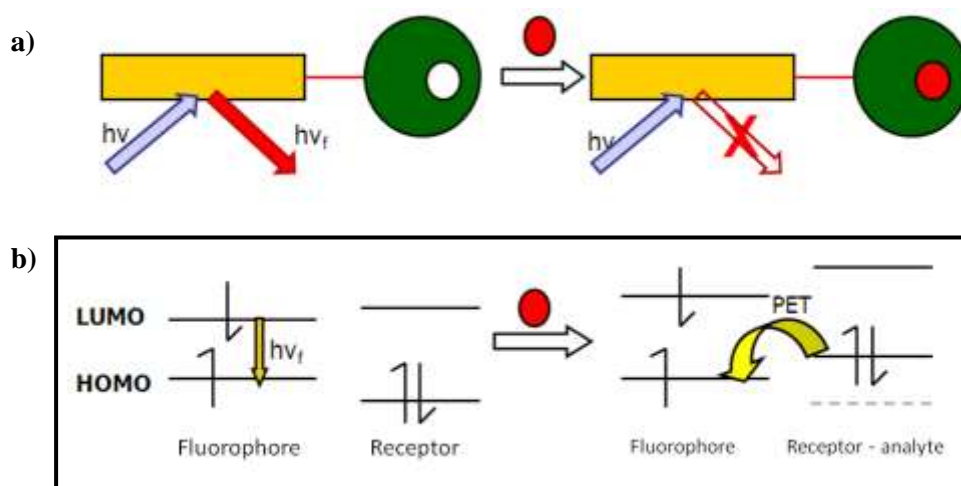
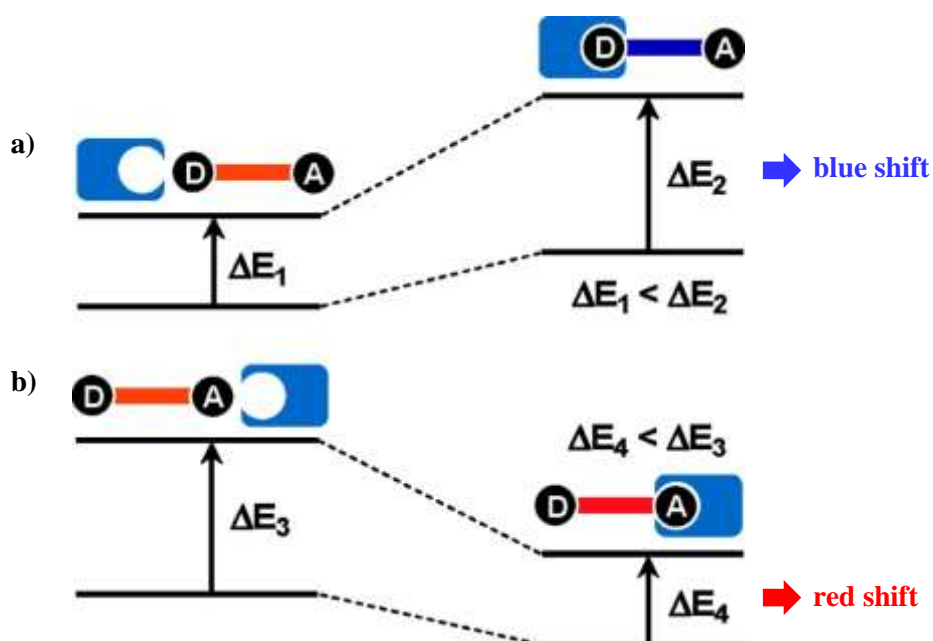


**Figure 1.3** a) Schematic and b) energy level representations of an ON-OFF sensor. The dashed line in the energy level representation of the acceptor-analyte shows the energy level prior to binding of analyte. [22]

### 1.4.2 Photoinduced charge transfer (PCT)

The photoinduced charge transfer phenomenon is intramolecular charge transfer from the electron-donating group to the electron-withdrawing group upon excitation by light. This charge transfer associates with the change of dipole moment. So, it can be anticipated that cations or anions in close interaction with the donor or the acceptor group will change the photophysical properties of the fluorophore. [23-25]

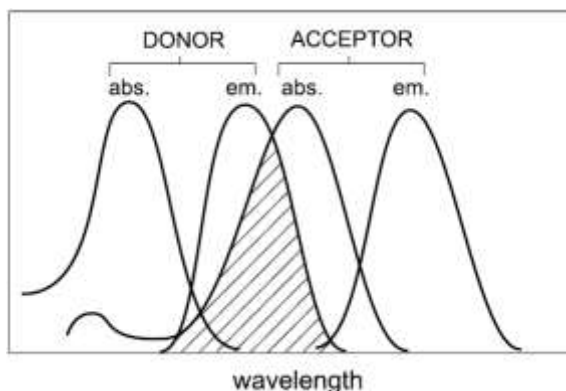
For example, the electron-donating group within a fluorophore interacts with a cation. The electron-donating character of the donor moiety is reduced and the excited state is stabilized by cation less than the ground state. The effective reduction of conjugation results in a blue shift of the absorption and emission spectra (see Fig. 1.4a)). On the contrary, when the cation bind with acceptor group, the excited state is stabilized by cation more than the ground state, causing the enhancement of electron-withdrawing character, and leading to a red shift of the absorption and emission spectra as displayed in Fig. 1.4b). [7, 26]



**Figure 1.4** PCT system of interaction with a) the donor group and b) the acceptor group [17]

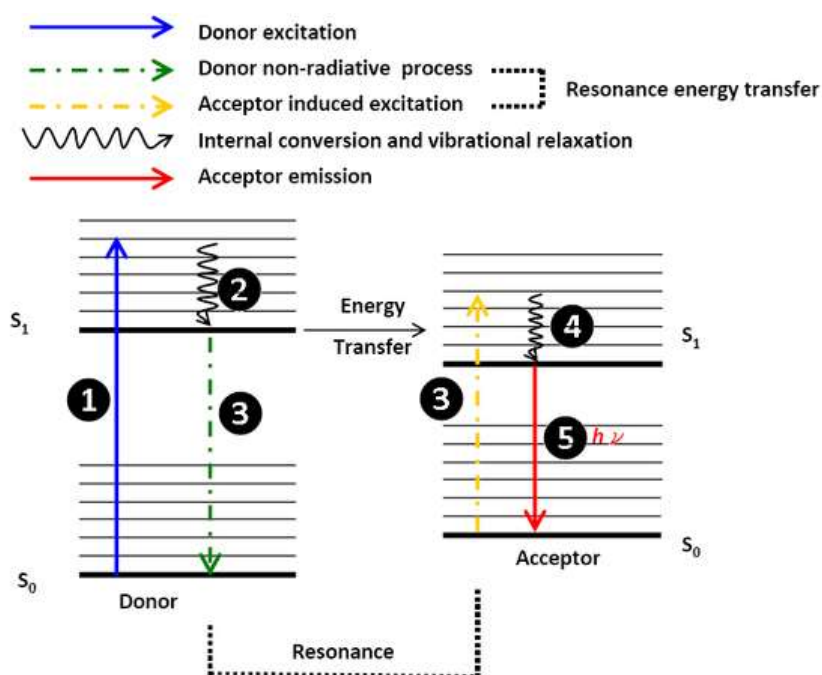
### 1.4.3 Fluorescence resonance energy transfer (FRET)

The phenomenon of fluorescence resonance energy transfer (FRET) is the transfer of energy from an excited donor molecule to an acceptor molecule through a non-radiative mechanism [7]. The three factors influence on FRET process including the range 10-100 °Å of distance between the donor and acceptor group, the overlap of spectrum between donor emission and acceptor absorption as shown in Fig. 1.5, the orientation of dipole moment between donor emission and acceptor absorption. [26-27]



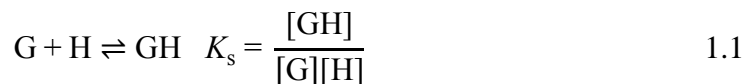
**Figure 1.5** The integral overlap between the emission spectrum of the donor and the absorption of the acceptor [7]

Fig. 1.6 displays the process of non-radiative transfer. The donor molecule is excited by a photon and then relaxes to the lowest singlet excited state ( $S_1$ ). After that, the return of electron to ground state ( $S_0$ ) effects to release energy and simultaneously excite the acceptor molecule. This non-radiative mechanism is referred to as “resonance”. Finally, the fluorescence emission of acceptor molecule is appeared after excitation at proximate absorption of acceptor.



**Figure 1.6** The schematic diagram of the fluorescence resonance energy transfer [28]

### 1.5 Formation of 1:1 complex [29-30]



$Y_0$  is the fluorescence intensity of the free host. In fluorometric experiments, the absorbance at the excitation wavelength should be less than 0.1.  $Y_0$  is proportional to the concentration of host  $c_H$ :

$$Y_0 = ac_H \quad 1.2$$

and in the presence of an excess of guest is completely complexed,  $Y$  reaches the limiting value  $Y_{lim}$ :

$$Y_{lim} = bc_H \quad 1.3$$

In spectrofluorometry,  $a$  and  $b$  are proportional to the molar absorption coefficients at the excitation wavelength and the fluorescent quantum yields of the host and complex, respectively. After addition the amount of guest at a concentration  $c_G$ , the fluorescence intensity becomes

$$Y = a[H] + b[GH] \quad 1.4$$

Mass balance equations for the host and guest are

$$c_H = [H] + [GH] \quad 1.5$$

$$c_G = [G] + [GH] \quad 1.6$$

From Equations 1.1 to 1.6, it is easy to derive the usual relation

$$\frac{Y - Y_0}{Y_{lim} - Y} = K_s[G] \quad 1.7$$

When  $Y_{lim}$  is not measurable because full complexation cannot be attained at a reasonable concentration of guest, it is better to use the following relation:

$$\boxed{\frac{Y_0}{Y - Y_0} = \frac{\alpha}{K_s[G]} + \alpha} \quad 1.8$$

Where  $\alpha = a/(b-a)$ . It is convenient to plot  $Y_0/(Y-Y_0)$  versus  $1/c_G$  provides that the approximation  $[G] \approx c_G$  is valid. The ratio of the ordinate at the origin to the slope yields  $K_s$ . Such a plot is called a double-reciprocal plot or a Benesi-Hildebrand plot.

### 1.6 Determination of stoichiometry of a complex by the method of continuous variation (Job's method) [7]

Information on the stoichiometry of a complex can be obtained from the continuous variation method. To consider a complex  $G_gH_h$  formed according to the equilibrium



with

$$\beta_{gh} = \frac{[G_gH_h]}{[G]^g[H]^h} \quad 1.10$$

The principle of the method as follows: the fluorescence intensity  $Y$  is measured for a series of solutions containing the host and the guest such that the sum of the total concentrations of host and guest is constant.

$$c_H + c_G = C = \text{constant} \quad 1.11$$

The position of the maximum of  $Y$  is then related to the ratio  $g/h$ . The intensity of complex is equal to  $Y_0$  and the value of  $Y$  is related to no guest added ( $x = 0$ ). When plotting the variations between fluorescence intensity and mole fraction  $X$ , it is convenient to subtract the fluorescence intensity that would be measured in the absence of guest at every concentration.



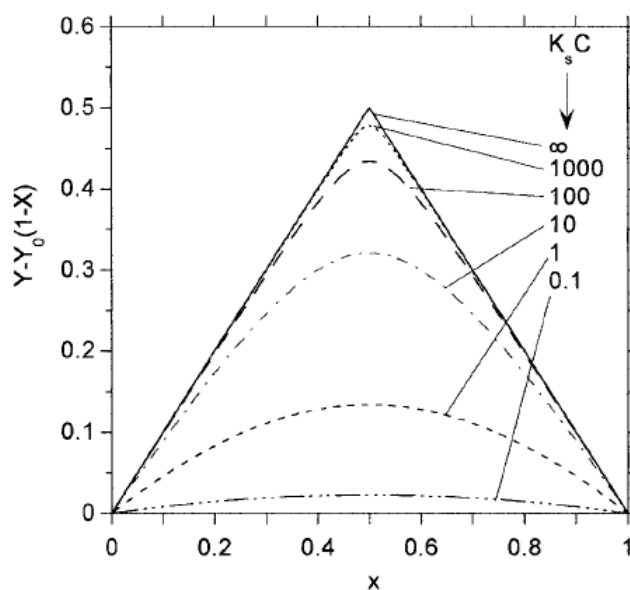


**Figure 1.7** Job's plots for a 1:1 complex [7]

### 1.7 Limit of detection [31]

Definition of detection limit is the lowest concentration of analyte that can be determined. The limit of detection of an analyte may be explained that the concentration of compound gives an instrument signal distinct from the blank or background signal. These meaning of the limit of detection are quite a deal of freedom to determine the correct definition, based on an appropriate interpretation of the phrase significantly different.

This is an optional definition for measurement of the limit of detection as the smallest measure,  $x_L$ . The  $x_L$  value is obtained from the equation 1.12

$$x_L = x_{bi} + 3s_{bi} \quad 1.12$$

Where  $x_{bi}$  is the representation of the blank signal and  $s_{bi}$  is the standard deviation of the blank.

The measurement units ( $x_L$ ) is converted into the concentration ( $c_L$ ), when, the sensitivity or slope ( $S = \Delta\text{concentration} / \Delta\text{intensity}$ ) is applied as corresponding to the equation 1.13

$$c_L = c_{bi} + 3s_{bi}S \quad 1.13$$

The blank concentration is zero, then

$$c_L = 3s_{bi}S \text{ or } c_L = 3s_{bi}/\text{slope} \quad 1.14$$

### 1.8 Principal component analysis (PCA) [32]

Principal component analysis (PCA) is a statistic method used to reduce a dimensionality of the data set into a new coordination system. To identify patterns in the data, the calculation of orthogonal eigenvectors from original data set is showed in terms of principle component (PCs). The first component PC1 contains the highest degree of variance and other PCs follow in order of decreasing variance. The mathematical transformation of the original data matrix ( $X$ ) can be described by equation:

$$X = T \cdot P + E \quad 1.15$$

where:

$X$  = original data matrix

$T$  = score matrix

$P$  = loading matrix

$E$  = error matrix

The graphical representation of PCA is displayed in Figure 1.8

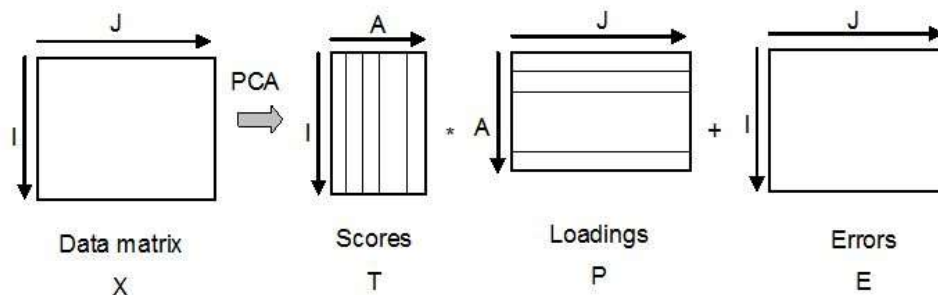


**Figure 1.8** Principal of the PCA [33]

The coordinations of the sample associate with the PC axis as the scores and can indicate the relationship between analytes. The original variables are reduced to a number of significant principle components by PCA method. This procedure can reduce the large original data set to a smaller data set that is utilized for simplified interpretation as indicated in Fig. 1.9.

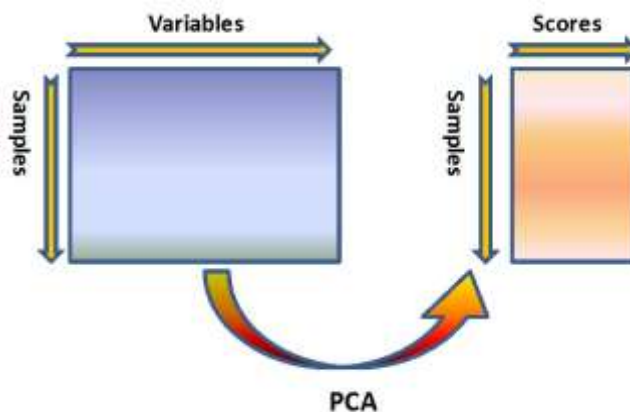


**Figure 1.9** PCA as a form of variable reduction [34]

Fig. 1.10 showed an example of PCA procedure for the reduction of original data from three-dimensional gene expression data to two new variables in term of principal component (PCs). The main variance is along PC1 and PC2 is orthogonal with PC1. This PCA method process well classifies the analytes.

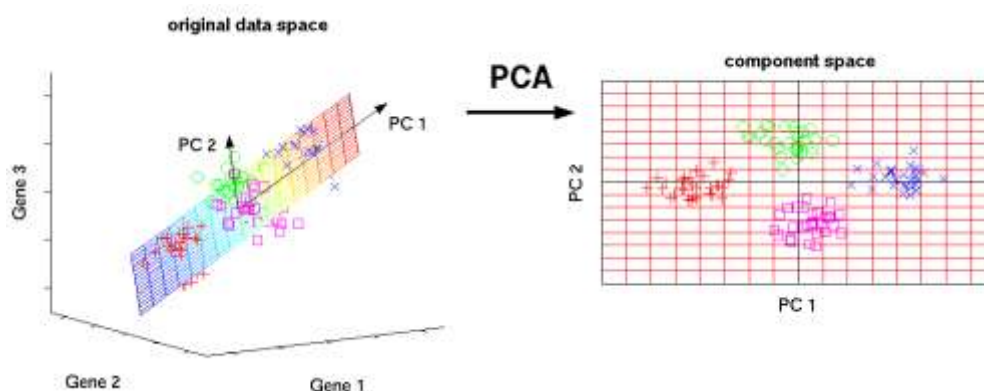


**Figure 1.10** Graphical representation of samples in the original data space (left) and the position of samples in PC spaces (right) [35]

## CHAPTER II

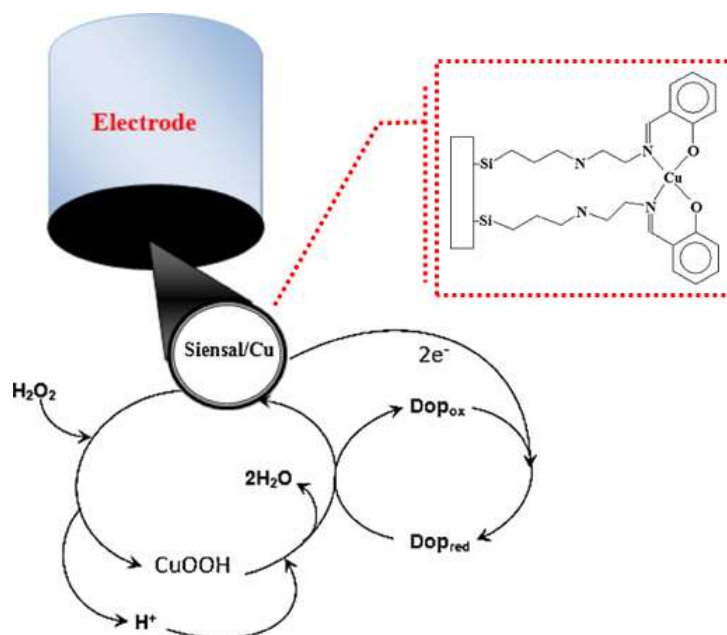
### LITERATURE REVIEWS

#### 2.1 Literature reviews

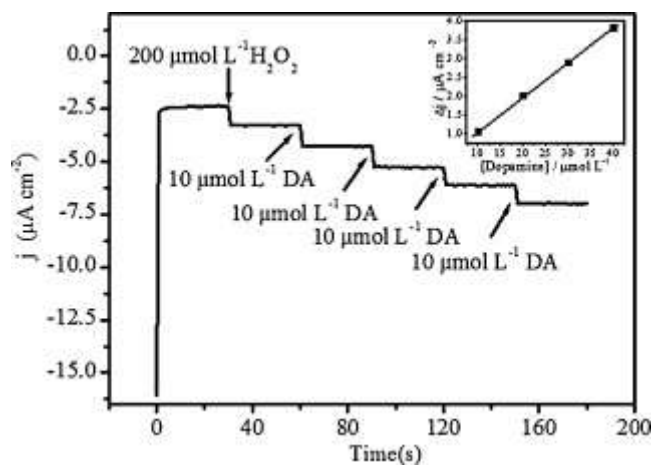
Catecholamine neurotransmitters, including dopamine (**DA**), norepinephrine (**NE**) and epinephrine (**EPI**), which are the class of biogenic amines, play an important role of neurotransmitters involving in the nervous system functions. [36-37] Unusual catecholamine concentration in brain tissue, urine and plasma serum is highly related to central nerve disease, such as Parkinson's disease [38-39] and Schizophrenia. So, the measurement of a quantity of dopamine is an essential task for pre-diagnosis of these diseases. For taking advantage, the diverse techniques for the detection of catecholamine have been developed in recent decades. [40-44]

##### 2.1.1 Determination of catecholamine by electrochemical technique

Dos Santos et al. [45] reported a novel amperometric sensor modified with ensal organic copper complexes on the surface of mesoporous silica for determination of dopamine (**DA**) by amperometry and cyclic voltammetry technique. Fig. 2.1 illustrated the proposed mechanism of **DA** oxidation on DMS/(ensal)<sub>2</sub>Cu/C electrode. The hydrogen peroxide (H<sub>2</sub>O<sub>2</sub>) generated Cu-OOH which oxidized **DA** species on the surface of electrode. The amperometric response of the prepared electrode toward **DA** added into the solution of H<sub>2</sub>O<sub>2</sub>. It demonstrated an excellent sensitivity of electrode at 21.2 nA L μmol<sup>-1</sup> cm<sup>-2</sup>.

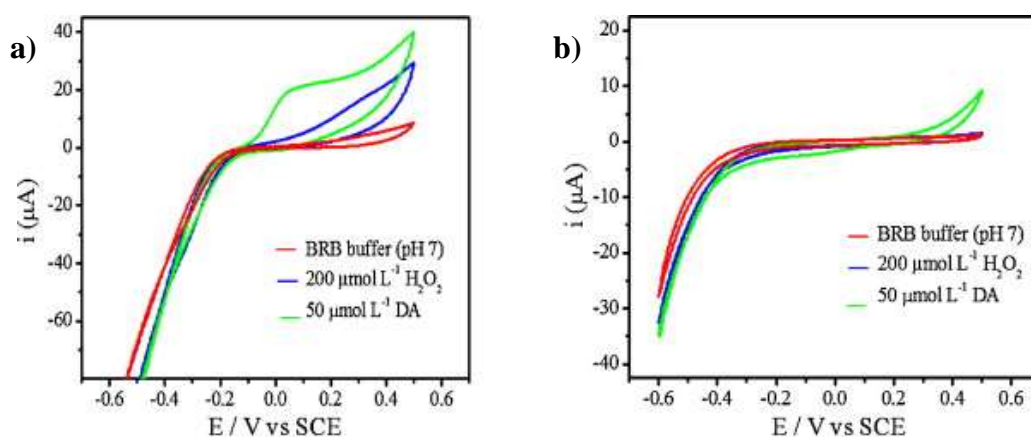


**Figure 2.1** Proposed mechanism of dopamine oxidation on the surface of DMS/(ensal)<sub>2</sub>Cu/C electrode



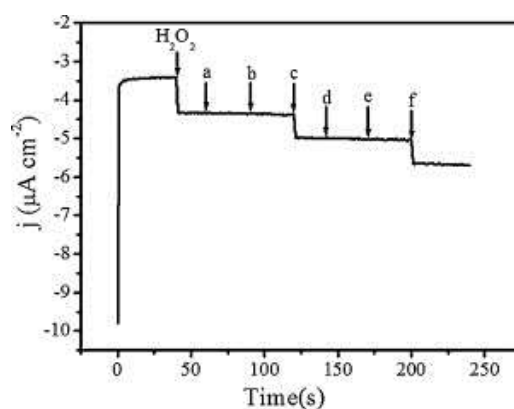
**Figure 2.2** Amperometric response of DA, each step corresponds to the increment of  $10 \mu\text{mol L}^{-1}$  DA containing  $200 \mu\text{mol L}^{-1}$  of  $\text{H}_2\text{O}_2$  and inset shows the analytical curve.

Fig. 2.3 showed the effect of copper complexes on the sensor response. The electrode modified with  $(\text{ensal})_2\text{Cu}$  in Fig. 2.3a showed signaling changes after adding **DA** or  $\text{H}_2\text{O}_2$ , while unmodified DMS/C electrode in Fig. 2.3b did not response to **DA** or  $\text{H}_2\text{O}_2$ . It implied that copper complexes acted as a catalyst for **DA** oxidation.



**Figure 2.3** Cyclic voltammograms obtained from a) DMS/C electrode modified with  $(\text{ensal})_2\text{Cu}$  and b) unmodified DMS/C electrode. Scan rate  $10 \text{ mVs}^{-1}$ ,  $0.04 \text{ mol L}^{-1}$  BRB at pH 7.0 containing  $1 \text{ mol L}^{-1}$  KCl.

The **DA** discrimination by this modified electrode did not obtain the interference of ascorbic acid (**AA**) and **NADH** at the same concentration of **DA** as shown in Fig. 2.4.



**Figure 2.4** Amperometric response of the addition of concentration in  $\mu\text{mol L}^{-1}$  of  $[\text{NADH}] = (\text{a}) 10, (\text{d}) 20, [\text{AA}] = (\text{b}) 10, (\text{e}) 20$  and  $[\text{DA}] = (\text{c}) 10, (\text{f}) 20$  into the electrochemical cell

Furthermore, this enzymeless biosensor indicated a wide response range as 10-130  $\mu\text{molL}^{-1}$ , a low detection limit of 0.52  $\mu\text{molL}^{-1}$  of **DA**, a long lifetime of 6 months for repeatability and a short response time of 1 s for detection of **DA**.

Abbaspour and Noori [46] invented an electrochemical sensor using a  $\beta$ -cyclodextrin (**CD**), poly (N-acetylaniline) and carbon nanotube composite modified on carbon paste electrode for simultaneous measurement of dopamine (**DA**) and serotonin (**5-HT**) as shown in Fig. 2.5.

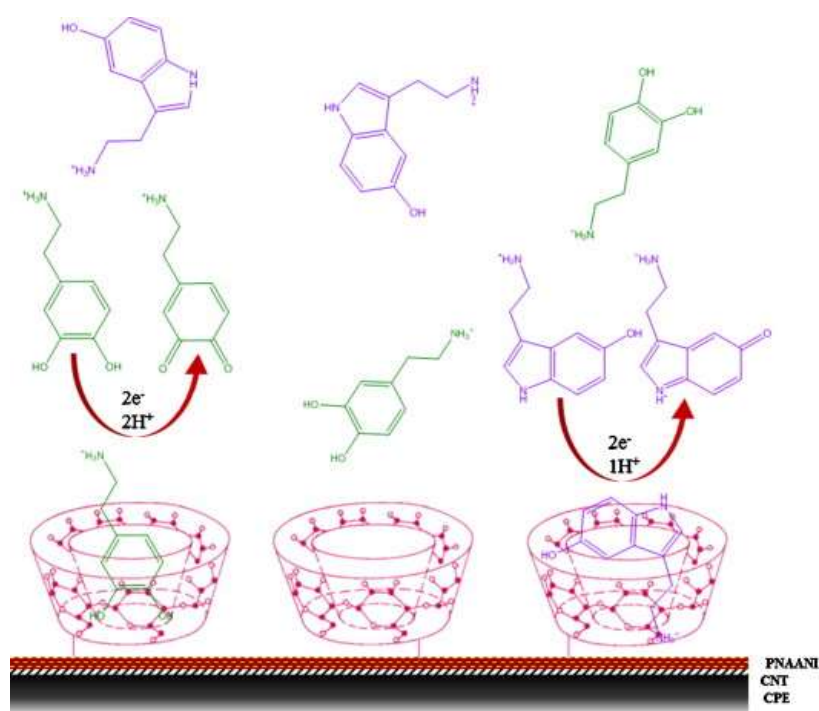


**Figure 2.5** The inclusion complex formation between  $\beta$ -cyclodextrin and **5-HT/DA** as guest molecules

The case of the cyclic voltammetry technique investigated the oxidation mechanism of **DA** and **5-HT** on the surface of the electrode.

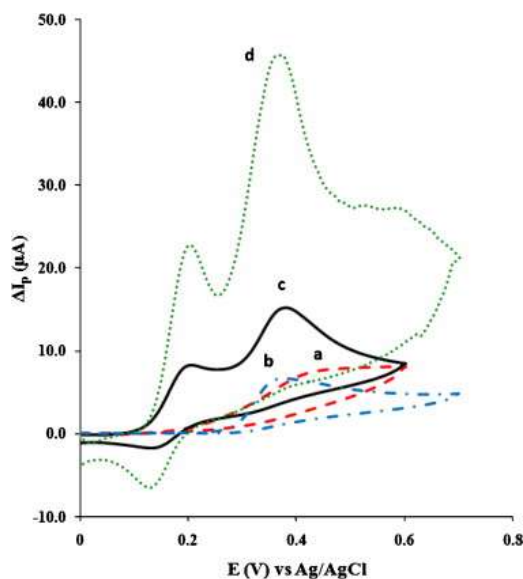


**Figure 2.6** Cyclic voltammograms of 100  $\mu\text{M}$  **5-HT** and **DA** in 0.05 M of phosphate buffer pH 7.4 on the bare (a, dashed), MWNT modified (b, dash-dotted), **CD/PNAANI** modified (c, solid) and **CD/PNAANI/CNT** modified (d, round-dotted) CPE (background currents are substrated for simplicity)

From Fig. 2.6, the overlapped anodic peaks of **DA** and **5-HT** at 428 mV on bare electrode (curve a) were separated significantly at 202 and 363 mV in the case of **CD/PNAANI/CNT** modified CPE (curve d). Moreover, this oxidation current was enhanced because of the catalytic effect of carbon nanotube and interaction of **CD** toward **5-HT** and **DA**. On the reverse scan, the disappearance of the reduction peak of **5-HT** was observed. It can be explained that the electrochemical oxidation of **5-HT** was totally irreversible. To investigate the analytical application of this biosensor for detection of **DA** and **5-HT** in bovine samples, it was found to detect **DA** and **5-HT** in micromolar levels. The detection limit of this sensor showed sub- $\mu\text{M}$  level and % recovery of this sensor is less than 5%.

Actually, the electrochemical technique has been highly attractive for detection of analytes in millisecond level with micrometer resolution. [47] However, limitation of this technique is in term of the interference of very similar potentials of oxidized catecholamines form. Since, the catechol group is easily oxidized providing



quinone moiety, [48-50] these techniques served as a poor selectivity for catecholamines detection.

### 2.1.2 Determination of catecholamine by NMR & mass spectroscopy

Paugam et al. [51] created a ditopic receptor **1** that consisted of 18-crown-6 for binding with ammonium ions and boronic acid for covalent bond of the catechol. This ditopic receptor was utilized the mimic transportation of dopamine through lipophilic membrane in biological system. To study a dopamine transport by using the standard U tube methodology [R], the solvent was divided two phase. The pH in aqueous phase was controlled by phosphate buffer at pH 7.4 and organic phase was chloroform solution. The selectivity of carrier **1** was verified by transport rate from Table 2.1. The carrier **1** showed a high selectivity with dopamine. The case of epinephrine without ammonium ion group caused a low rate enhancement. Other amines and saccharides showed very weak interaction with carrier **1**.

**Table 2.1** Transport rates for catecholamines, glucosides, and uridine in the presence and absence of carrier **1**

entry	transported compound	no carrier (±15%)	carrier <b>1</b> (±15%)	rate enhancement
1	dopamine	2.2	356	160
2	norepinephrine	2	120	60
3	epinephrine	3.4	6.8	2
4	tyramine	70	70	1
5	<i>p</i> -nitrophenyl $\beta$ -glucoside	1.3	3.9	3
6	<i>p</i> -nitrophenyl $\beta$ -manoside	1.6	3.3	2
7	uridine	0.2	0.2	1

A structure of the transported dopamine-**1** complex in Fig 2.7 was supported by mass spectroscopy. The negative ion FAB showed the intense peak at 564 m/z [**1**+H<sup>+</sup>] in aqueous phase and 562 m/z [**1**-H<sup>-</sup>] in chloroform phase.

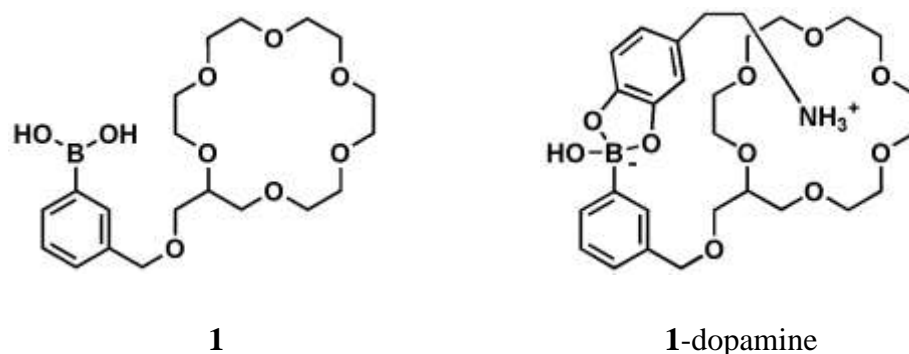


**Figure 2.7** The structure of carrier **1** and complexation of carrier **1** with dopamine

Kim et al. [52] designed tripodal oxazoline-based receptors (in Fig. 2.8), which imitate a hydrophobic pocket proghosticated for a human D2 receptor. Receptor **2** was the best recognition of dopamine observing from the association constants as indicated in Table 2.2. The complexation of **2** toward tyramine and 2-phenylethylamine guests displayed sequentially a lower binding constant. The interaction of receptor **2** with analytes was underwent the hydrogen bonding of ammonium ion and nitrogen atom on tripodal oxazoline, aromatic  $\pi$ - $\pi$  stacking interaction and hydrophobic nature of analytes.



**Figure 2.8** Proposed interactions of designed receptor **2** with dopamine•HCl in water and CPK view of an inclusion complex between **2** and dopamine ammonium ion

**Table 2.2** Association constants obtained for complexation of receptor **2** toward various organoammonium ions in D<sub>2</sub>O by <sup>1</sup>H-NMR titrations

guest <sup>a</sup>	$K_{\text{assoc}(1:1)}$ [M <sup>-1</sup> ] <sup>b</sup>	$-\Delta G$ [kJ mol <sup>-1</sup> ]	$\Delta\delta_{\text{sat}}$ [ppm] <sup>c</sup>	stoichiometry <sup>d</sup>
2-phenethylamine	82 ± 12%	10.99	0.32	1:1
tyramine	101 ± 7%	11.51	0.33	1:1
dopamine	161 ± 16%	12.67	0.36	1:1
catechol	< 1			1:1
ethanolamine	< 1			1:1
acetylcholine	< 1			1:1
noradrenaline	67 ± 6%	10.48	0.21	1:1
DL-tyrosine methyl ester	65 ± 11%	10.41	0.22	1:1
GABA	< 1			1:1

<sup>a</sup>As the hydrochloride salt. <sup>b</sup>Errors are calculated as standard deviations from the nonlinear regression. <sup>c</sup>Largest shifts from selected CH protons. <sup>d</sup>Determined by Job plots and curve fitting of titration curves.

Considering, the structure of analytes related to the trend of association constant values. In table 2.2 showed the order of dopamine (two –OH groups) > tyramine (one –OH group) > 2-phenylethylamine (no -OH group). It can be explained that the hydroxyl group of analytes can interact with sulfonate group or phenyl ether oxygen in water. Furthermore, the binding mode of complexing was examined by the <sup>1</sup>H-NMR spectrum in Fig. 2.9. The <sup>1</sup>H-NMR spectrum of oxazoline phenyl protons displayed upfield shift caused by  $\pi$ - $\pi$  stacking interaction between receptor **2** and aromatic ring of dopamine.

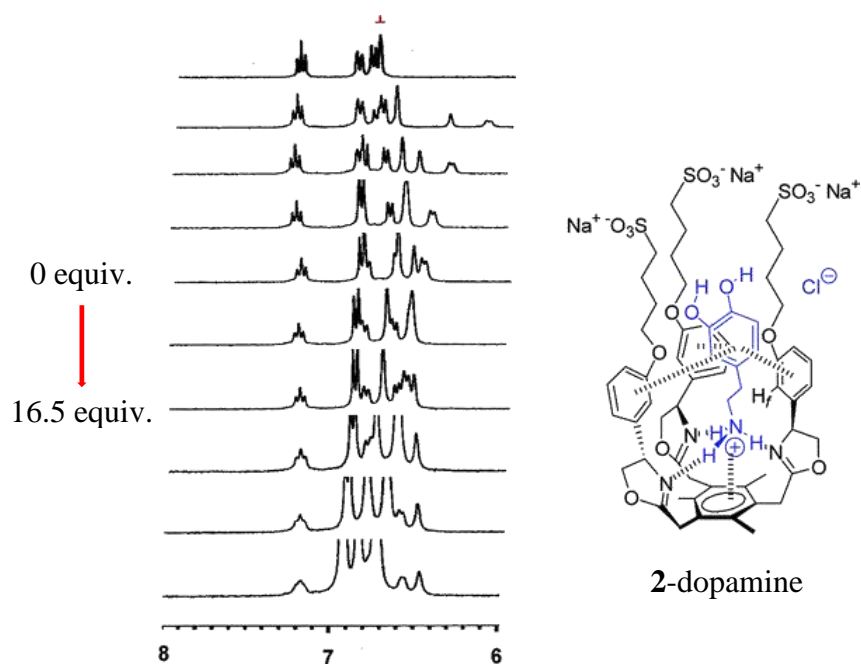


**Figure 2.9**  $^1\text{H-NMR}$  spectral changes at proton  $\text{H}_f$  of **2** (40 mM) at upon addition of dopamine hydrochloride (0 to 16.5 equiv.) in water

### 2.1.3 Determination of catecholamine by fluorescence spectrophotometry

Widely known, the detection of specific catecholamine, neurotransmitters, by artificial chemosensors under fluorescence spectroscopy [53-54] which is a versatile technique with high sensitivity, rapid response, and easy performance, is currently of interest subject to pursue.

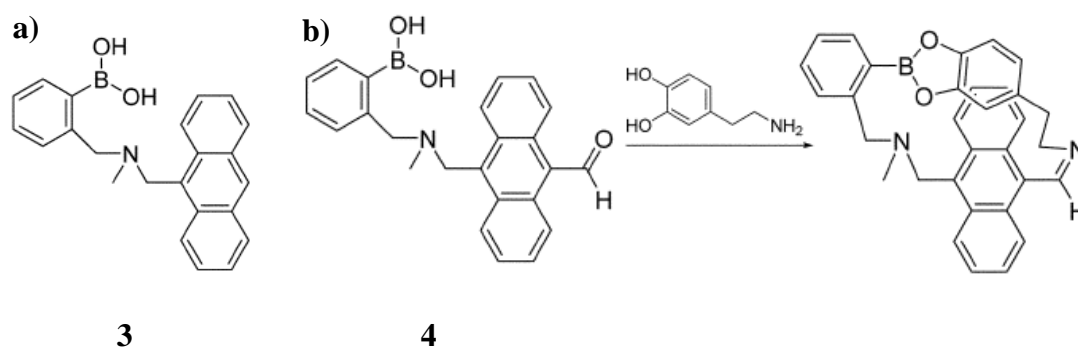


**Figure 2.10** a) Structure of sensor **3** and b) proposed binding mode of sensor **4** with dopamine

Jang et al. [55] synthesized two new anthracene derivatives (**3** and **4**) containing boronic acid group for detecting dopamine in aqueous solution as shown in Fig. 2.10. They reported that both compounds exhibited large fluorescence quenching effects with epinephrine, dopamine and catechol at pH 7.4 as shown in Fig. 2.11. This phenomenon can be described by a photoinduced electron transfer (PET) process. The electron rich on catechol is probably playing as a quencher of anthracene when the complex was occurred.

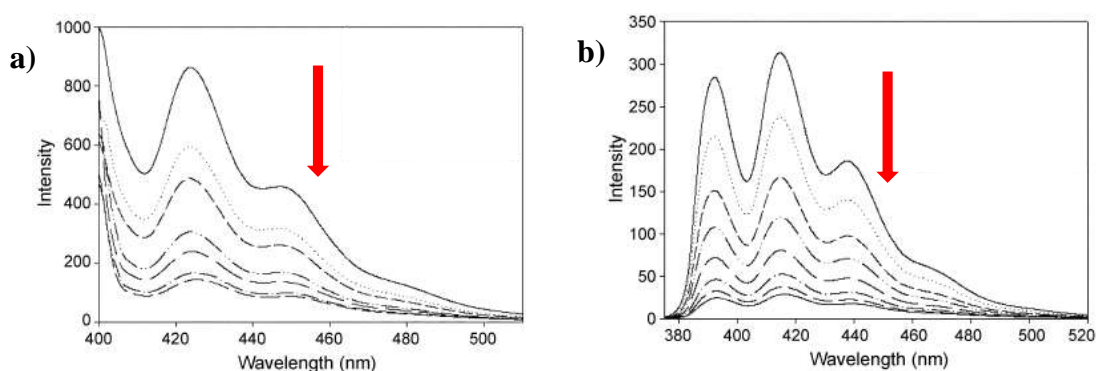


**Figure 2.11** Fluorescence spectra of a) sensor **4** (3 μM) upon the addition of dopamine in MeOH (excitation at 397 nm) b) sensor **3** (3 μM) upon the addition of dopamine in 50% MeOH/0.05M HEPES buffer at pH 7.4 (excitation at 367 nm)

Concerning on the capability of sensor **3** and **4** with dopamine, sensor **4** containing aldehyde group exhibited two fold better complexing with dopamine in methanol than sensor **3** did. Because aldehyde group of sensor **4** would bind with amino group of dopamine to produce the imine bond.

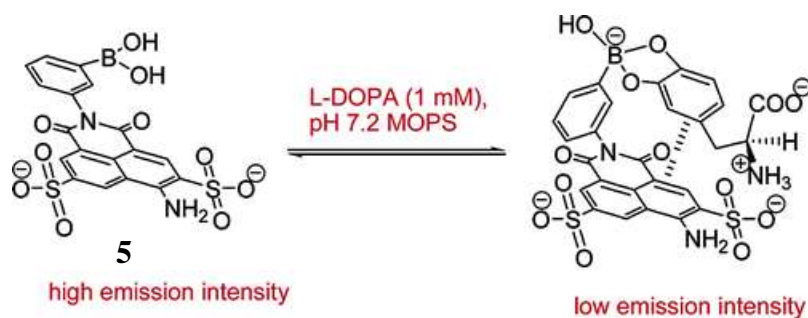


**Figure 2.12** The complexation of sensor **5** with **L-DOPA** in buffer solution

Coskun et al. [56] presented the fluorescent chemosensor **5** based on a phenylboronic naphthalimide (Lucifer yellow dyes) for recognition of **L-DOPA** through a combination of reversible boronic ester formation, electrostatic interaction and  $\pi$ - $\pi$  interactions as shown in Fig. 2.12. Upon the addition of **L-DOPA**, the fluorescence intensity at 535 nm was gradually decreased. (as shown in Fig. 2.13)

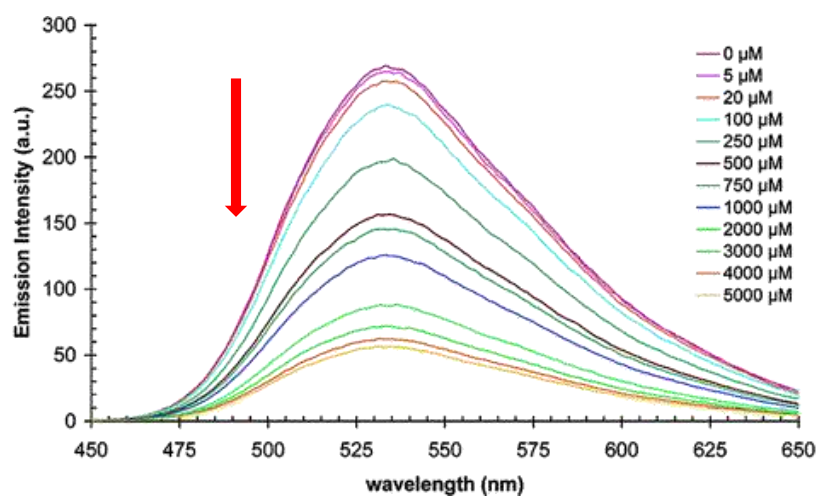


**Figure 2.13** Fluorescence spectra of 5  $\mu$ M chemosensor **5** in the presence of gradual increasing of **L-DOPA** concentrations in 0.1 M MOPS buffer pH 7.2 and excitation at 430 nm.

The complexation of chemosensor **5** and **L-DOPA** showed dissociation constant of  $6.1 \times 10^{-4}$  M for 1:1 complexation by Benesi Hildebrand analysis. The fluorescence changes of other analytes were depicted in Fig. 2.14.

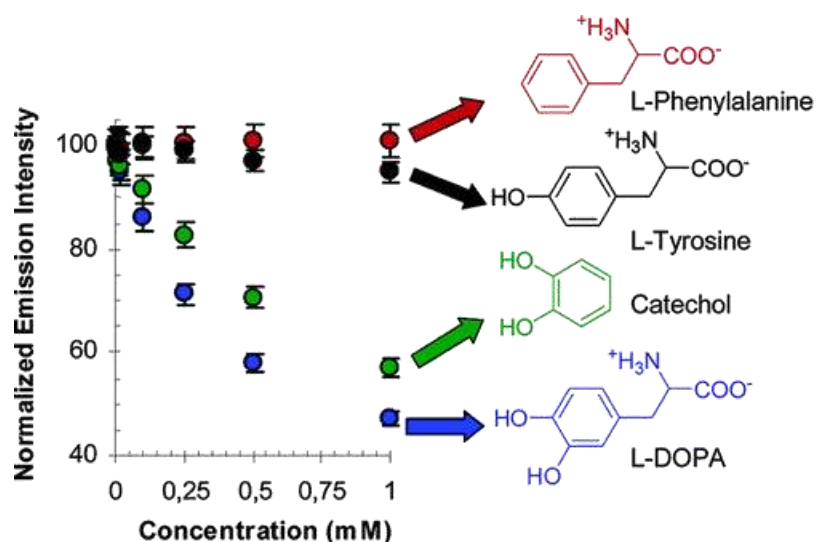


**Figure 2.14** Normalized peak emission intensity of **5** toward catechol, **L-DOPA** and other amino acid in buffered aqueous solution (0.1 M MOPS, pH 7.2) and excitation wavelength at 430 nm

The catechol analyte showed a decrease of the fluorescence intensity estimate with **L-DOPA**. L-Phenylalanine and L-Tyrosine did not change the emission intensity. It seems that both analytes cannot interact with fluorescence chemosensor **5**. To study the multiple binding mode of complex,  $^1\text{H-NMR}$  titration in buffer solution was carried out. An aromatic proton of phenyl boronic acid showed upfield shift after the increasing amount of **L-DOPA**. The energy minimized structure of the complex addressed the binding behavior of the chemosensor **5** and **L-DOPA** with charge transfer interaction and electrostatic interaction between sulfonate and ammonium groups.

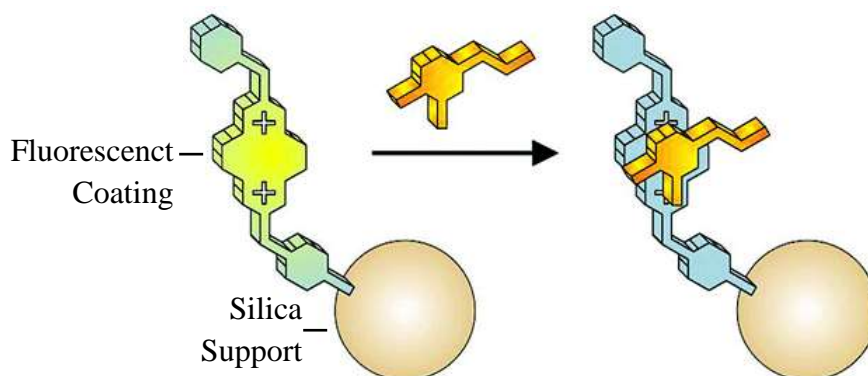


**Figure 2.15** The complexation of fluorescence probe of 2,7-diazapyrenium dication modified on silica particles toward dopamine

Raymo and Cejas [57] designed fluorescence probe of 2,7-diazapyrenium dication modified on silica particles for detection of dopamine at the particle/water interface. They hypothesized that the electron-rich catechol of dopamine complexed with the electron-deficient 2,7-diazapyrenium dications by charge transfer interaction and electrostatic forces as shown in Fig. 2.15.

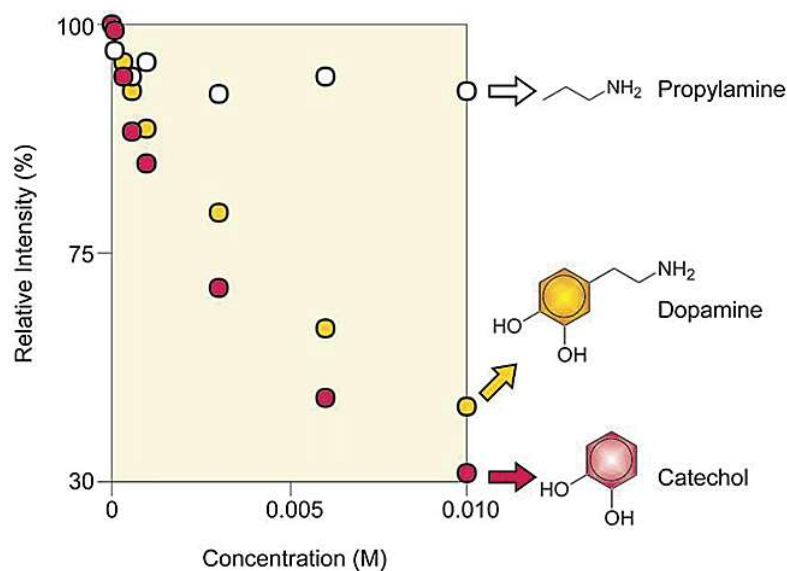


**Figure 2.16** Relative emission intensity of fluorescent particles (0.3 mg/mL, sodium phosphate buffer, pH = 7.0, 32°C,  $\lambda_{em} = 432$  nm) in the presence of various concentrations of catechol, dopamine or propylamine



To prove ability of fluorescence particle toward dopamine in aqueous media at pH 7, the fluorescence intensity at 432 nm decreased rapidly after the gradual addition of dopamine. For other analytes, the emission intensity of fluorescence probe to propylamine did not significantly change, while the catechol analyte could interfere the detection of dopamine by a high fluorescence quenching as indicated in Fig. 2.16. Moreover, the association constants of 1:1 complexes of host and guest in the case of catechol and dopamine were  $260 \pm 10$  and  $180 \pm 7$ , respectively.

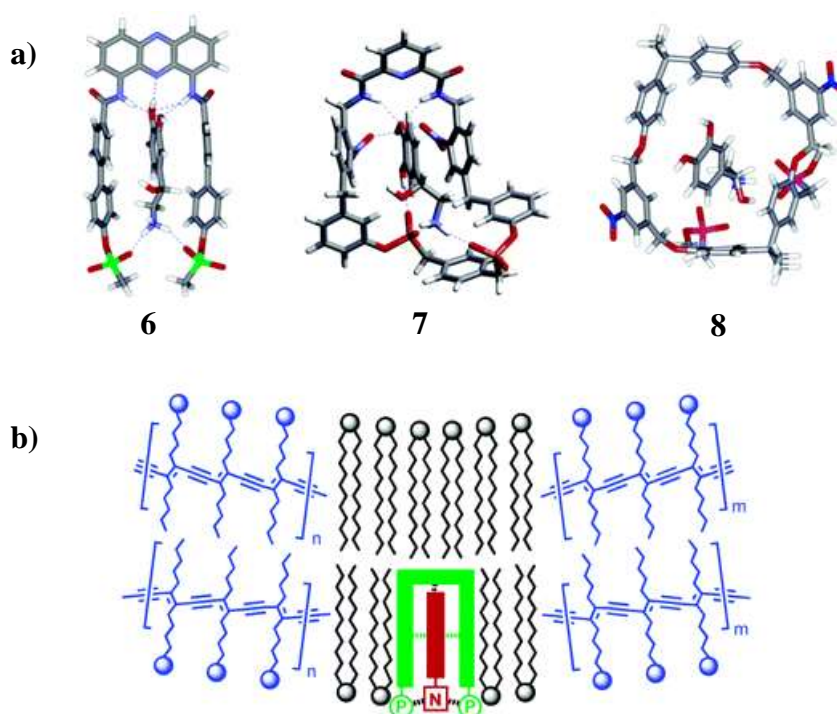


**Figure 2.17** a) Structure of receptor-noradrenaline complexes b) schematic structure of the receptor/phospholipid/PDA assemblies. Blue: PDA. Black: phospholipids. Green: host. Red: ligand

Kolusheva et al. [58] described the recognition of catecholamine using the synthetic fluorescence sensor holding with phospholipid/polydicetylene (PDA) vesicle. The receptor incorporated in PDA could enhance the fluorescence intensity for detection of catecholamine due to the static receptor in aqueous solution. From Fig. 2.17a, receptor **6** was found to selectively bind with noradrenaline, while receptor **7** preferred to bind dopamine and receptor **8** was designed to recognize a large

analytes. The assembled incorporation of receptor in phospholipid and PDA could form complexes with catecholamine in aqueous solution.

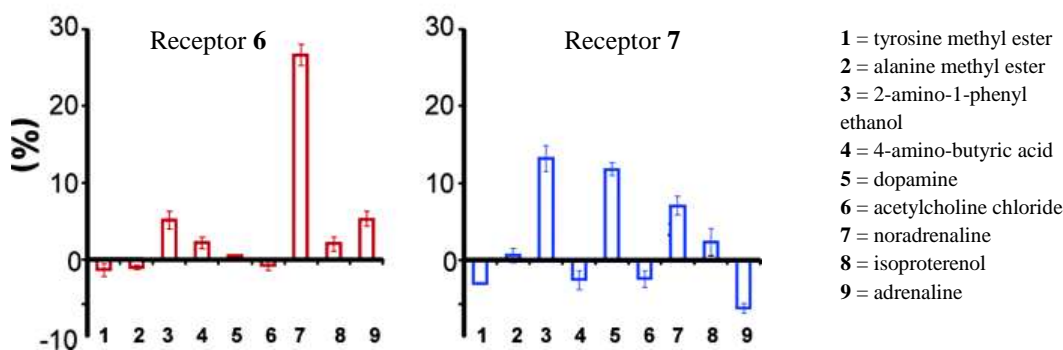


**Figure 2.18** Fluorescence emissions (560 nm, excitation 490 nm) were induced by ligand addition to host/DMPC/PDA vesicles. The values shown (calculated as percentage intensities compared to host/DMPC/PDA) vesicle.

To verify the selectivity of receptor **6** and **7**, the **6** DMPC/PDA vesicle demonstrated a large enhancement of highly of fluorescence intensity after adding noradrenaline (**7**), while sensor **7**/DMPC/PDA showed a strong fluorescence spectrum in the case of 2-amino-1-phenylethanol (**3**) and dopamine (**5**) as indicated in Fig. 2.18. Moreover, the calibration curve was constructed between relative fluorescence emission at 560 nm and concentration of analytes in urine. It displayed a wide range in micromolar level and is useful for quantitative determination of catecholamine in urine samples.

Tao et al. [60] designed the colorimetric and fluorometric dual channel sensor based on bovine serum albumin-stabilized Au nanocluster (BSA-AuNCs) for high sensitivity and selectivity of detection of dopamine (DA). The BSA-AuNCs showed a strong fluorescence intensity. Upon binding with excess DA, the fluorescence emission band of BSA-AuNCs extremely decreased under photoinduce electron transfer (PET) mechanism from electrostatic interaction between DA and BSA-AuNCs. On the other hand, the complex of DA and BSA-AuNCs can inhibit the phenomenon of peroxidase-like catalytic color reaction which offers an excellent sensing purpose of DA detection.

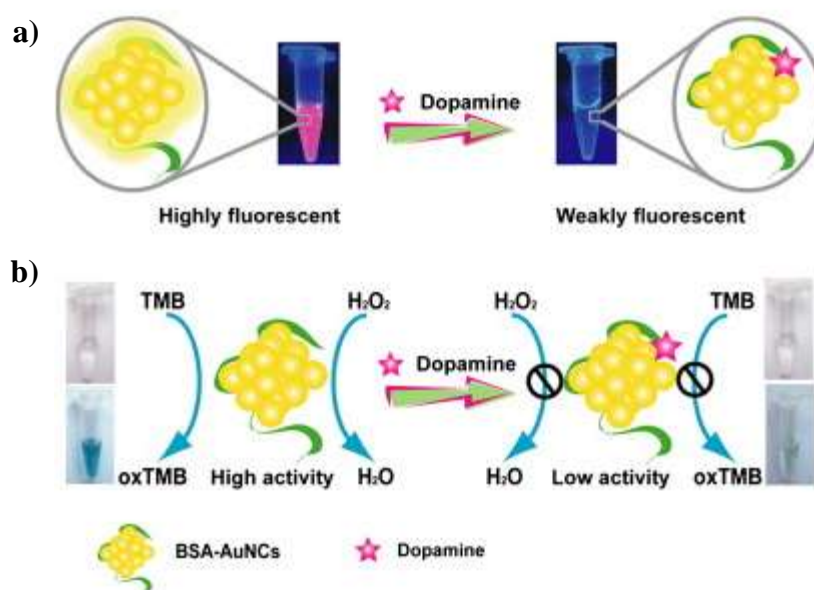


**Figure 2.19** a) The fluorescence response of the BSA-AuNCs with DA. b) Schematic representation of peroxidase-like catalytic color reaction for sensitive sensing of DA

The visual detection of DA showed color change from sky blue to colorless after adding DA. This colorimetric and fluorometric probe showed a high potential selectivity toward DA among interfering from other analytes as indicated in Fig. 2.20. Moreover, this dual channel sensor has been successfully demonstrated an effective detection of DA in real sample in both case of serum and PC12 cells.

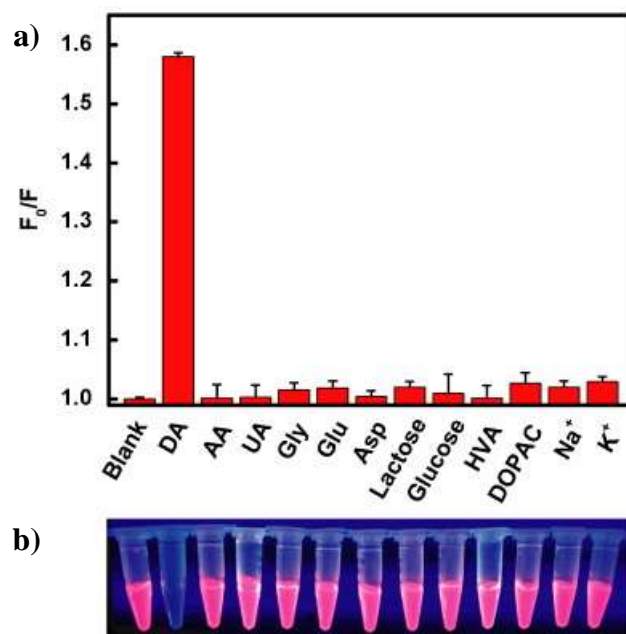


**Figure 2.20** a) The fluorescence responses of the BSA-AuNCs in the presence of 100  $\mu\text{M}$  DA or other analytes. b) Photographs of BSA-AuNCs solutions in the presence of 1 mM DA or other analytes under UV light

#### 2.1.4 Ratiometric sensors under FRET mechanism

Served factors give the influence on the fluorescent intensity change such as an environmental conditions, probe concentration and instrumental efficiency. [61-62] Ratiometric probe can eliminate most or all vagueness by self-calibration of emission intensities at two wavelengths. [63-68] Therefore, many researches have paid attention to design the fluorescence chemosensor under fluorescence resonance energy transfer (FRET) mechanism between FRET donor and acceptor which shows a longer wavelength. [69-72]

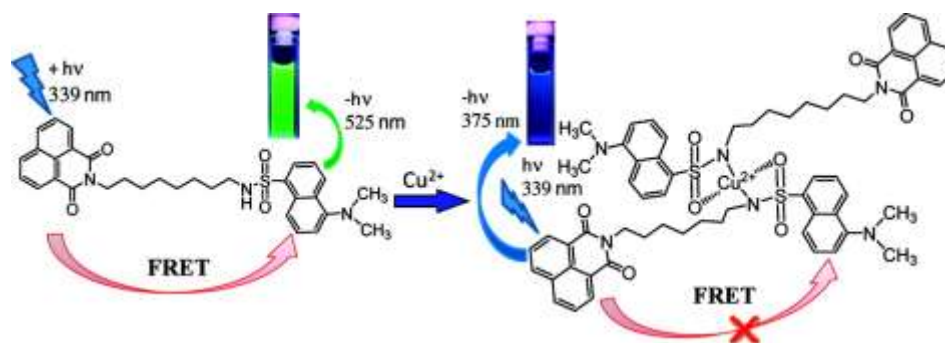


**Figure 2.21** The complexation of sensor **9** toward  $\text{Cu}^{2+}$  under inhibition of FRET process

Jisha et al. [73] synthesized the molecular sensor **9** based on naphthalimide and dansyl moiety linked with the polymethylene group for measurement of various metal ions in 20% acetonitrile containing neutral micelles TX-100. From Fig. 2.22a, this sensor exhibited dual emission band at 375 and 525 nm of naphthalimide and dansyl group, respectively under fluorescence resonance energy transfer (FRET) mechanism. After adding  $\text{Cu}^{2+}$  ion, the emission band at 525 nm was decreased, while the fluorescence intensity at 375 nm was enhanced owing to the inhibition of FRET mechanism as shown in Fig. 2.21. To prove a selectivity of sensor, they reveal that the sensor **9** displayed a high selectivity for  $\text{Cu}^{2+}$  ions compared to various metal ions observing from the decrease of emission band at 525 nm in concomitant with the fluorescent enhancement of naphthalimide moiety at 375 nm as shown in Fig. 2.22b. Further, the Job's plot of complex between sensor **9** and  $\text{Cu}^{2+}$  ions showed 2:1 stoichiometry with the association constant ( $K_{\text{assoc}}$ ) of  $5.2 \pm 0.1 \times 10^{10} \text{ M}^{-1}$  calculated by Benesi-Hidebrand method.

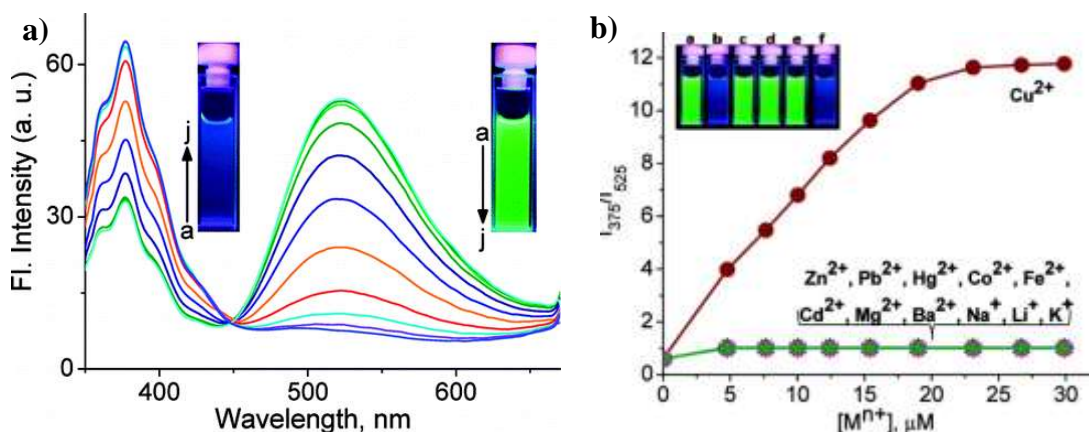


**Figure 2.22** a) The fluorescent titration spectra of sensor **9** with  $\text{Cu}^{2+}$  ion and b) relative emission intensity change of sensor **9** toward various metal ions in 20% acetonitrile containing 2 mM of neutral micelle TX-100 and excitation wavelength at 339 nm

Lee and Kang [74] developed a biosensor for measuring the quantity of dopamine. Since the amount of dopamine was an important factor in the diagnosis of the Parkinson's disease. In this study, they researched the effect of dopamine concentration through fluorescence resonance energy transfer (FRET) mechanism between dendrimer-QD and Alexa Fluor 488-labeled antibody acting as donor and acceptor, respectively, as shown in Fig. 2.23.

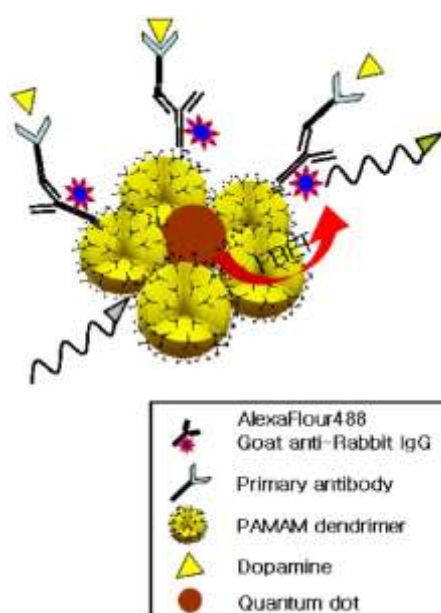


**Figure 2.23** FRET process between dendrimer-QD and Alexa Fluor 488-labeled

The effect of dopamine concentration on the FRET mechanism was confirmed by using enzyme-linked immunosorbant assay (ELISA). The conjugation between the rabbit anti-dopamine polyclonal antibody and goat anti-rabbit antibody acted as primary antibody and secondary antibody, respectively. From Fig. 2.24, the increase of the antigen-antibody reaction of dopamine induced the enhancement of the process in 30 min. This implied that the reaction of antigen-antibody was carried out in the short range of the time.

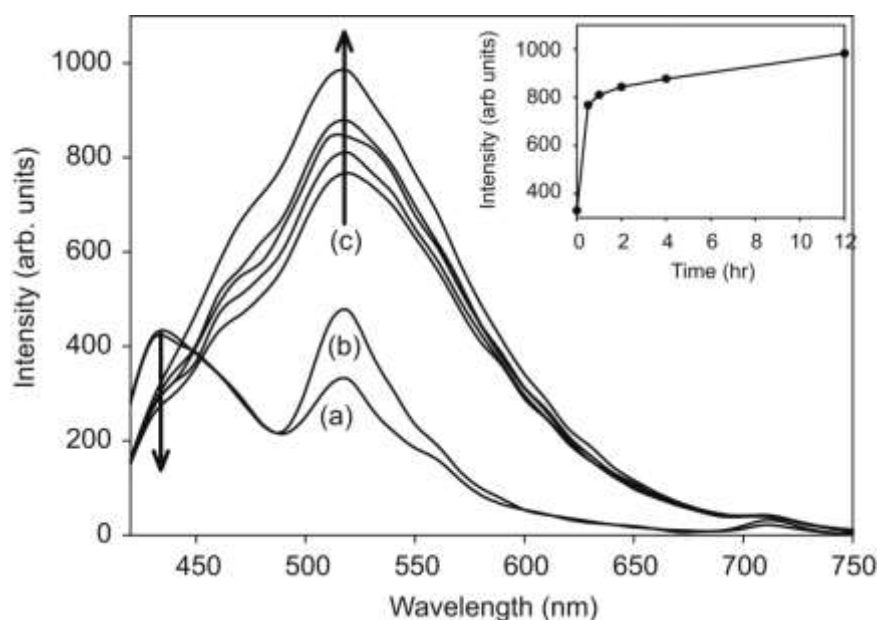


**Figure 2.24** ELISA data of FRET mechanism of polyamidoamine (PAMAM) dendrimer (G5)-CdS with AlexaFluor 488-conjugated antibody: (a) dendrimer-QD and AlexaFluor 488 antibody conjugation, (b) dendrimer-QD secondary antibody and primary antibody conjugation and (c) the effect of 10 mM of anti-dopamine-dopamine conjugation on time period shows (30 min – 12 h), Inset shows change of fluorescence intensity at 520 nm.

Furthermore, Fig. 2.25 displayed the fluorescence enhancement of AlexaFluor 488 or FRET process as a function of the dopamine concentration. FRET efficiency of this system is 0.96.

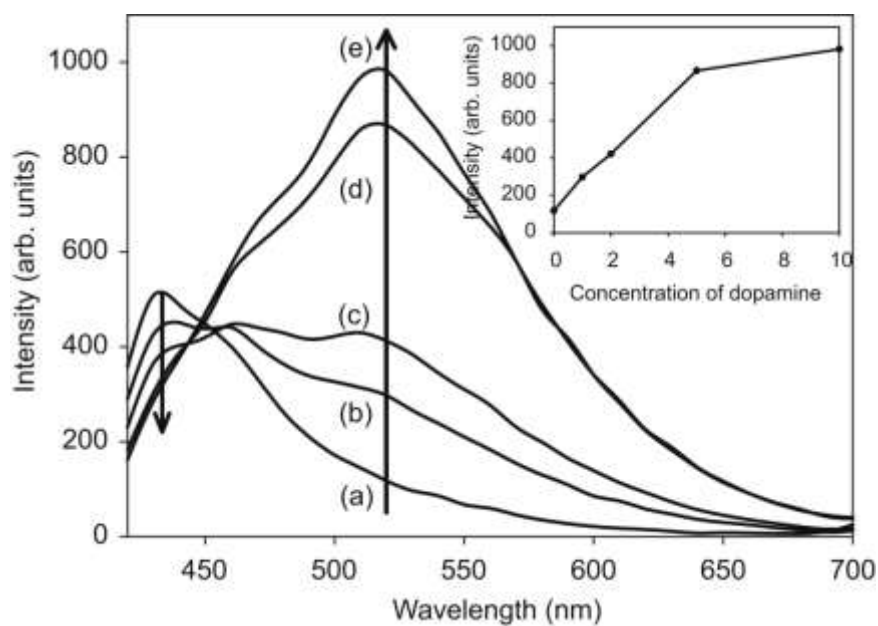


**Figure 2.25** Fluorescent intensity change under FRET process between dendrimer-QD and AlexaFluor 488-conjugated antibody: (a) 0, (b) 1, (c) 2, (d) 5, and (e) 10 mM, Inset shows the change of emission intensity of dendrimer-QD with various dopamine concentration at 520 nm.



## 2.2 Objectives and scope of this research

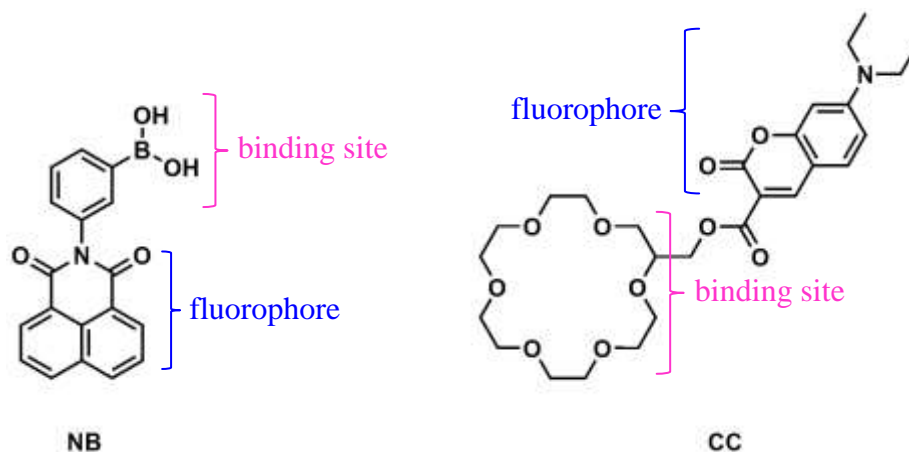


**Figure 2.26** Structure of fluorescence chemosensors **NB** and **CC**

The goal of our research is to develop fluorescence chemosensors for determination of catecholamine neurotransmitter in biological system. We attempt to discriminate each catecholamine derivatives. This approach is beneficial for pre-diagnosis of central nervous system disease and for study of enzymatic process in catecholamine biosynthesis [75]. Therefore, two fluorescence chemosensors **NB** and **CC** were designed and synthesized in this research. As shown in Fig. 2.26, The sensor **NB** contains boronic acid as a binding unit to covalently bond with catechol unit and naphthalimide group as a fluorophore. New sensor **CC** was designed based on crown ether and coumarin acting as binding site and fluorophore moiety, respectively.

The sensing properties of these sensors toward biogenic amines were investigated in 10% DMSO:phosphate buffer pH 7.4 by fluorescence spectrophotometry and mass spectroscopy. For our purpose this concept, the catecholamines function as a linker analyte between sensor **NB** act as FRET donor and sensor **CC** act as FRET acceptor under fluorescence resonance energy transfer (FRET) mechanism. Furthermore, the PCA analysis is utilized for classification of biogenic amine analytes by fluorescence spectral data. Additionally, we also applied this conceptually sensing purpose in real biological systems of human urine samples.

## CHAPTER III

### EXPERIMENTAL SECTION

#### 3.1 General procedures

##### 3.1.1 Analytical instrument

Nuclear Magnetic Resonance (NMR) spectra were recorded on a Varian Mercury Plus 400 and Bruker DRX 400 MHz nuclear magnetic resonance spectrometer. The chemical shifts were reported in part per million (ppm) using the residual proton or carbon signal in deuterated solvents as internal reference. Elemental analysis was carried out on CHONS/O analyzer (Perkin Elmers PE 2400 series II) by ignition combustion gas chromatography separated by frontal analysis and qualitative detected by thermal conductivity detector. MALDI-TOF mass spectra were carried out on Bruker Daltonics MALDI-TOF by using  $\alpha$ -hydroxy cyanocinnamic acid (CCA) as a matrix. All fluorescence spectra were measured by a Varian Cary Eclipse Probe fluorescence spectrophotometer by personal computer data processing unit. The light source is Cary Eclipse a pulsed xenon lamp and a detector is a photomultiplier tube.

##### 3.1.2 Materials

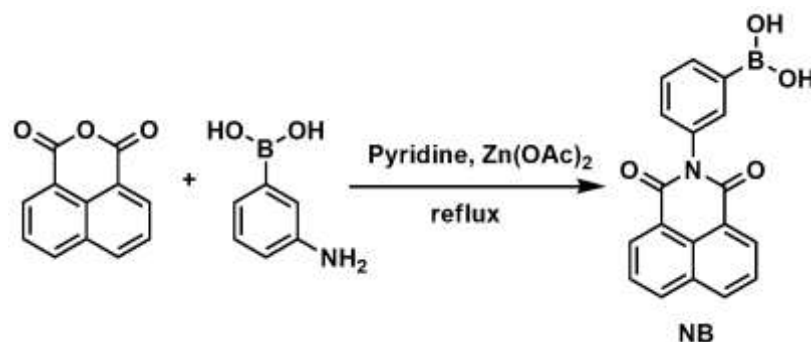
All materials and solvents were purchased from Aldrich, Fluka, Merck and TCI as standard analytical grade and used without further purification. Commercial grade solvents such as acetone, dichloromethane, methanol and ethanol were purified by distillation before using. Thin-layer chromatography (TLC) was performed on silica and alumina gel plates (Kieselgel 60 F<sub>254</sub>, 1mm, Merck). Dimethyl sulfoxide as AR grade used in fluorescence measurement was used without drying.

In this research, we synthesized the 6 sensors including sensor **NB**, sensor **DC**, sensor ***m*-BA**, sensor **L2-Zn**, sensor ***o*-AB** and sensor **CC** for complexation study toward biogenic amines.

## 3.2 Synthesis

### 3.2.1 Synthesis of boronic/naphthalimide based sensor

#### 3.2.1.1 Preparation of *N*-(1,8-Naphthaloyl)-3-aminophenylboronic acid (NB)



Into a two-neck round bottom flask equipped with a magnetic bar and a Dean-Stark equipment to remove water, corresponding 3-aminophenylboronic acid hemisulfate (0.225 g, 1.21 mmol), 1,8-naphthalene dicarboxylic acid anhydride (0.2 g, 1.01 mmol), molecular sieves, and of zinc acetate (30 mg, 0.14 mmol) were stirred in 20 mL of pyridine under nitrogen atmosphere. The reaction mixture was refluxed for 12 hours. Pyridine was removed by a rotary evaporator and replaced with dichloromethane. The crude product was purified by precipitation with methanol. The precipitate was filtered and washed with methanol and dichloromethane to obtain a cream color solid **NB** in 56% yield.

#### Characterization data for sensor **NB**

**<sup>1</sup>H-NMR (400 MHz, DMSO-*d*<sub>6</sub>):**  $\delta$  (in ppm) = 8.48 (d,  $J$  = 6.4 Hz, 3H, ArH), 8.15 (s, 2H, BOH), 7.88 (t,  $J$  = 6.4 Hz 3H, ArH), 7.69 (s, 1H, ArH), 7.48 (t,  $J$  = 5.6 Hz, 1H, ArH), 7.42 (d,  $J$  = 6.0 Hz, 1H, ArH)

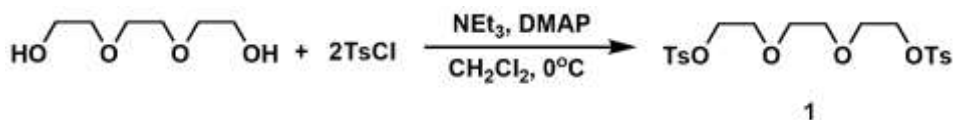
**<sup>13</sup>C-NMR (400 MHz, DMSO-*d*<sub>6</sub>):**  $\delta$  (in ppm) = 163.71, 135.29, 134.46, 133.83, 131.46, 130.75, 130.69, 128.01, 127.83, 127.24, 122.55

**MALDI-TOF mass:** Anal. Calcd for [C<sub>18</sub>H<sub>12</sub>BNO<sub>4</sub>]<sup>+</sup>  $m/z$  = 317.09

Found  $m/z$  = 317.38 [M]<sup>+</sup>

### 3.2.2 Synthesis of diazacrown ether/dansyl based sensor

#### 3.2.2.1 Preparation of 2,2'-(ethane-1,2-diylbis(oxy))bis(ethane-2,1-diyl) bis(4-methylbenzenesulfonate) (**1**)



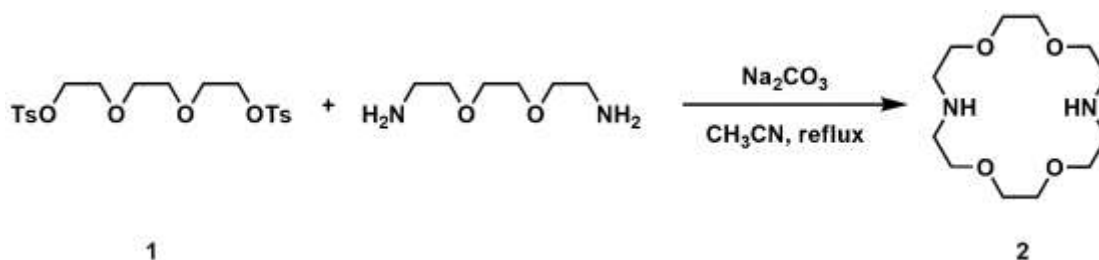
Into a two-neck round bottom flask equipped with a magnetic bar, a solution of triethylene glycol (8.00 g, 52 mmol), DMAP and triethylamine (21.74 mL, 156 mmol) was stirred in 50 mL of dry dichloromethane at room temperature for 30 min under nitrogen atmosphere. The solution of tosylchloride (20.00 g, 104 mmol) in 40 mL of dichloromethane was added into the reaction mixture at 0°C and stirred at room temperature for 24 hours. After reaction completed, the reaction mixture was treated with 3M HCl and extracted with dichloromethane. The organic layer was dried over anhydrous sodium sulfate and evaporated to dryness in vacuum. The residue was precipitated in dichloromethane and methanol to afford a white solid **1** in 69% yield.

#### Characterization data for **1**

**<sup>1</sup>H-NMR (400 MHz, CDCl<sub>3</sub>):** δ (in ppm) = 7.79 (d, *J* = 8.4 Hz, 2H, Ar*H*), 7.34 (d, *J* = 8.0 Hz, 2H, Ar*H*), 4.13 (t, *J* = 4.6 Hz, 2H, OCH<sub>2</sub>), 3.65 (t, *J* = 4.8 Hz, 2H, OCH<sub>2</sub>), 3.53 (s, 2H, OCH<sub>2</sub>), 2.44 (s, 3H, ArCH<sub>3</sub>)

**<sup>13</sup>C-NMR (400 MHz, CDCl<sub>3</sub>):** δ (in ppm) = 144.82, 133.11, 129.83, 127.95, 70.70, 69.17, 68.76, 21.60

### 3.2.2.2 Preparation of 1,4,10,13-tetraoxa-7,16-diazacyclooctadecane (2)



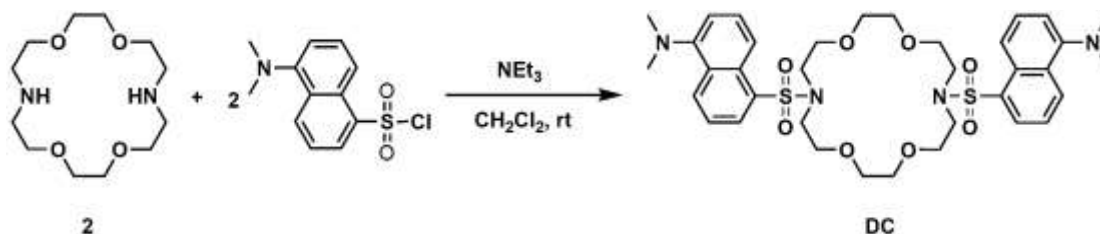
Into a two-neck round bottom flask equipped with a magnetic bar, a solution of ethylenedioxyamine (2.95 mL, 20.12 mmol) and sodium carbonate (20.35 g, 192 mmol) in 100 mL acetonitrile was stirred at room temperature for 30 min under nitrogen atmosphere. A solution of compound **1** (8.85 g, 19.3 mmol) in 25 mL acetonitrile was added dropwise into the reaction mixture which was further refluxed for 3 day. Sodium carbonate was filtered off and the solvent was removed under vacuum. The crude product was purified by column chromatography on alumina with 500 mL of 10% EtOH:THF to obtain a white solid **2** in 40% yield.

#### Characterization data for **2**

**<sup>1</sup>H-NMR (400 MHz, CDCl<sub>3</sub>):**  $\delta$  (in ppm) = 3.55 (t,  $J$  = 4.6 Hz, 16H, OCH<sub>2</sub>), 2.76 (t,  $J$  = 6.0 Hz, 8H, NCH<sub>2</sub>), 2.32 (s, 2H, CH<sub>2</sub>NH)

**<sup>13</sup>C-NMR (400 MHz, CDCl<sub>3</sub>):**  $\delta$  (in ppm) = 70.89, 70.69, 70.37, 70.32, 70.29, 70.21, 70.09, 69.85, 69.79, 49.32, 49.23, 21.14

### 3.2.2.3 Preparation of Dansyl azacrown (DC)



Compound **2** (0.300 g, 1.14 mmol) was dissolved in 30 mL of dichloromethane, followed by addition of triethylamine (3.19 mL, 22.88 mmol). The reaction mixture was stirred at room temperature for 30 min. The solution of dansyl chloride (0.679 g, 2.52 mmol) in dichloromethane was added to the reaction. The reaction mixture was stirred at room temperature for 24 h. The solvent was removed under vacuum to give the crude product which was purified by precipitation with  $\text{CH}_2\text{Cl}_2/\text{MeOH}$  to obtain a white solid **DC** in 45% yield.

#### Characterization data for sensor DC

**$^1\text{H-NMR}$  (400 MHz,  $\text{CDCl}_3$ ):**  $\delta$  (in ppm) = 8.51 (d,  $J = 8.0$  Hz, 2H, ArH), 8.28 (d,  $J = 8.4$  Hz, 2H, ArH), 8.13 (d,  $J = 7.6$  Hz, 2H, ArH), 7.51 (m, 4H, ArH), 7.16 (d,  $J = 7.2$  Hz, 2H, ArH), 3.60 (s, 16H,  $\text{OCH}_2$ ), 3.49 (s, 8H,  $\text{NCH}_2$ ), 2.87 (s, 12H,  $\text{NCH}_3$ )

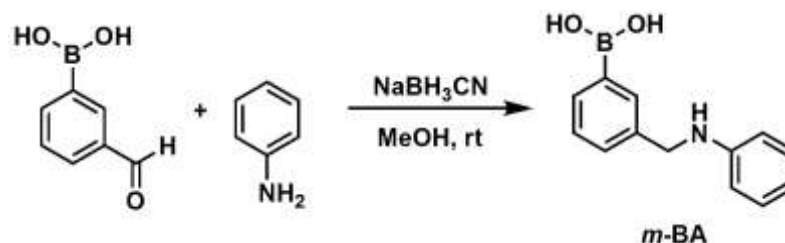
**$^{13}\text{C-NMR}$  (400 MHz,  $\text{CDCl}_3$ ):**  $\delta$  (in ppm) = 151.74, 135.43, 130.17, 130.12, 128.79, 123.13, 119.60, 115.23

**MALDI-TOF mass:** Anal. Calcd for  $[\text{C}_{36}\text{H}_{48}\text{N}_4\text{O}_8\text{S}_2]^+$   $m/z = 728.29$

Found  $m/z = 729.34$   $[\text{M} + \text{H}]^+$

### 3.2.3 Synthesis of boronic/amino phenyl based sensor

#### 3.2.3.1 Preparation of 3-((phenylamino)methyl)phenylboronic acid (*m*-BA)



Into a two-neck round bottom flask equipped with a magnetic bar, 3-formyl phenyl boronic acid (0.15 g, 1 mmol), aniline (0.09 mL, 1 mmol) and sodium cyanoborohydride (1.24 g, 2 mmol) were dissolved in methanol (10 mL). The reaction mixture was stirred at room temperature for 24 hours under nitrogen atmosphere. Methanol was removed by a rotary vacuum evaporator. After that, the crude product was purified by column chromatography on silica with 20% EtOAc/CH<sub>2</sub>Cl<sub>2</sub> to obtain a white solid *m*-BA in 74% yield.

#### Characterization data for sensor *m*-BA

**<sup>1</sup>H-NMR (400 MHz, CH<sub>3</sub>OD):** δ (in ppm) = 7.75 (s, 1H, ArH), 7.61 (m, 1H, ArH), 7.40 (d, 1H, *J* = 7.6 Hz, ArH), 7.28 (d, 1H, *J* = 8.0 Hz, ArH), 7.05 (t, 2H, *J* = 7.8 Hz, ArH), 6.59 (m, 3H, ArH), 4.63 (s, 1H, NH), 4.28 (s, 2H, CH<sub>2</sub>)

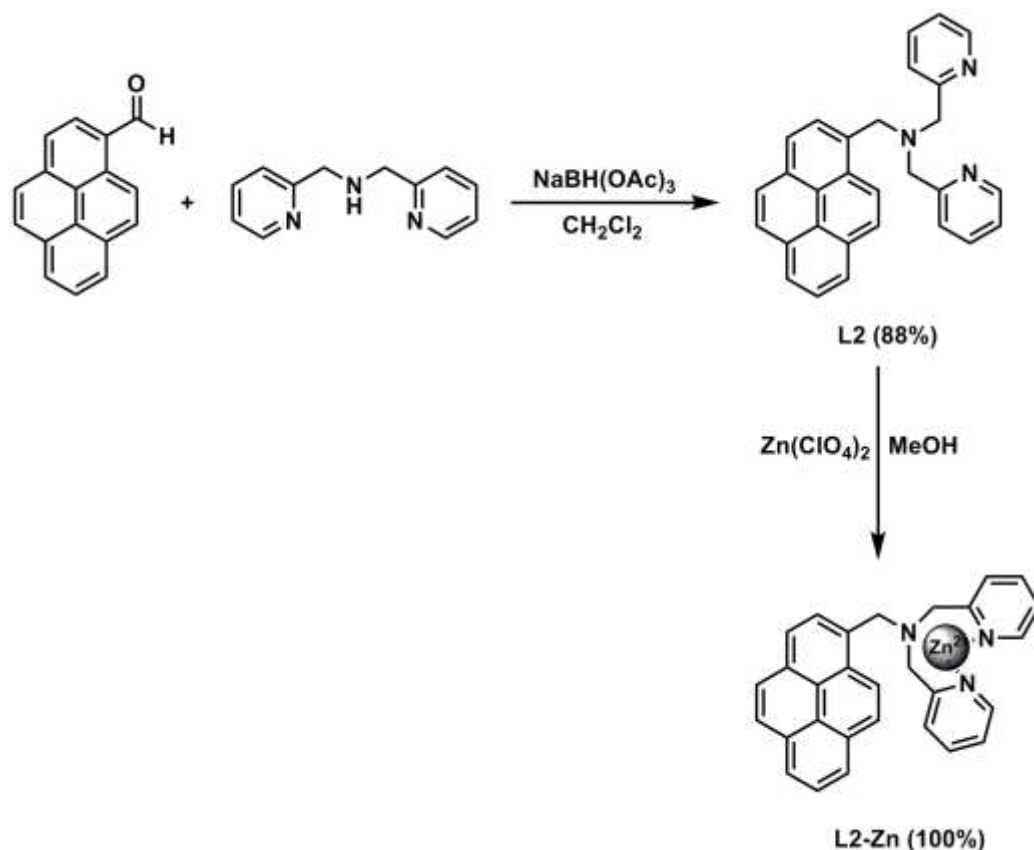
**<sup>13</sup>C-NMR (400 MHz, CH<sub>3</sub>OD):** δ (in ppm) = 150.07, 140.38, 134.01, 130.44, 129.45, 128.42, 117.85, 113.98, 48.48

**MALDI-TOF mass:** Anal. Calcd for [C<sub>13</sub>H<sub>14</sub>BNO<sub>2</sub>]<sup>+</sup> *m/z* = 227.11

Found *m/z* = 227.29 [M]<sup>+</sup>

### 3.2.4 Synthesis of picolyl amine/pyrene based sensor

#### 3.2.4.1 Preparation of sensor L2-Zn [76]



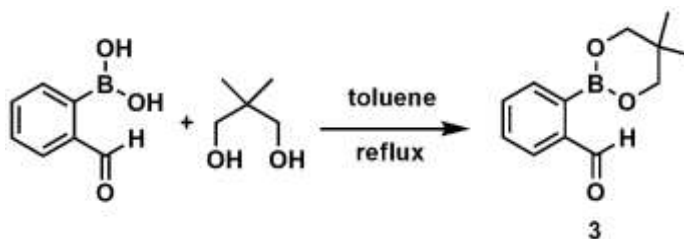
Into a two-neck round bottom flask equipped with a magnetic bar, sodium tris(acetoxo)borohydride (0.28 g, 1.32 mmol), pyrenecarboxaldehyde (0.23 g, 1 mmol) and dipicolylamine (0.20 g, 1 mmol) in 10 mL  $\text{CH}_2\text{Cl}_2$  were stirred under nitrogen atmosphere at room temperature for 5 h. The reaction mixture was neutralized with sodium hydrogen carbonate and extracted with  $\text{CH}_2\text{Cl}_2$  and then the solvent was evaporated under vacuum. The residue was purified by column chromatography on silica gel with 5% MeOH in dichloromethane as eluent to afford a yellow oil which ultimately solidifies when dry (0.36 g, 88%).

Into a two-neck round bottom flask equipped with a magnetic bar, a solution of  $\text{Zn(ClO}_4)_2$  in 5 mL MeOH (0.171 g, 0.47 mmol) was added dropwise into a solution of **L2** (0.112 g, 0.27 mmol) in 5 mL MeOH. Upon stirring overnight at room temperature, the precipitate was filtered and washed with MeOH to give **L2-Zn** (0.21 g, 100%) as a light yellow powder.



### 3.2.5 Synthesis of boronic/anthraquinone based sensor

#### 3.2.5.1 Preparation of 2-(5,5-dimethyl-1,3,2-dioxaborinan-2-yl)benzaldehyde (**3**)



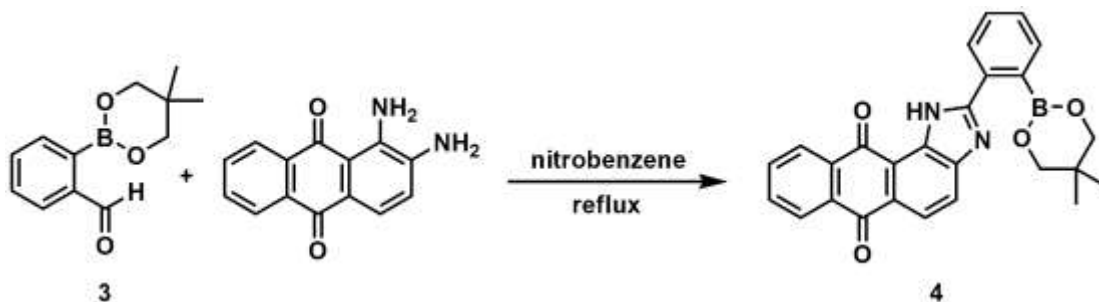
Into a two-neck round bottom flask equipped with a magnetic bar and a Dean-Stark equipment to remove water, 2-formyl phenylboronic acid (0.300 g, 2 mmol), 1,2-propanediol (0.208 g, 2 mmol) and molecular sieves were mixed in toluene (50 mL). The reaction mixture was refluxed for overnight under nitrogen atmosphere. Then, molecular sieves in solution were filtered and the solvent was removed under vacuum to obtain a white solid **3** in quantitative yield.

#### Characterization data for **3**

**<sup>1</sup>H-NMR (400 MHz, CDCl<sub>3</sub>):**  $\delta$  (in ppm) = 10.45 (s, 1H, CHO), 7.89 (d, 1H, *ArH*),  $J = 7.6$  Hz, 7.79 (d, 1H,  $J = 7.2$  Hz, *ArH*), 7.52 (m, 2H, *ArH*), 3.79 (s, 4H, OCH<sub>2</sub>), 1.05 (s, 6H, C(CH<sub>3</sub>)<sub>2</sub>)

**<sup>13</sup>C-NMR (400 MHz, CDCl<sub>3</sub>):**  $\delta$  (in ppm) = 194.84, 134.35, 132.90, 129.92, 128.26, 72.54, 21.90

### 3.2.5.2 Preparation of 2-(2-(5,5-dimethyl-1,3,2-dioxaborinan-2-yl)phenyl)-1H-anthra[1,2-d]imidazole-6,11-dione (4)



Into a two-neck round bottom flask equipped with a magnetic bar, the corresponding 2-formyl phenylboronate ester **3** (0.231 g, 1.06 mmol) in nitrobenzene (5 mL) was added dropwise to a solution of 1,2-diamino-1,4-anthraquinone (0.253 g, 1.06 mmol) in nitrobenzene (15 mL). The reaction mixture was slowly heated up to 150°C for 24 hours under nitrogen atmosphere. The solution was cooled to room temperature and the residue was precipitated with hexane to afford a brown solid **4** in 47% yield.

#### Characterization data for 4

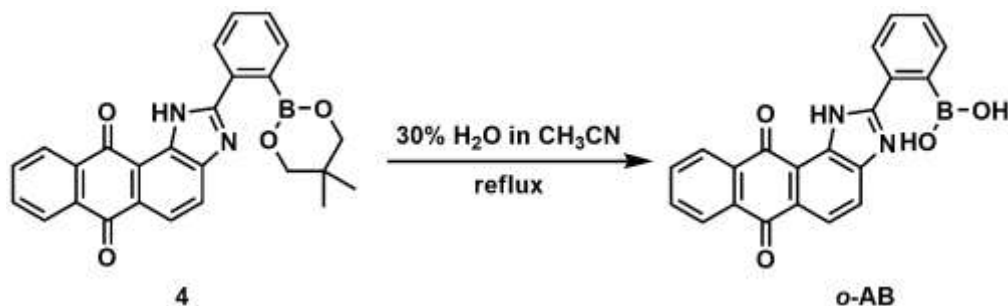
**<sup>1</sup>H-NMR (400 MHz, DMSO-*d*<sub>6</sub>):**  $\delta$  (in ppm) = 13.70 (s, 1H, *NH*), 8.69 (d,  $J = 7.4$  Hz, 1H, *ArH*), 8.35 (d,  $J = 7.2$  Hz, 1H, *ArH*), 8.20 (s, 2H, *OH*), 8.18-8.01 (m, 4H, *ArH*), 7.90-7.83 (m, 3H, *ArH*), 7.49 (t,  $J = 7.5$  Hz, 1H, *ArH*)

**<sup>13</sup>C-NMR (400 MHz, DMSO-*d*<sub>6</sub>):**  $\delta$  (in ppm) = 182.29, 134.47, 134.26, 133.14, 132.12, 131.46, 130.09, 128.60, 127.80, 126.78, 126.22, 124.40, 121.29, 71.70, 21.86

**MALDI-TOF mass:** Anal. Calcd for [C<sub>26</sub>H<sub>21</sub>BN<sub>2</sub>O<sub>4</sub>]<sup>+</sup>  $m/z = 436.16$

Found  $m/z = 436.48$

### 3.2.5.3 Preparation of 2-(6,11-dioxo-6,11-dihydro-1H-anthra[1,2-d]imidazol-2-yl)phenylboronic acid (*o*-AB)



The protecting group of **4** (1.06 mmol) was removed by refluxing in 10 mL of 30% H<sub>2</sub>O:CH<sub>3</sub>CN. The precipitate was filtered and washed with diethylether to give a yellow solid ***o*-AB** in the quantitative yield.

#### Characterization data for sensor *o*-AB

<sup>1</sup>H-NMR (400 MHz, DMSO-*d*<sub>6</sub>): δ (in ppm) = 13.76 (s, 1H, NH), 13.34 (s, 1H, ArH-N), 8.72 (d, *J* = 7.6 Hz, 1H, ArH), 8.39 (d, *J* = 7.1 Hz, 1H, ArH), 8.25 (s, 2H, OH), 8.20-8.03 (m, 4H, ArH), 7.80-7.95 (m, 3H, ArH), 7.56 (t, *J* = 7.6 Hz, 1H, ArH)

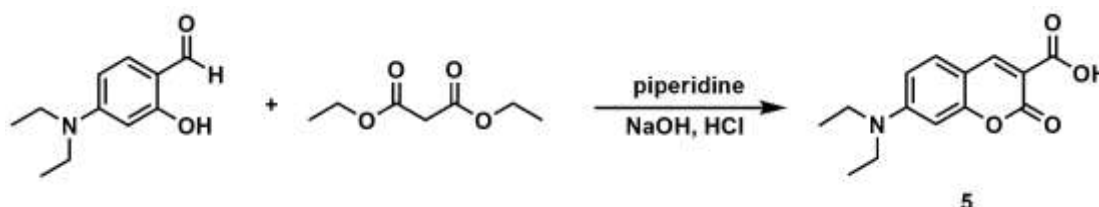
<sup>13</sup>C-NMR (400 MHz, DMSO-*d*<sub>6</sub>): δ (in ppm) = 181.46, 134.52, 134.33, 132.14, 132.78, 131.12, 129.10, 128.56, 128.05, 127.78, 126.30, 124.23, 121.34

**MALDI-TOF mass:** Anal. Calcd for [C<sub>21</sub>H<sub>13</sub>BN<sub>2</sub>O<sub>4</sub>]<sup>+</sup> *m/z* = 368.10

Found *m/z* = 493.47 [M + C<sub>6</sub>H<sub>5</sub>NO<sub>2</sub> + 2H]<sup>+</sup>

### 3.2.6 Synthesis of crown ether/coumarin based sensor

#### 3.2.6.1 Preparation of 7-diethylamino-2-oxo-2H-chromen-3-carboxylic acid (**5**)



Into a two-neck round bottom flask equipped with a magnetic bar, 4-diethylaminosalicylaldehyde (0.386 g, 2 mmol), diethylmalonate (0.61 mL, 4 mmol), and piperidine (0.2 mL) were dissolved in absolute ethanol (6 mL). The reaction mixture was stirred and refluxed for 6 hours under nitrogen atmosphere. Then 10% NaOH (6 mL) solution was added to the reaction and refluxed for 15 min. The solution was cooled to room temperature and acidified to pH 2 using concentrated hydrochloric acid at 0°C affording a precipitate deposit which was filtered out, washed with water, then recrystallized with ethanol to give an orange crystal (**5**, 74%).

#### Characterization data for **5**

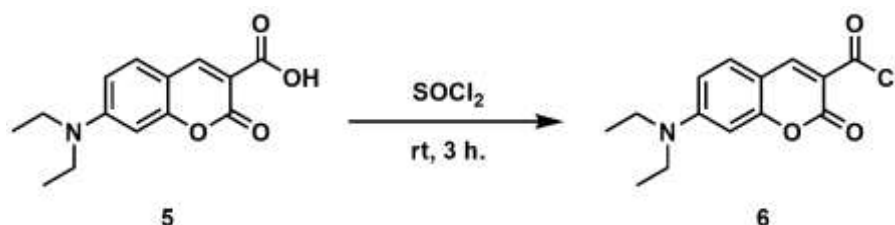
**<sup>1</sup>H-NMR (400 MHz, CDCl<sub>3</sub>):**  $\delta$  (in ppm) = 12.37 (s, 1H, COOH), 8.67 (s, 1H, ArH), 7.46 (d,  $J = 9.2$  Hz, 1H, ArH), 6.71 (dd,  $J = 4.27$  Hz, 1H, ArH), 6.53 (d,  $J = 2.0$  Hz, 1H, ArH), 3.49 (q,  $J = 7.07$  Hz, 4H, CH<sub>2</sub>CH<sub>3</sub>), 1.26 (t,  $J = 7.2$  Hz, 6H, CH<sub>2</sub>CH<sub>3</sub>)

**<sup>13</sup>C-NMR (400 MHz, CDCl<sub>3</sub>):**  $\delta$  (in ppm) = 165.52, 164.42, 158.07, 153.78, 150.27, 131.94, 110.91, 108.59, 105.70, 96.89, 45.34, 12.39

**MALDI-TOF mass:** Anal. Calcd for [C<sub>14</sub>H<sub>15</sub>NO<sub>4</sub>]<sup>+</sup>  $m/z = 261.10$

Found  $m/z = 261.32$

### 3.2.6.2 Preparation of 7-diethylamino-2-oxo-2H-chromen-3-carboxylic chloride (6)



Into a two-neck round bottom flask equipped with a magnetic bar, **5** (0.187 g, 0.7 mmol) was added to dry thionyl chloride (3 mL) and the suspension was stirred at room temperature for 3 hours under nitrogen atmosphere. The precipitate was washed with dichloromethane under vacuum to give a yellow solid **6** in a quantitative yield.

#### Characterization data for **6**

<sup>1</sup>H-NMR (400 MHz, CDCl<sub>3</sub>): δ (in ppm) = 8.68 (s, 1H, ArH), 7.49 (d, *J* = 4.4 Hz, 1H, ArH), 6.76 (m, 1H, ArH), 6.59 (s, 1H, CCH), 3.50 (q, *J* = 6.9 Hz, 4H, CH<sub>2</sub>CH<sub>3</sub>), 1.28 (t, *J* = 3.4 Hz, 6H, CH<sub>2</sub>CH<sub>3</sub>)



**MALDI-TOF mass:** Anal. Calcd for  $[\text{C}_{27}\text{H}_{39}\text{NO}_{10}]^+$   $m/z = 537.26$

Found  $m/z = 537.89$   $[\text{M}]^+$

**ESI-HRMS:** Anal. Calcd for  $[\text{C}_{27}\text{H}_{39}\text{NO}_{10} + \text{H}]^+$   $m/z = 538.2647$

Found  $m/z = 538.2676$

Anal. Calcd for  $[\text{C}_{27}\text{H}_{39}\text{NO}_{10} + \text{Na}]^+$   $m/z = 560.2466$

Found  $m/z = 560.2514$

Anal. Calcd for  $[\text{C}_{27}\text{H}_{39}\text{NO}_{10} + \text{K}]^+$   $m/z = 576.2206$

Found  $m/z = 576.2254$

**Elemental Analysis:** Anal. Calcd. For  $\text{C}_{27}\text{H}_{39}\text{NO}_{10}$ : C, 60.32; H, 7.31; N, 2.61

Found: C, 60.21; H, 7.47; N, 2.42

**IR spectrum (ATR ( $\text{cm}^{-1}$ )):** 2864.21 (C-H stretch)  $\text{cm}^{-1}$ , 1751.66 (C=O stretch in ester)  $\text{cm}^{-1}$ , 1615.50-1505.90 (C-C stretches in aromatic ring)  $\text{cm}^{-1}$ , 1213.65 (C-N stretch)  $\text{cm}^{-1}$ , 1100.74 (C-O stretch)  $\text{cm}^{-1}$

### 3.3 Complexation studies

#### 3.3.1 Complexation studies of sensor **NB** and sensor **DC** with **DA** by fluorescence spectrophotometry technique

Initially, the solution of  $1 \times 10^{-5}$  M of sensor **NB** and sensor **DC** were prepared in DMSO. A stock solution of  $1 \times 10^{-3}$  M of **DA** in 0.01 M phosphate buffer pH 7.4 was prepared in the volumetric flasks. The solution of **DA** was added directly to 2.00 mL of  $1 \times 10^{-5}$  M of sensor **NB** in 10% DMSO:phosphate buffer of a 1-cm quartz cuvette by micropipette and stirred for 5 min. Next, the mixture solution was stirred for 10 min after adding  $1 \times 10^{-5}$  M solution of sensor **DC** in a quartz cuvette. Fluorescence spectra were measured under the following condition:

*Start: 350 nm*

*End: 800 nm*

*Excitation: 340 nm*

*Excitation slit: 5.0*

*Emission slit: 5.0*

#### 3.3.2 Complexation studies of sensor **m-BA** and sensor **L2-Zn** with **DA** by fluorescence spectrophotometry technique

Typically, the solution of  $1 \times 10^{-4}$  M of sensor **m-BA** and sensor **L2-Zn** were prepared in methanol. A stock solution of  $1 \times 10^{-3}$  M of **DA** in 0.01 M phosphate buffer pH 8.2 was prepared in the volumetric flasks. The solution of **DA** was added directly to 2.00 mL of  $1 \times 10^{-5}$  M of sensor **m-BA** in 50% MeOH:phosphate buffer (0.01 M, pH 8.2) of a 1-cm quartz cuvette by micropipette and stirred for 5 min. Then,  $1 \times 10^{-5}$  M solution of sensor **L2-Zn** was added in the same quartz cuvette. Fluorescence spectra were measured under the following condition:



*Start: 300 nm*

*End: 800 nm*

*Excitation: 290 nm*

*Excitation slit: 5.0*

*Emission slit: 5.0*

### **3.3.3 Complexation studies of sensor **L2-Zn** and sensor **o-AB** with **DA** by fluorescence spectrophotometry technique**

Typically,  $1 \times 10^{-3}$  M of sensor **L2-Zn** and sensor **o-AB** were prepared in DMSO. A stock solution of 0.01 M of **DA** in 0.01 M phosphate buffer pH 7.4 was prepared in the volumetric flasks. The solution of **DA** was added directly to 2.00 mL of  $1 \times 10^{-5}$  M of sensor **o-AB** in a 1-cm quartz cuvette by micropipette and stirred for 5 min. After that,  $1 \times 10^{-5}$  M solution of sensor **L2-Zn** was added in the same quartz cuvette and stirred for 10 min. Fluorescence spectra were monitored under the following condition:

*Start: 350 nm*

*End: 800 nm*

*Excitation: 340 nm*

*Excitation slit: 5.0*

*Emission slit: 5.0*

### 3.3.4 Complexation studies of sensor **NB** with various guests by fluorescence spectrophotometry technique

Typically, a stock solution of  $1 \times 10^{-4}$  M solution of sensor **NB** in DMSO was prepared. A stock solution of  $2 \times 10^{-3}$  M of various guests including dopamine (**DA**), norepinephrine (**NE**), epinephrine (**EPI**), tyramine (**TY**), L-glutamic acid (**Glu**), L-lysine (**Lys**), histidine (**His**) and histamine (**Hist**) in 0.01 M phosphate buffer pH 7.4 were prepared in the volumetric flasks as shown in Table 3.1. The solution of various guests was added directly to 2.00 mL of  $1 \times 10^{-5}$  M of sensor **NB** in a 1-cm quartz cuvette by micropipette and stirred for 5 min. The fluorescence spectra were recorded after each addition as listed in Table 3.2 under the following condition:

*Start: 350 nm*

*End: 800 nm*

*Excitation: 340 nm*

*Excitation slit: 5.0*

*Emission slit: 5.0*

**Table 3.1** Amounts of guests used for studies of fluorescence spectrophotometry technique.

Guest	Molecular weight ( $\text{gmol}^{-1}$ )	Weight (mg)	Volume (mL)
<b>DA</b>	189.64	0.76	2
<b>NE</b>	205.64	0.82	2
<b>EPI</b>	183.20	0.73	2
<b>TY</b>	137.18	0.55	2

Guest	Molecular weight ( $\text{g mol}^{-1}$ )	Weight (mg)	Volume (mL)
<b>Glu</b>	147.13	0.59	2
<b>Lys</b>	146.19	0.58	2
<b>His</b>	155.16	0.62	2
<b>Hist</b>	111.15	0.44	2

**Table 3.2** Amounts of guests used for studies of fluorescence spectrophotometry technique.

Guest	[Guest] (M)	Guest added ( $\mu\text{L}$ )	Guest:NB ratios
<b>DA</b>	$2 \times 10^{-3}$	500	100:1
<b>NE</b>	$2 \times 10^{-3}$	500	100:1
<b>EPI</b>	$2 \times 10^{-3}$	500	100:1
<b>TY</b>	$2 \times 10^{-3}$	500	100:1
<b>Glu</b>	$2 \times 10^{-3}$	500	100:1
<b>Lys</b>	$2 \times 10^{-3}$	500	100:1
<b>His</b>	$2 \times 10^{-3}$	500	100:1
<b>Hist</b>	$2 \times 10^{-3}$	500	100:1

### 3.3.5 Fluorescence image of sensor **NB** with various guests

Generally, a stock solution of  $5 \times 10^{-4}$  M was prepared in 1 mL of DMSO. A stock solution of  $1 \times 10^{-2}$  M of various guests including **DA**, **NE**, **EPI**, **TY**, **Glu**, **Lys**, **His** and **Hist** in 0.1 M phosphate buffer pH 7.4 was prepared in the volumetric flask as shown in Table 3.3. The solution of various guests was added directly to 2.00 mL of  $5 \times 10^{-5}$  M of sensor **NB** in each vial by micropipette and stirred for 5 min. Then, the mixture solutions were exposed under the black light.

**Table 3.3** The amount ratio of guest and sensor **NB** used for study the fluorescence image.

Vial	Guest	V <sub>Guest</sub> (mL)	V <sub>NB</sub> (mL)	Guest: <b>NB</b> ratios
1	-	0.00	0.20	100:1
2	<b>DA</b>	1.00	0.20	100:1
3	<b>NE</b>	1.00	0.20	100:1
4	<b>EPI</b>	1.00	0.20	100:1
5	<b>TY</b>	1.00	0.20	100:1
6	<b>Glu</b>	1.00	0.20	100:1
7	<b>Lys</b>	1.00	0.20	100:1
8	<b>His</b>	1.00	0.20	100:1
9	<b>Hist</b>	1.00	0.20	100:1

### 3.3.6 Job's plot studies of NB with DA, NE and EPI

Typically, the stock solution of sensor **NB** and catecholamine guests was prepared in 10% DMSO:phosphate buffer (0.01M, pH 7.4) at concentration of  $1 \times 10^{-5}$  M in 5 mL volumetric flask.

The portion of sensor **NB** solution was mixed with portions of the stock solution of catecholamine guests to give the final concentration of guests according to Table 3.4. The mixture was kept stirring at room temperature for 5 min and then the fluorescence spectra of complex were recorded from 350-800 nm upon the excitation at 340 nm at ambient temperature.

**Table 3.4** Mole fraction and volume of sensor **NB** ( $1 \times 10^{-5}$  M) and catecholamine guests ( $1 \times 10^{-5}$  M) for Job's plot experiment.

Sample	Mole fraction of <b>NB</b>	Mole fraction of guest	V of <b>NB</b> (mL)	V of guest (mL)
1	1.0	0.0	2.00	0.00
2	0.9	0.1	1.80	0.20
3	0.8	0.2	1.60	0.40
4	0.7	0.3	1.40	0.60
5	0.6	0.4	1.20	0.80
6	0.5	0.5	1.00	1.00
7	0.4	0.6	0.80	1.20
8	0.3	0.7	0.60	1.40
9	0.2	0.8	0.40	1.60
10	0.1	0.9	0.20	1.80
11	0.0	1.0	0.00	2.00

### 3.3.7 Complexation studies of sensor **NB** with **DA**, **NE** and **EPI** by fluorescence spectrophotometric titration technique

A stock solution of  $1 \times 10^{-4}$  M of sensor **NB** in DMSO was prepared. The stock solution of  $2 \times 10^{-3}$  M of guests including **DA**, **NE** and **EPI** in 0.01 M phosphate buffer pH 7.4 was prepared in the volumetric flasks. The solution of guests was added directly to 2.00 mL of  $1 \times 10^{-5}$  M of sensor **NB** in a 1-cm quartz cuvette by micropipette and stirred for 5 min. The fluorescence spectra were recorded after each addition as listed in Table 3.5, 3.6 and 3.7 under the following condition:

*Start: 350 nm*

*End: 800 nm*

*Excitation: 340 nm*

*Excitation slit: 5.0*

*Emission slit: 5.0*

**Table 3.5** The concentration of **DA** used for complexation studies with sensor **NB** and the ratios of **NB:DA**.

Entry	DA/NB	[NB] (M)	[DA] (M)	V of DA (mL)	V total (mL)
1	0	$1.00 \times 10^{-5}$	0.00	0.000	2.000
2	0.2	$9.99 \times 10^{-6}$	$2.00 \times 10^{-6}$	0.002	2.002
3	0.4	$9.98 \times 10^{-6}$	$3.99 \times 10^{-6}$	0.004	2.004
4	0.6	$9.97 \times 10^{-6}$	$5.98 \times 10^{-6}$	0.006	2.006
5	0.8	$9.96 \times 10^{-6}$	$7.97 \times 10^{-6}$	0.008	2.008
6	1	$9.95 \times 10^{-6}$	$9.95 \times 10^{-6}$	0.010	2.010
7	2	$9.90 \times 10^{-6}$	$1.98 \times 10^{-5}$	0.020	2.020
8	3	$9.85 \times 10^{-6}$	$2.96 \times 10^{-5}$	0.030	2.030
9	4	$9.80 \times 10^{-6}$	$3.92 \times 10^{-5}$	0.040	2.040
10	5	$9.75 \times 10^{-6}$	$4.88 \times 10^{-5}$	0.050	2.050
11	6	$9.70 \times 10^{-6}$	$5.83 \times 10^{-5}$	0.060	2.060
12	7	$9.65 \times 10^{-6}$	$6.76 \times 10^{-5}$	0.070	2.070
13	8	$9.60 \times 10^{-6}$	$7.69 \times 10^{-5}$	0.080	2.080
14	10	$9.52 \times 10^{-6}$	$9.52 \times 10^{-5}$	0.100	2.100
15	12	$9.43 \times 10^{-6}$	$1.13 \times 10^{-4}$	0.120	2.120
16	15	$9.30 \times 10^{-6}$	$1.40 \times 10^{-4}$	0.150	2.150
17	20	$9.09 \times 10^{-6}$	$1.82 \times 10^{-4}$	0.200	2.200

Entry	DA/NB	[NB] (M)	[DA] (M)	V of DA (mL)	V total (mL)
18	25	$8.89 \times 10^{-6}$	$2.22 \times 10^{-4}$	0.250	2.250
19	30	$8.69 \times 10^{-6}$	$2.61 \times 10^{-4}$	0.300	2.300
20	35	$8.51 \times 10^{-6}$	$2.98 \times 10^{-4}$	0.350	2.350
21	40	$8.33 \times 10^{-6}$	$3.33 \times 10^{-4}$	0.400	2.400
22	45	$8.16 \times 10^{-6}$	$3.67 \times 10^{-4}$	0.450	2.450
23	50	$8.00 \times 10^{-6}$	$4.00 \times 10^{-4}$	0.500	2.500
24	55	$7.84 \times 10^{-6}$	$4.31 \times 10^{-4}$	0.550	2.550
25	60	$7.69 \times 10^{-6}$	$4.62 \times 10^{-4}$	0.600	2.600
26	65	$7.55 \times 10^{-6}$	$4.91 \times 10^{-4}$	0.650	2.650
27	70	$7.41 \times 10^{-6}$	$5.19 \times 10^{-4}$	0.700	2.700
28	75	$7.27 \times 10^{-6}$	$5.45 \times 10^{-4}$	0.750	2.750
29	80	$7.14 \times 10^{-6}$	$5.71 \times 10^{-4}$	0.800	2.800



**Table 3.6** The concentration of **NE** used for complexation studies with sensor **NB** and the ratios of **NB:NE**.

Entry	NE/NB	[NB] (M)	[NE] (M)	V of NE (mL)	V total (mL)
1	0.0	$1.00 \times 10^{-5}$	0.00	0.000	2.000
2	0.2	$9.99 \times 10^{-6}$	$2.00 \times 10^{-6}$	0.002	2.002
3	0.4	$9.98 \times 10^{-6}$	$3.99 \times 10^{-6}$	0.004	2.004
4	0.6	$9.97 \times 10^{-6}$	$5.98 \times 10^{-6}$	0.006	2.006
5	0.8	$9.96 \times 10^{-6}$	$7.97 \times 10^{-6}$	0.008	2.008
6	1.0	$9.95 \times 10^{-6}$	$9.95 \times 10^{-6}$	0.010	2.010
7	1.4	$9.94 \times 10^{-6}$	$1.19 \times 10^{-5}$	0.012	2.012
8	2	$9.90 \times 10^{-6}$	$1.98 \times 10^{-5}$	0.020	2.020
9	3	$9.85 \times 10^{-6}$	$2.96 \times 10^{-5}$	0.030	2.030
10	4	$9.80 \times 10^{-6}$	$3.92 \times 10^{-5}$	0.040	2.040
11	5	$9.76 \times 10^{-6}$	$4.88 \times 10^{-5}$	0.050	2.050
12	6	$9.71 \times 10^{-6}$	$5.83 \times 10^{-5}$	0.060	2.060
13	7	$9.66 \times 10^{-6}$	$6.76 \times 10^{-5}$	0.070	2.070
14	8	$9.62 \times 10^{-6}$	$7.69 \times 10^{-5}$	0.080	2.080
16	10	$9.52 \times 10^{-6}$	$9.52 \times 10^{-5}$	0.100	2.100
17	12	$9.43 \times 10^{-6}$	$1.13 \times 10^{-4}$	0.120	2.120
18	14	$9.35 \times 10^{-6}$	$1.31 \times 10^{-4}$	0.140	2.140
19	16	$9.26 \times 10^{-6}$	$1.48 \times 10^{-4}$	0.160	2.160

Entry	NE/NB	[NB] (M)	[NE] (M)	V of NE (mL)	V total (mL)
20	18	$9.17 \times 10^{-6}$	$1.65 \times 10^{-4}$	0.180	2.180
21	20	$9.09 \times 10^{-6}$	$1.82 \times 10^{-4}$	0.200	2.200
22	22	$9.01 \times 10^{-6}$	$1.98 \times 10^{-4}$	0.220	2.220
26	40	$8.33 \times 10^{-6}$	$3.33 \times 10^{-4}$	0.400	2.400
27	45	$8.16 \times 10^{-6}$	$3.67 \times 10^{-4}$	0.450	2.450
28	50	$8.00 \times 10^{-6}$	$4.00 \times 10^{-4}$	0.500	2.500
29	55	$7.84 \times 10^{-6}$	$4.31 \times 10^{-4}$	0.550	2.550
30	60	$7.69 \times 10^{-6}$	$4.62 \times 10^{-4}$	0.600	2.600
31	70	$7.41 \times 10^{-6}$	$5.19 \times 10^{-4}$	0.700	2.700
32	80	$7.14 \times 10^{-6}$	$5.71 \times 10^{-4}$	0.800	2.800

**Table 3.7** The concentration of **EPI** used for complexation studies with sensor **NB** and the ratios of **NB:EPI**.

Entry	<b>EPI/NB</b>	[NB] (M)	[EPI] (M)	V of <b>EPI</b> (mL)	V total (mL)
1	0	$1.00 \times 10^{-5}$	0.00	0.000	0.000
2	0.2	$9.99 \times 10^{-6}$	$2.00 \times 10^{-6}$	0.002	2.002
3	1	$9.95 \times 10^{-6}$	$9.95 \times 10^{-6}$	0.010	2.010
4	2	$9.90 \times 10^{-6}$	$1.98 \times 10^{-6}$	0.020	2.020
5	3	$9.85 \times 10^{-6}$	$2.96 \times 10^{-5}$	0.030	2.030
6	4	$9.80 \times 10^{-6}$	$3.92 \times 10^{-5}$	0.040	2.040
7	5	$9.76 \times 10^{-6}$	$4.88 \times 10^{-5}$	0.050	2.050
8	6	$9.71 \times 10^{-6}$	$5.83 \times 10^{-5}$	0.060	2.060
9	7	$9.66 \times 10^{-6}$	$6.76 \times 10^{-5}$	0.070	2.070
10	8	$9.61 \times 10^{-6}$	$7.69 \times 10^{-5}$	0.080	2.080
11	9	$9.57 \times 10^{-6}$	$8.61 \times 10^{-5}$	0.090	2.090
12	10	$9.52 \times 10^{-6}$	$9.52 \times 10^{-5}$	0.100	2.100
13	11	$9.48 \times 10^{-6}$	$1.04 \times 10^{-4}$	0.110	2.110
14	12	$9.43 \times 10^{-6}$	$1.13 \times 10^{-4}$	0.120	2.120
15	13	$9.39 \times 10^{-6}$	$1.22 \times 10^{-4}$	0.130	2.130
16	14	$9.35 \times 10^{-6}$	$1.31 \times 10^{-4}$	0.140	2.140
17	15	$9.30 \times 10^{-6}$	$1.40 \times 10^{-4}$	0.150	2.150
18	16	$9.26 \times 10^{-6}$	$1.48 \times 10^{-4}$	0.160	2.160

Entry	NE/NB	[NB] (M)	[EPI] (M)	V of EPI (mL)	V total (mL)
19	17	$9.22 \times 10^{-6}$	$1.57 \times 10^{-4}$	0.170	2.170
20	19	$9.13 \times 10^{-6}$	$1.74 \times 10^{-4}$	0.190	2.190
21	20	$9.09 \times 10^{-6}$	$1.82 \times 10^{-4}$	0.200	2.200
22	22	$9.01 \times 10^{-6}$	$1.98 \times 10^{-4}$	0.220	2.220
27	40	$8.33 \times 10^{-6}$	$3.33 \times 10^{-4}$	0.400	2.400
28	45	$8.16 \times 10^{-6}$	$3.67 \times 10^{-4}$	0.450	2.450
29	50	$8.00 \times 10^{-6}$	$4.00 \times 10^{-4}$	0.500	2.500

### 3.3.8 Determination of detection limit of sensor NB with DA, NE and EPI by fluorescence spectrophotometry

Typically, a stock solution of  $1 \times 10^{-4}$  M of sensor **NB** was prepared in 5 mL of DMSO. A final concentration of sensor **NB** at  $1 \times 10^{-5}$  M in 10% DMSO:phosphate buffer (0.01 M, pH 7.4) was added to a 1-cm quartz cuvette by micropipette and stirred for a min. Fluorescence spectra of sensor **NB** were recorded for 10 times at ambient temperature under the following condition.

*Start: 350 nm*

*End: 800 nm*

*Excitation: 340 nm*

*Excitation slit: 5.0*

*Emission slit: 5.0*

### 3.3.9 Complexation studies of sensor **CC** with various guests by fluorescence spectrophotometry technique

A stock solution of  $1 \times 10^{-3}$  M of sensor **CC** was prepared in DMSO. A stock solution of  $2 \times 10^{-3}$  M of various guests including **DA**, **NE**, **EPI**, **TY**, **Glu**, **Lys**, **His** and **Hist** in 0.1 M phosphate buffer pH 7.4 was prepared in the volumetric flasks. The solution of 15-crown-5 (0.1 mL) was added to the solution of sensor **CC** ( $5 \times 10^{-5}$  M) and stirred for 10 min. After that, 100 equiv. of the various guests was added directly to the solution mixture in a 1-cm quartz cuvette by micropipette and the mixture solution was stirred for 5 min. The fluorescence spectra were recorded after each addition collected in Table 3.8 under the following condition:

*Start: 350 nm*

*End: 800 nm*

*Excitation: 340 nm*

*Excitation slit: 5.0*

*Emission slit: 5.0*

**Table 3.8** Amounts of guests used for studies fluorescence spectrophotometry technique.

Guests	[Guest] (M)	Guest added ( $\mu$ L)	Guest:CC ratios
<b>DA</b>	$2 \times 10^{-3}$	500	100:1
<b>NE</b>	$2 \times 10^{-3}$	500	100:1
<b>EPI</b>	$2 \times 10^{-3}$	500	100:1
<b>TY</b>	$2 \times 10^{-3}$	500	100:1

Guests	[Guest] (M)	Guest added ( $\mu$ L)	Guest:CC ratios
<b>Glu</b>	$2 \times 10^{-3}$	500	100:1
<b>Lys</b>	$2 \times 10^{-3}$	500	100:1
<b>His</b>	$2 \times 10^{-3}$	500	100:1
<b>Hist</b>	$2 \times 10^{-3}$	500	100:1

### 3.3.10 Complexation studies of sensor NB and sensor CC with various guests by fluorescence spectrophotometry technique

A stock solution of  $1 \times 10^{-3}$  M of sensor **NB** and sensor **CC** were prepared in DMSO. A stock solution of  $2 \times 10^{-3}$  M of various guests including **DA**, **NE**, **EPI**, **TY**, **Glu**, **Lys**, **His** and **Hist** in 0.1 M phosphate buffer pH 7.4 was prepared in the volumetric flasks. The solution of each guests were added to the solution of sensor **NB** ( $1 \times 10^{-5}$  M) and stirred for 5 min. A 0.1 mL of 15-crown-5 was added to the solution mixture and stirred for 10 min. The solution of sensor **CC** ( $5 \times 10^{-5}$  M) was added in the same 1-cm quartz cuvette by micropipette and stirred for 5 min. The fluorescence spectra were recorded at room temperature as listed in Table 3.9 under the following condition:

*Start: 350 nm*

*End: 800 nm*

*Excitation: 340 nm*

*Excitation slit: 5.0*

*Emission slit: 5.0*

**Table 3.9** Amounts of guests used for studies fluorescence spectrophotometry technique.

Guests	[Guest] (M)	Guest added ( $\mu$ L)	Guest:CC ratios
<b>DA</b>	$2 \times 10^{-3}$	1000	100:1
<b>NE</b>	$2 \times 10^{-3}$	1000	100:1
<b>EPI</b>	$2 \times 10^{-3}$	1000	100:1
<b>TY</b>	$2 \times 10^{-3}$	1000	100:1
<b>Glu</b>	$2 \times 10^{-3}$	1000	100:1
<b>Lys</b>	$2 \times 10^{-3}$	1000	100:1
<b>His</b>	$2 \times 10^{-3}$	1000	100:1
<b>Hist</b>	$2 \times 10^{-3}$	1000	100:1

### 3.3.11 Principal component analysis (PCA) method for analysis of complexation

#### 3.3.11.1 PCA method for complexation of sensor NB with various guests

The solution of various guests (100 equiv.) was added directly to 2.00 mL of  $1 \times 10^{-5}$  M of sensor **NB** in a 1-cm quartz cuvette by micropipette and stirred for 5 min. The fluorescence spectra of complexation were measured from 350-800 nm at the excitation of 340 nm. The complexation was reproducibly detected for 5 times in each guest. The evaluation of PCA was calculated by using MATLAB 7.11 (version R2011a) program.

### 3.3.11.2 PCA method for complexation of sensor CC with various guests

The solution of 15-crown-5 (0.1 mL) was added to the solution of sensor **CC** ( $5 \times 10^{-5}$  M) and stirred for 10 min. After that, 100 equiv. of the various guests was added directly to the solution mixture in a 1-cm quartz cuvette by micropipette and stirred for 5 min. The fluorescence spectra of complexation were recorded from 350-800 nm at the excitation of 340 nm. The complexation was reproducibly detected for 5 times in each guest. The evaluation of PCA was calculated by using MATLAB 7.11 (version R2011a) program.

### 3.3.11.3 PCA method for complexation of sensor NB and sensor CC with various guests

The solution of each guests (100 equiv.) were added to the solution of sensor **NB** ( $1 \times 10^{-5}$  M) and stirred for 5 min. Then, 0.1 mL of 15-crown-5 was added to the solution mixture and stirred for 10 min. Last one, the solution of sensor **CC** ( $5 \times 10^{-5}$  M) was added in the same 1-cm quartz cuvette by micropipette and stirred for 5 min. The fluorescence spectra of complexation were monitored from 350-800 nm at the excitation of 340 nm. The complexation was reproducibly detected for 5 times in each guest. The evaluation of PCA was calculated by using MATLAB 7.11 (version R2011a) program.

### 3.3.12 Complexation study of sensor NB with EPI in human urine sample

A stock solution of  $1 \times 10^{-4}$  M of sensor **NB** was prepared in DMSO. The stock solution of  $2 \times 10^{-3}$  M of **EPI** analyte was prepared in 0.01 M phosphate buffer pH 7.4 and synthetic urine was prepared in milli-Q water as indicated in Table 3.10.

For calibration curve, the synthetic urine was spiked into the  $1 \times 10^{-5}$  M of sensor **NB** solution by the 100-fold diluted solution of urine. The **EPI** solution was added to the mixture solution as various concentrations (10-70  $\mu$ M) and stirred for 5 min. The fluorescence spectra were record from 350-800 nm at the excitation of



340 nm. Therefore, a calibration curve was built from the plot of  $I-I_0$  at 490 nm versus concentration of **EPI**.

Then, the urine samples were spiked into the  $1 \times 10^{-5}$  M of sensor **NB** solution by the 100-fold diluted solution of urine. The 40  $\mu$ M of **EPI** solution was added to the mixture solution, stirred for 5 min and repeated for three times. The fluorescence spectra were record from 350-800 nm at the excitation of 340 nm. After that, the found amount and percent recovery were calculated from the calibration curve.

**Table 3.10** Composition of synthetic urine [77]

Species	Concentration (g l <sup>-1</sup> )	Concentration (mmol l <sup>-1</sup> )
CaCl <sub>2</sub> .H <sub>2</sub> O	0.65	Ca: 4.3
MgCl <sub>2</sub> .6H <sub>2</sub> O	0.651	Mg:3.2
NaCl	4.6	SO <sub>4</sub> : 16
Na <sub>2</sub> SO <sub>4</sub>	2.3	Citrate: 2.3
Na <sub>3</sub> C <sub>6</sub> H <sub>8</sub> O <sub>7</sub> .2H <sub>2</sub> O	0.65	Oxalate: 0.149
Na <sub>2</sub> C <sub>2</sub> O <sub>4</sub>	0.020	
KH <sub>2</sub> PO <sub>4</sub>	2.8	PO <sub>4</sub> : 20.5
KCl	1.6	
NH <sub>4</sub> Cl	1	NH <sub>4</sub> : 19
CO(NH <sub>2</sub> ) <sub>2</sub>	25	
C <sub>4</sub> H <sub>7</sub> N <sub>3</sub> O	1.1	
Total Na = 118 mEq		
Total K = 42 mEq		
pH = 5.8		

### 3.3.13 Complexation study of sensor **NB** and sensor **CC** with **NE** by mass spectroscopy

A stock solution of 0.1 M of sensor **NB**, sensor **CC** and **NE** were prepared in DMSO- $d_6$ . A stock solution of 0.1 M of NaOH was prepared in D<sub>2</sub>O. The solution of  $5 \times 10^{-3}$  M of NaOH was added to the solution of sensor **NB** ( $1 \times 10^{-2}$  M) and stirred for 1 min. Then, the  $1 \times 10^{-2}$  M of **NE** analyte was added to the solution mixture and stirred for 5 min. After that, the solution of sensor **CC** ( $1 \times 10^{-2}$  M) was add the solution mixture and stirred for 10 min. The mass spectrum of the complex was recorded by MALDI-TOF mass spectroscopy.

## CHAPTER IV

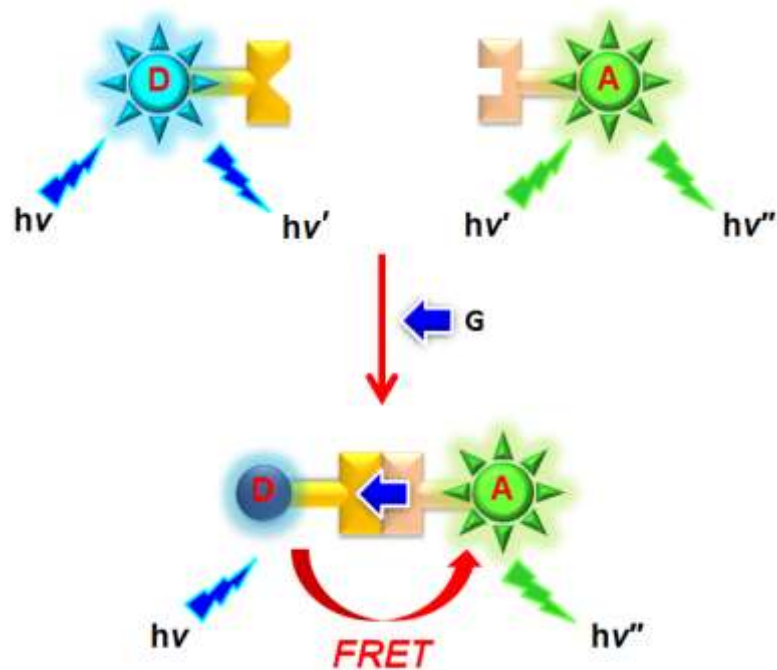
### RESULTS AND DISCUSSION

#### 4.1 Design and synthesis of boronic acid based sensors

Our research has focused on design and development of molecular sensor for measurement of catecholamine neurotransmitter in imitatively biological system. Usually, chemosensors are comprised of binding units and sensory units linked with the spacer. Following host-guest chemistry [78], recognition events occur via covalent bond and non-covalent interactions including hydrogen bonding, electrostatic interactions, ion-dipole interactions and cation- $\pi$  interactions and  $\pi$ - $\pi$  stacking interactions. [1, 79] Herein, these recognitions displayed significant role in biological environment regarding to the sensitivity and selectivity.

Molecular sensor were designed and synthesized for sensitive and selective detection of catecholamine through fluorescence resonance energy transfer (FRET) process. Considerably, the structure of catecholamines consists of two functional groups including catechol and amino group. Therefore, the sensor should contain two binding sites for the selective binding of each part based catecholamine guests. Our concept hypothesized that the catecholamine acts as a bridging analyte between FRET donor and FRET acceptor of two fluorescence sensors. As anticipated, the complete complexation of both sensors with a proper analyte demonstrated the shift of donor fluorophore to the new emission band of acceptor fluorophore. This phenomenon is called FRET mechanism as shown in scheme 4.1.

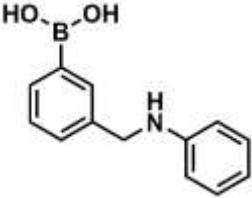
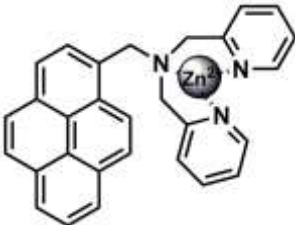
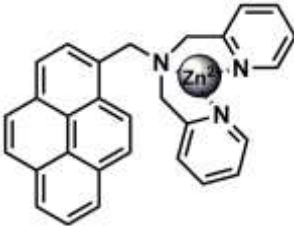
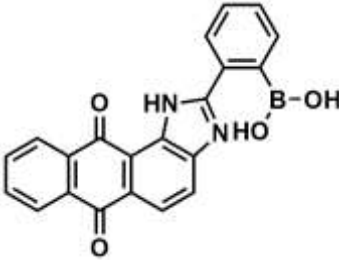
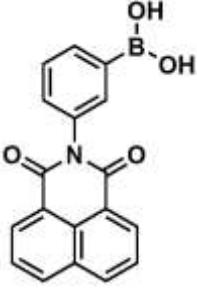
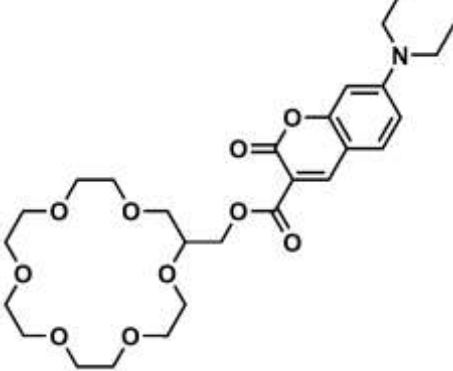
In this work, we have taken an attempt to investigate the properly coupled fluorophore with a regard of FRET process by studying the FRET efficiency of four couples of fluorescence sensor as a following in table 4.1.



**Scheme 4.1** Conceptual hypothesis under FRET mechanism

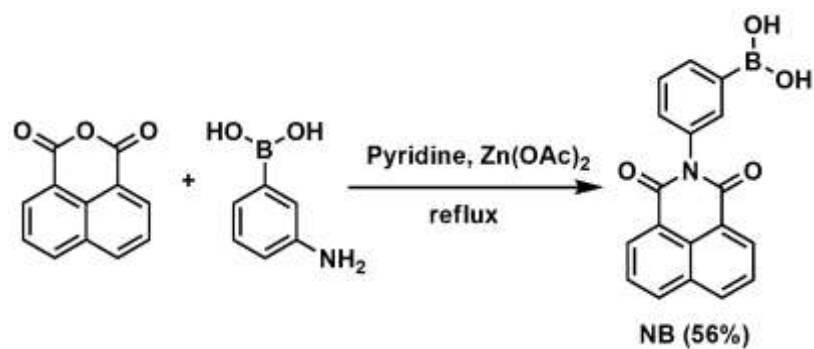
**Table 4.1** The FRET donor and FRET acceptor used for study of the complexation.

Couple	FRET donor	FRET acceptor
1	<p><b>NB</b></p> <p><math>\lambda_{\text{ex}} = 340 \text{ nm}</math>  <math>\lambda_{\text{em}} = 384 \text{ nm}</math></p>	<p><b>DC</b></p> <p><math>\lambda_{\text{ex}} = 353 \text{ nm}</math>  <math>\lambda_{\text{em}} = 494 \text{ nm}</math></p>

Couple	FRET donor	FRET acceptor
2	 <p style="text-align: center;"><b><i>m</i>-BA</b></p> <p style="text-align: center;"><math>\lambda_{\text{ex}} = 290 \text{ nm}</math> <math>\lambda_{\text{em}} = 329 \text{ nm}</math></p>	 <p style="text-align: center;"><b>L2-Zn</b></p> <p style="text-align: center;"><math>\lambda_{\text{ex}} = 345 \text{ nm}</math> <math>\lambda_{\text{em}} = 388 \text{ nm}</math></p>
3	 <p style="text-align: center;"><b>L2-Zn</b></p> <p style="text-align: center;"><math>\lambda_{\text{ex}} = 345 \text{ nm}</math> <math>\lambda_{\text{em}} = 388 \text{ nm}</math></p>	 <p style="text-align: center;"><b><i>o</i>-AB</b></p> <p style="text-align: center;"><math>\lambda_{\text{ex}} = 420 \text{ nm}</math> <math>\lambda_{\text{em}} = 603 \text{ nm}</math></p>
4	 <p style="text-align: center;"><b>NB</b></p> <p style="text-align: center;"><math>\lambda_{\text{ex}} = 340 \text{ nm}</math> <math>\lambda_{\text{em}} = 384 \text{ nm}</math></p>	 <p style="text-align: center;"><b>CC</b></p> <p style="text-align: center;"><math>\lambda_{\text{ex}} = 420 \text{ nm}</math> <math>\lambda_{\text{em}} = 475 \text{ nm}</math></p>

## 4.2 Synthesis

### 4.2.1 Preparation of sensor NB



**Scheme 4.2** Synthesis pathway of sensor **NB**

*N*-(1,8-Naphthaloyl)-3-aminophenylboronic acid (**NB**) was prepared in a single-step reaction by nucleophilic substitution between 3-aminophenylboronic acid hemisulfate and 1,8-naphthalene dicarboxylic acid anhydride to give a light yellow solid with 56% yield. From the <sup>1</sup>H-NMR data of sensor **NB** in Fig. 4.1, the range of aromatic protons at 7.42-8.48 ppm assigned to aromatic protons of both naphthalimide group and boronic acid. MALDI-TOF mass showed the intensified peak at 317.38 m/z with agreement of the structure of sensor **NB**.

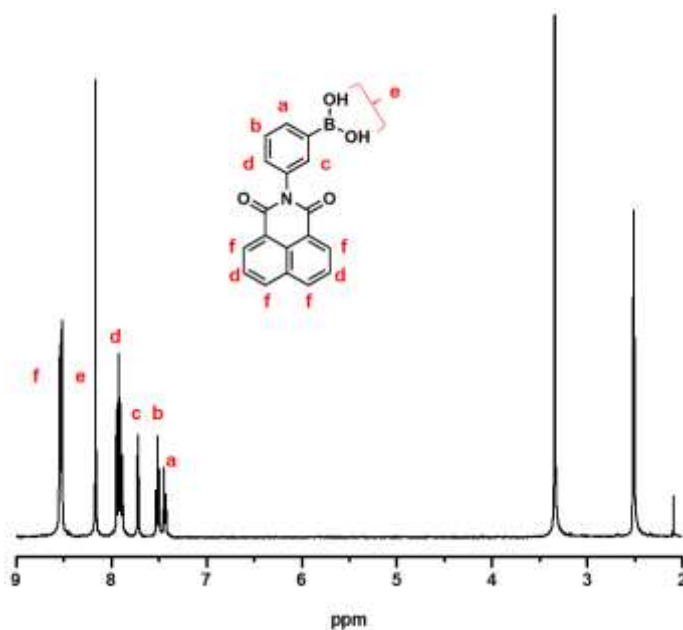
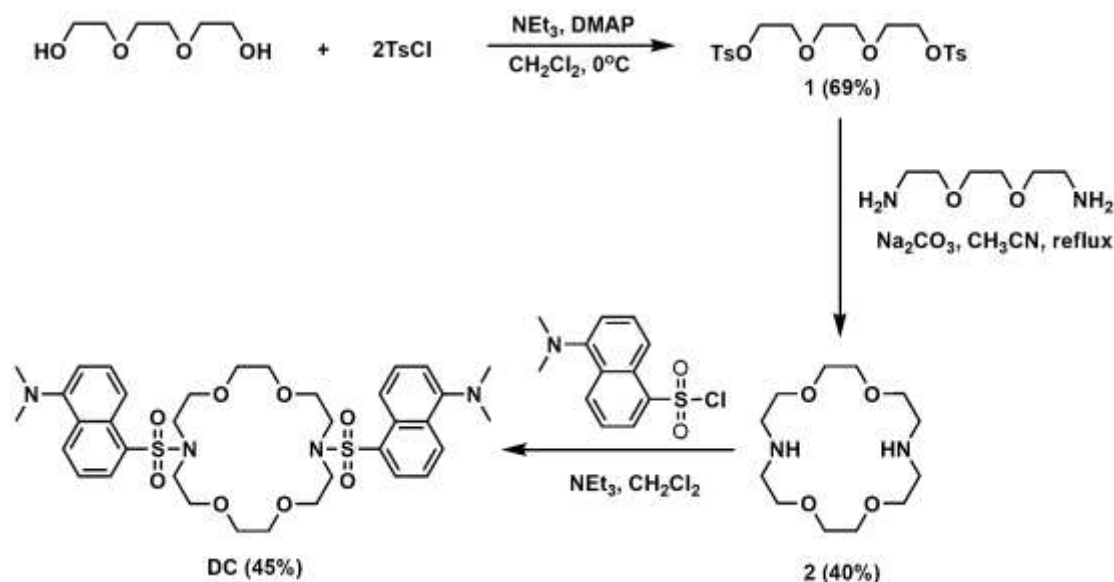


**Figure 4.1** The <sup>1</sup>H-NMR spectrum of sensor **NB** in DMSO-*d*<sub>6</sub> at 400 MHz

#### 4.2.2 Preparation of sensor DC



**Scheme 4.3** Synthesis pathway of sensor **DC**

For sensor **DC** chemosensor, compound **1** was synthesized by nucleophilic substitution between triethylene glycol and tosyl chloride to give a white solid in 69% yield. The  $^1\text{H-NMR}$  spectrum showed the characteristic peaks of aromatic protons of tosyl group at 7.34-7.79 ppm. Furthermore, the ethylene protons shifted to downfield from 3.40 to 4.18 ppm.

Compound **2** was prepared by the reaction between compound **1** and ethylenedioxy amine to give a white solid in 40% yield. The  $^1\text{H-NMR}$  spectrum showed the broad peak of amine group ( $-\text{CH}_2\text{NH}$ ) at 2.32 ppm. Moreover, the observation of disappearance of tosylate groups supports the structure of **2**.

Finally, the desired product (**DC**) was obtained from nucleophilic substitution of amine group based compound **2** and dansyl chloride. The  $^1\text{H-NMR}$  data of the sensor **DC** displayed the aromatic protons of dansyl group at 7.16-8.51 ppm. Moreover, the broad peak of amine group disappeared in the  $^1\text{H-NMR}$  spectrum of Fig. 4.2. The observation of an intense peak at 729.34 m/z from MALDI-TOF mass spectrum confirmed the structure of sensor **DC**.

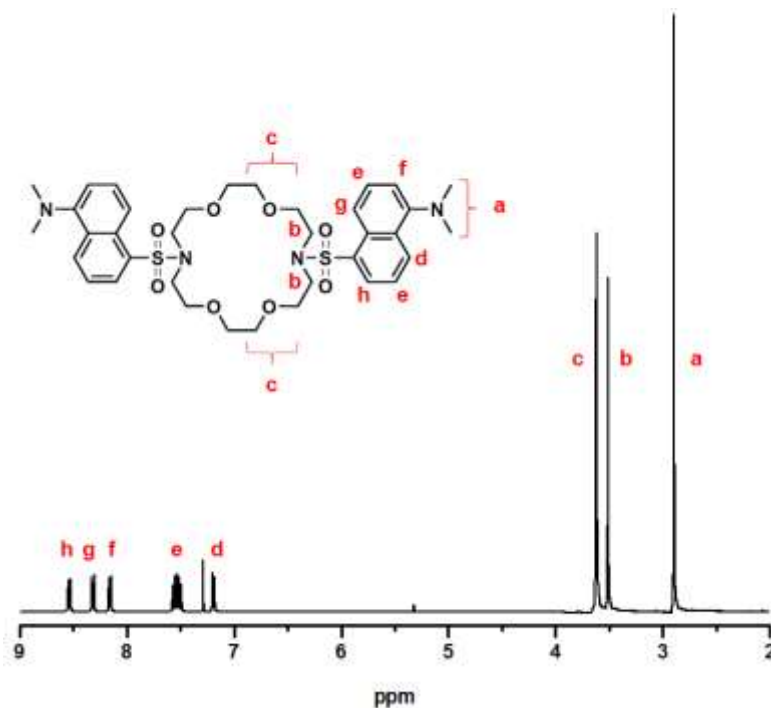
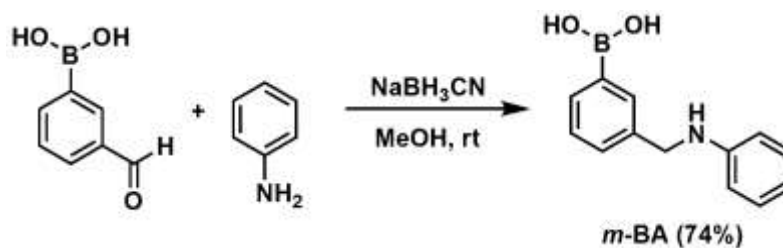


**Figure 4.2** The  $^1\text{H}$ -NMR spectrum of sensor **DC** in  $\text{CDCl}_3$  at 400 MHz

#### 4.2.3 Preparation of sensor *m*-BA



**Scheme 4.4** Synthesis pathway of sensor *m*-BA

To prepare sensor *m*-BA by one pot reaction, phenyl boronic acid reacted with aniline in methanol under shift base reaction. In situ, the imine moiety was reduced by sodium cyanoborohydride to obtain a white solid in 74% yield. Importantly, the  $^1\text{H}$ -NMR spectrum displayed a board peak of a proton of secondary amine at 4.63 ppm and aromatic protons in the range of 7.75-6.56 ppm as indicated in Fig. 4.3. The intense peak at 227.285 m/z from MALDI-TOF mass spectrum supported the structure of sensor *m*-BA.



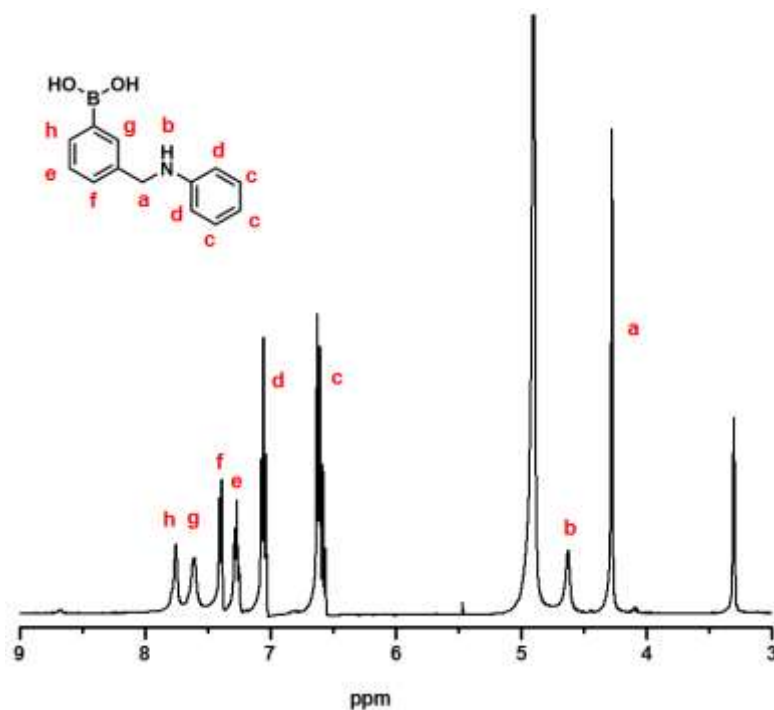
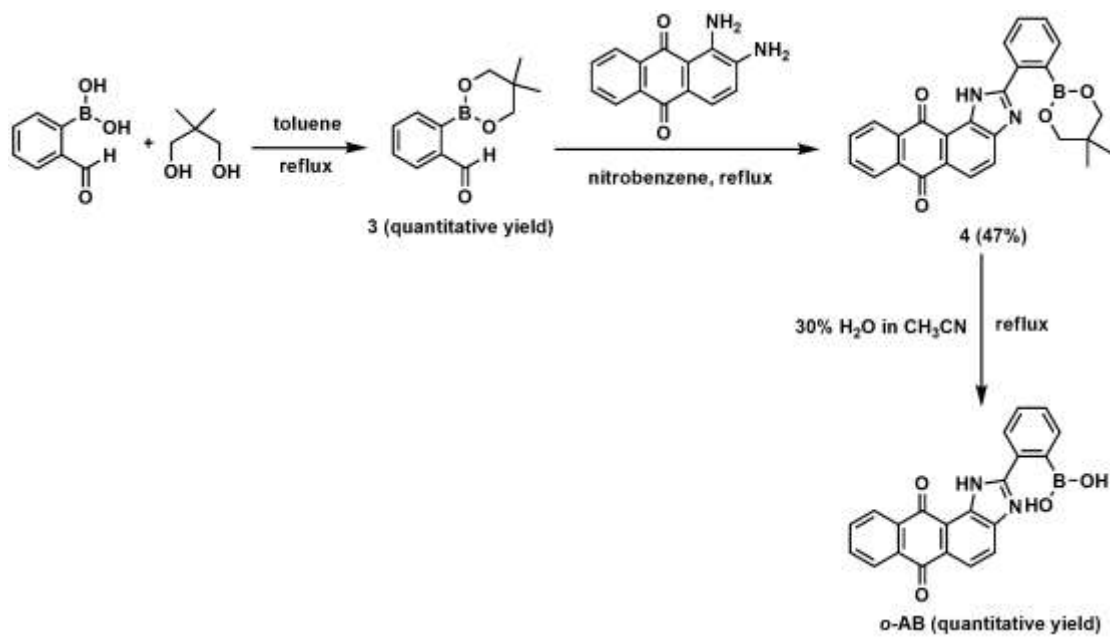


Figure 4.3 The  $^1\text{H-NMR}$  spectrum of *m*-BA in  $\text{CD}_3\text{OD}$  at 400 MHz

#### 4.2.4 Preparation of sensor *o*-AB



Scheme 4.5 Synthesis pathway of sensor *o*-AB

The sensor ***o*-AB** was synthesized by using the protected ortho-formyl phenylboronate (**3**) and commercial available of 1,2-diamino-1,4-anthraquinone. The compound **4** was purified by precipitation with hexane in nitrobenzene to afford a brown solid in 47% yield. The  $^1\text{H-NMR}$  spectrum of compound **4** presented the imidazole proton at 13.53 ppm because of the hydrogen bonding between this proton and oxygen atom of anthraquinone. The sensor ***o*-AB** was obtained by deprotection with 30%  $\text{H}_2\text{O}:\text{CH}_3\text{CN}$ . From the  $^1\text{H-NMR}$  spectrum in Fig. 4.4, the protons on  $-\text{CH}_2$  and  $-\text{CH}_3$  group of 1,2-propadiol were disappeared at 3.70 and 1.07, respectively.

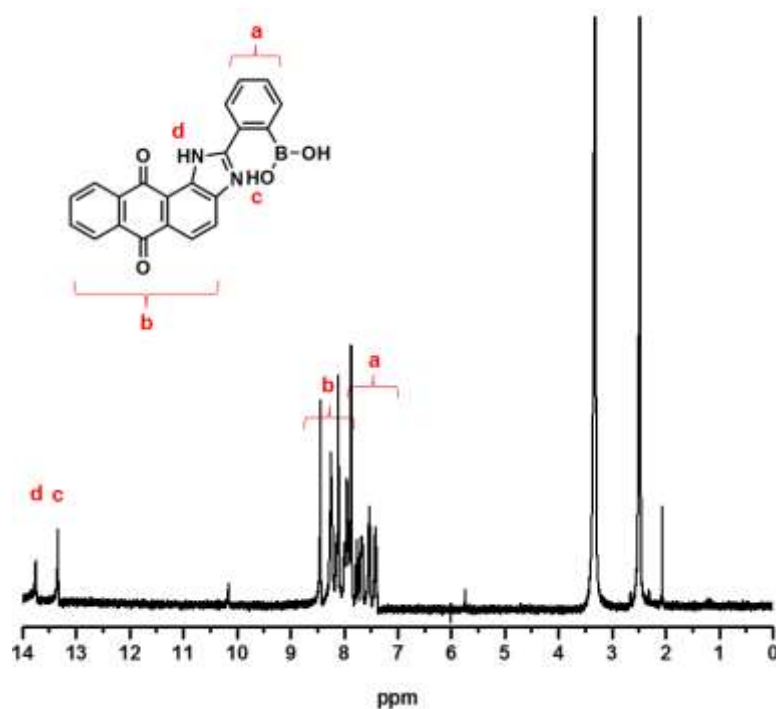
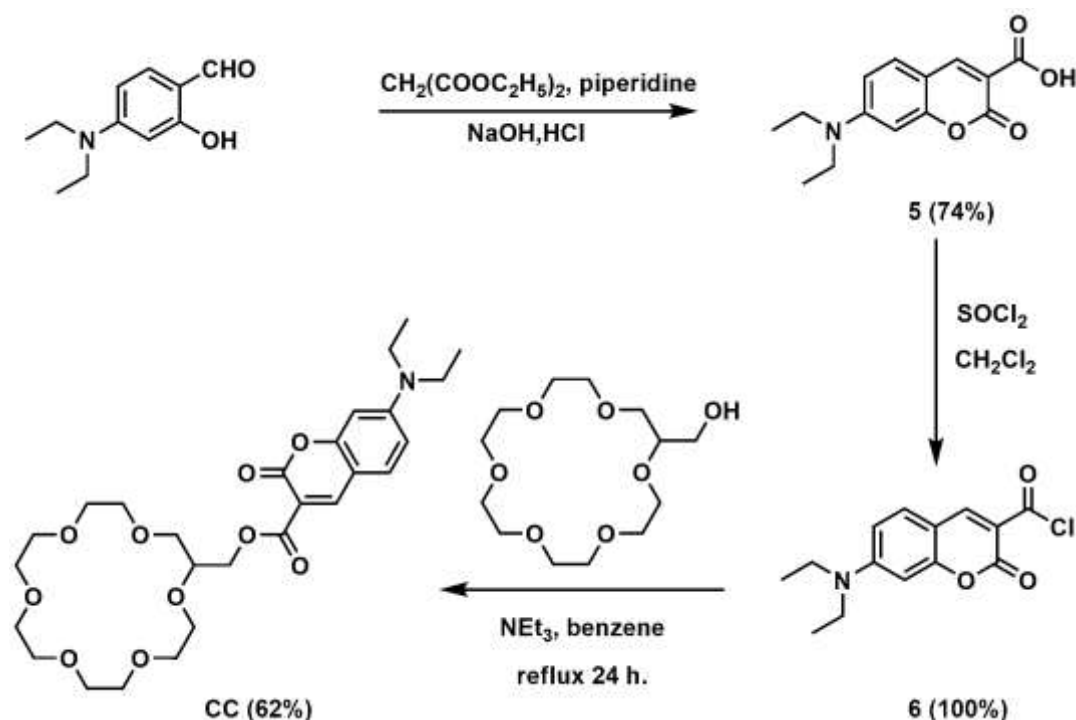


**Figure 4.4** The  $^1\text{H-NMR}$  spectrum of ***o*-AB** in  $\text{DMSO-}d_6$  at 400 MHz

#### 4.2.5 Preparation of sensor CC



**Scheme 4.6** Synthesis pathway of sensor **CC**

Sensor **CC** was prepared in three steps. First step, the product **5** was synthesized by nucleophilic substitution between diethylaminosalicylaldehyde and diethylmalonate to give an orange crystal in 74% yield. The  $^1\text{H-NMR}$  spectrum exhibited the characteristic peak of acetic acid proton at 12.37 ppm and a singlet peak of the additional aromatic protons at 8.66 ppm. The next step demonstrated the conversion of acetic acid group to acid chloride in product **6** by reaction of compound **5** with thionyl chloride to give a yellow powder of **6** in quantitative yield. From  $^1\text{H-NMR}$  spectrum, the disappearance of acetic proton at 12.37 ppm was observed due to the replacement of chloride atom at hydroxyl group. In final step, sensor **CC** was obtained by coupling reaction of **6** and 2-hydroxymethyl-18-crown-6 by nucleophilic substitution and triethylamine as base. Considerably, a singlet proton of coumarin showed upfield shift from 8.68 to 8.35 and other aromatic protons presented upfield shift possibly caused by the electron donor group of methylene bridge as shown in Fig. 4.5. In addition, the  $^{13}\text{C-NMR}$  spectrum showed ester group signal at 163.97 and

158.54. MALDI-TOF mass spectra also supported the structure of sensor **CC** with the intense peak of  $m/z$  at 537.887.

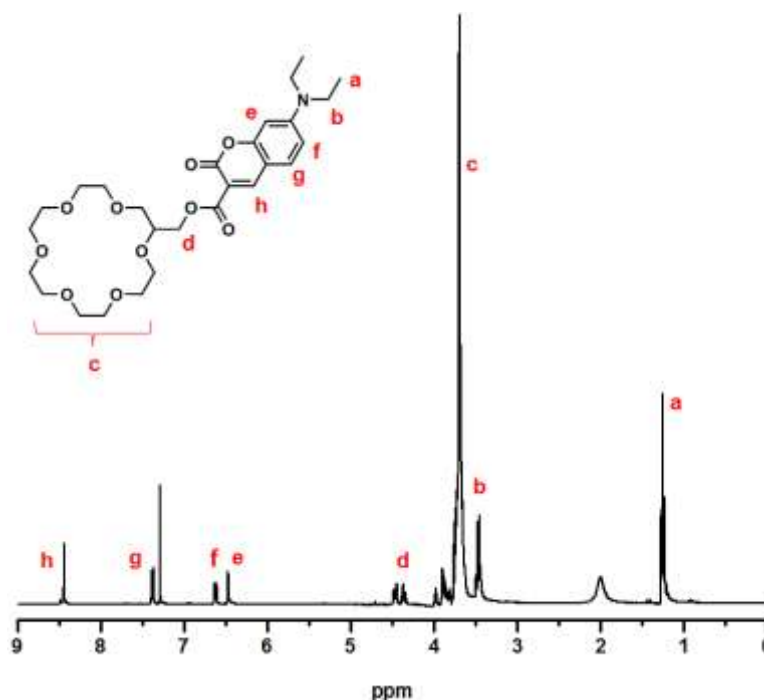


**Figure 4.5** The  $^1\text{H}$ -NMR spectrum of sensor **CC** in  $\text{CDCl}_3$  at 400 MHz

### 4.3 Complexation studies

#### 4.3.1 Complexation studies of sensor **NB** and sensor **DC** with dopamine (**DA**) by fluorescence spectrophotometry technique

We designed the fluorescence sensor **NB** and sensor **DC** for detection of **DA** under FRET mechanism as shown in Fig. 4.6. The sensor **NB** assigned as FRET donor ( $\lambda_{\text{ex}} = 340 \text{ nm}$ ,  $\lambda_{\text{em}} = 384 \text{ nm}$ ) contains boronic acid as a binding unit to bond covalently with catechol unit and naphthalimide group as a fluorophore, while the sensor **DC** acting as FRET acceptor consists of 18-crown-6 moiety as a binding site for ammonium ion and coumarin as a fluorophore ( $\lambda_{\text{ex}} = 353 \text{ nm}$ ,  $\lambda_{\text{em}} = 494 \text{ nm}$ ).

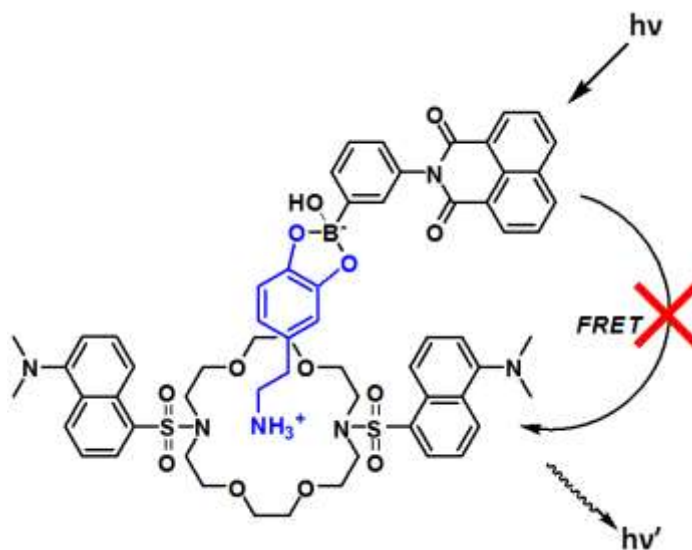


**Figure 4.6** The conceptually proposed structure and mechanism of **NB-DA-DC** complex under FRET mechanism.

To investigate the complexation in 10% DMSO:phosphate buffer (0.01 M, pH 7.4), The excess dopamine was added to the solution of sensor **NB**. Consequently, the fluorescence intensity at 384 nm was decreased through PET mechanism. Then, the addition of sensor **DC** into mixture solution was stirred at varying time. From Fig 4.7 showed the fluorescence quenching at 494 nm and enhancement at 462 nm. Unfortunately, the complexation of both sensors with **DA** did not occur under FRET mechanism. Moreover, we revealed that both sensors could not bind simultaneously with **DA** due to the interference of sodium ion in phosphate buffer as shown in Fig.4.7. The interaction of sodium ion with diazacrown ether of sensor **DC** blocked the interaction of ammonium ion based **DA** and diazacrown ether of sensor **DC**.

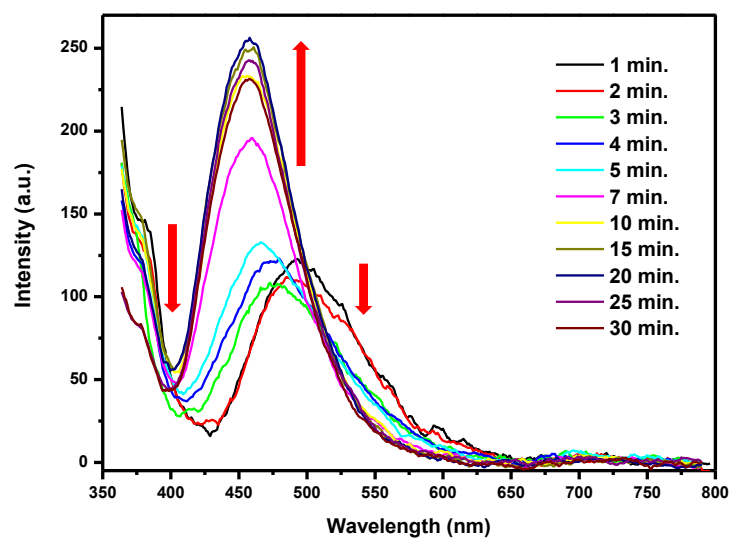


**Figure 4.7** Fluorescence spectra of sensor **NB** ( $1 \times 10^{-5}$  M) and sensor **DC** ( $1 \times 10^{-6}$  M) in the presence of excess dopamine in 10% DMSO:phosphate buffer (0.01 M, pH 7.4) vary time ( $\lambda_{\text{ex}} = 353$  nm)

To prove the hypothesis, the fluorescence spectra of sensor **DC** without adding **DA** showed an enhancement and small blue shift as a function of time as shown in Fig. 4.8. These fluorescence changes could be explained that sodium ion in buffer solution binds with crown ether of sensor **DC** and subsequent to inhibit the PET process of sensor **DC**. Therefore, this system could not serve as the dopamine sensing by FRET process.

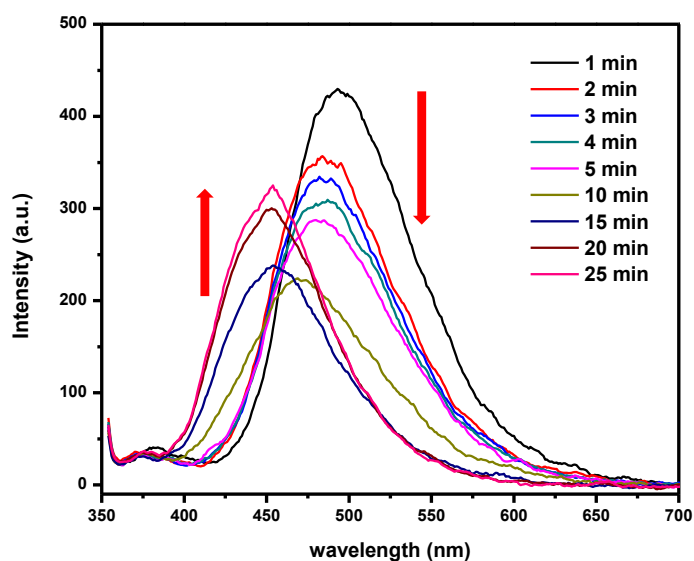


**Figure 4.8** Fluorescence spectra of sensor **DC** ( $1 \times 10^{-5}$  M) in 10% DMSO:phosphate buffer (0.01 M, pH 7.4) vary time ( $\lambda_{\text{ex}} = 353$  nm)

#### 4.3.2 Complexation studies of sensors *m*-BA and sensor L2-Zn with DA by fluorescence spectrophotometry technique

To avoid the interference of sodium ion in buffer solution, we designed molecular sensor without diazacrown ether. The new design of sensor *m*-BA and sensor L2-Zn was synthesized for detection of DA by FRET process as depicted in Fig. 4.9. Sensor *m*-BA, namely FRET donor, contains boronic acid as binding unit ( $\lambda_{\text{ex}} = 290$  nm,  $\lambda_{\text{em}} = 329$  nm). Preliminary, the complex of sensor *m*-BA with diol group displayed fluorescence enhancement [80] which was excellent property for donor molecule. The sensor L2-Zn as FRET acceptor contains zinc complex which was expected to coordinate with amino group of DA. The sensor L2-Zn consists of pyrene as a fluorophore giving the excitation wavelength at 345 nm and the emission band at 388 nm.

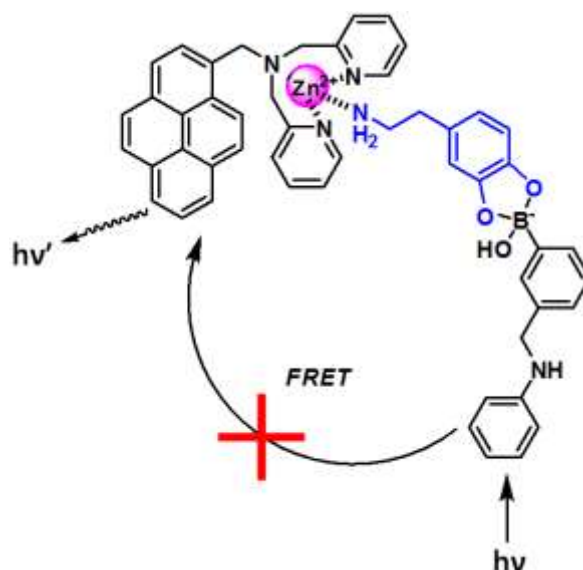


**Figure 4.9** The conceptually proposed structure and mechanism of (*m*-BA)-DA-(L2-Zn) complex under FRET mechanism

The self-assembled complexation of both sensors with **DA** in 50% MeOH:phosphate buffer (0.01 M, pH 8.0) was investigated. From Fig.4.10, the fluorescence intensity of pyrene at 388 nm was gradually developed upon the increment of sensor **L2-Zn** and excess **DA**. The new emission band was occurred at 462 nm owing to excimer species or  $\pi$ - $\pi$  stacking interaction of pyrene. This occurrence of a new band does not stemmed from FRET mechanism, because the fluorescence changes at 462 nm as a result of the increment of amount sensor **L2-Zn**. We hypothesized that both fluorescence sensors are able to absorb the energy at the same wavelength. The complex of sensor **L2-Zn** and dopamine could preferential adsorb the energy with a higher molar absorptivity over the complex of sensor **m-BA** and dopamine.



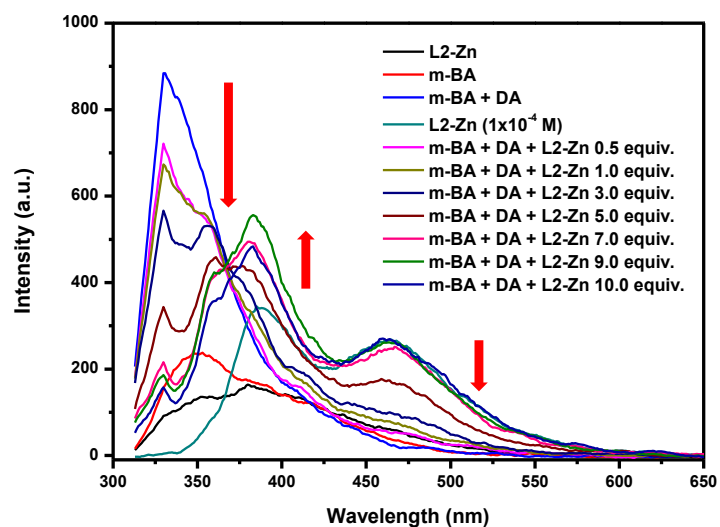


**Figure 4.10** Fluorescence spectra of sensor **L2-Zn** and sensor **m-BA** ( $1 \times 10^{-5}$  M) in 50% MeOH:phosphate buffer (0.01 M, pH 8.0) in the presence of **DA** 50 equiv. ( $\lambda_{\text{ex}} = 290$  nm)

Unfortunately, the solution of **DA** without sensor in 50% MeOH:phosphate at the same excitation of 290 nm, gives an emission band at 326 nm which overlabs with the fluorescence signal of sensor **m-BA** spectrum (as shown in Fig. 4.11). Thus, it is difficult to identify a signal change assigned by the complexation. This couple FRET process is not proper for catecholamine sensing.

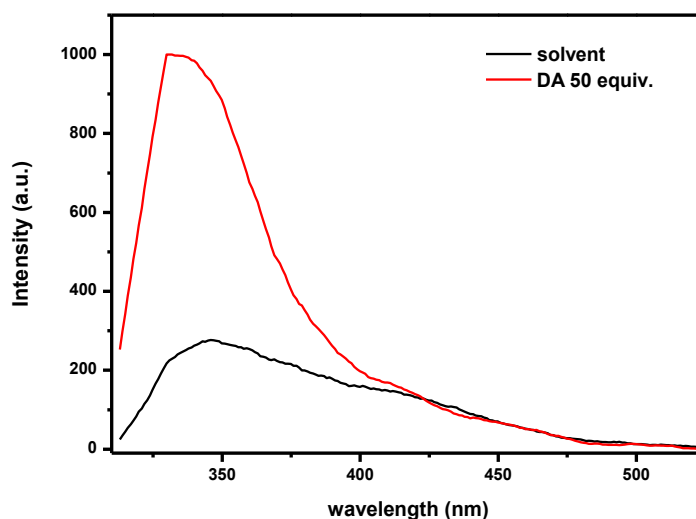


**Figure 4.11** Fluorescence spectra of solvent and **DA** (50 equiv.) in 50% MeOH:phosphate buffer (0.01 M, pH 8.0) with excitation at 290 nm

### 4.3.3 Complexation studies of sensor **L2-Zn** and sensor ***o*-AB** with **DA** by fluorescence spectrophotometry technique

Consequently, the new probe ***o*-AB** was designed for detection of **DA** under FRET mechanism as indicated in Fig. 4.12. Sensor **L2-Zn** acting as FRET donor bearing zinc ion was expected to form ion-dipole interaction with amino group of **DA** and pyrene as a fluorophore ( $\lambda_{\text{ex}} = 345 \text{ nm}$ ,  $\lambda_{\text{em}} = 388 \text{ nm}$ ). The FRET acceptor of sensor ***o*-AB** consists of the boronic acid for binding with catechol group of **DA** and anthraquinone as a fluorophore with the excitation and emission wavelength at 420 and 603 nm, respectively.

To explore the binding ability between both sensors and **DA** in 10% DMSO:phosphate buffer (0.01 M, pH 7.4). The emission band of sensor **L2-Zn** at 388 nm and sensor ***o*-AB** at 603 nm was decreased upon the increment of **DA** as indicated in Fig 4.12. The fluorescence quenching of both sensors was a consequence of PET mechanism by electron donation from catecholamine to fluorophore. Hence, this couple fluorophores did not allow the effective FRET process.

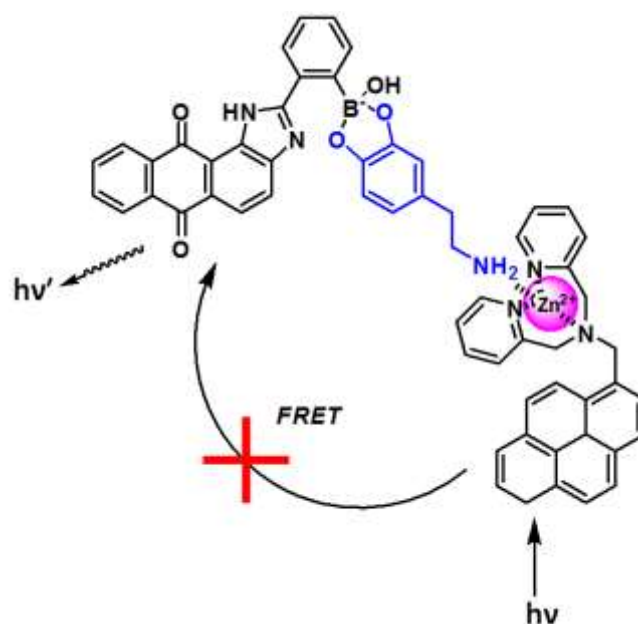


**Figure 4.12** The conceptually proposed structure and mechanism of (L2-Zn)-DA-o-AB complex under FRET mechanism

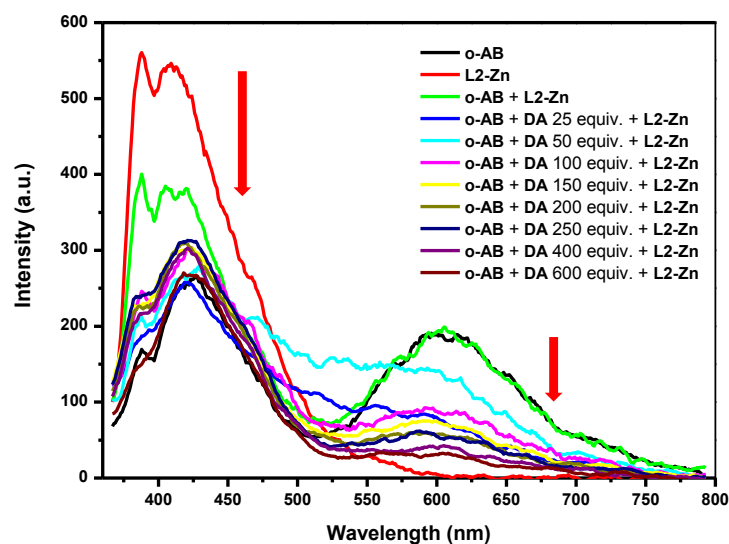
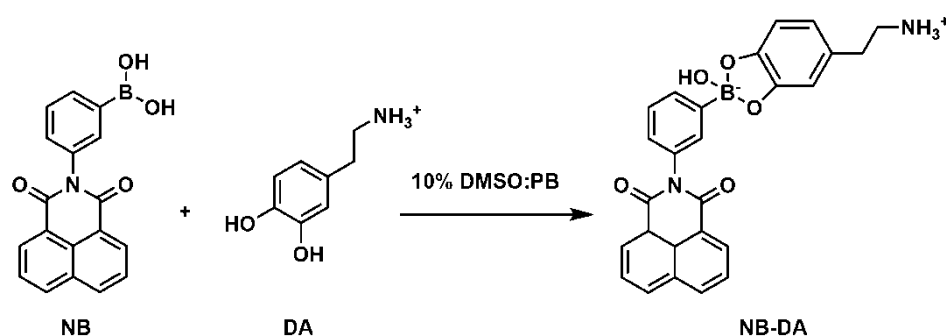


**Figure 4.13** Fluorescence spectra of sensor L2-Zn ( $1 \times 10^{-5}$  M) and sensor o-AB ( $1 \times 10^{-5}$  M) in 10% DMSO:phosphate buffer (0.01 M, pH 7.4) with varying the amount of DA ( $\lambda_{\text{ex}} = 345$  nm)

#### 4.3.4 Complexation studies of sensor **NB** with various guests by fluorescence spectrophotometry technique

In this section, the creation of sensor **NB** contains boronic acid moiety as a binding unit and naphthalimide moiety as a fluorophore. In our hypothesis, the condensation reaction between boronic acid group of sensor **NB** and catechol group of analytes was expected to be performed in Scheme 4.7. This approach could be monitored by fluorescence technique.



**Scheme 4.7** The condensation reaction of sensor **NB** with **DA** in 10% DMSO:phosphate buffer (0.01 M, pH 7.4)

The selectivity of sensor **NB** was examined in biological system (10% DMSO:phosphate buffer (0.01 M, pH 7.4)) toward 100 equiv. of various biogenic amines including dopamine (**DA**), norepinephrine (**NE**), epinephrine (**EPI**), tyramine (**TY**), L-glutamic acid (**Glu**), L-lysine (**Lys**), histidine (**His**) and histamine (**Hist**) as indicated in Fig. 4.14.

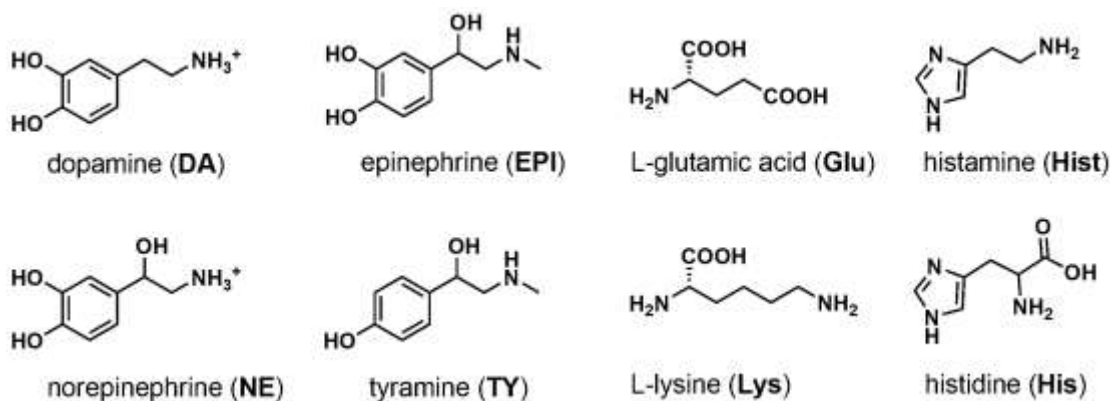


**Figure 4.14** The structures of various biogenic amines

The chemosensor **NB** showed the characteristic emission band at 384 nm. As shown in Fig. 4.15, the fluorescence spectra of sensor **NB** with **DA** and **NE** displayed a large fluorescence quenching at 384 nm. These results can be explained by photoinduced electron transfer (PET) process from a phenyl group of **DA** to naphthalimide moiety of sensor **NB**. Alternatively, the emission band of sensor **NB** upon complexing with **EPI** exhibits a strong fluorescence intensity with a concomitant of a large red shift from 384 nm to 490 nm. This phenomenon stemmed from the photoinduced charge transfer (PCT) mechanism as described in Scheme 4.8. The boronate ester based and naphthalimide of **NB-EPI** complex acted as an acceptor group while secondary amine on side chain performed the donor group. The orientation of dipole moment of complex **NB-EPI** was increased from the donor part to acceptor part of complex. Consequently, the intramolecular charge transfer from the secondary amine to boronate ester based naphthalimide induced a large red-shift and strong emission band. In the case of **DA** and **NE**, the PET process is more dominant than PCT process because the complex of sensor **NB** and **DA** or **NE** did not affect on their dipole moments. On the other hand, other analytes without the catechol group including **TY**, **Glu**, **Lys**, **His** and **Hist** could not induce the fluorescence changes implying that these analytes did not bind with boronic acid based sensor **NB**.

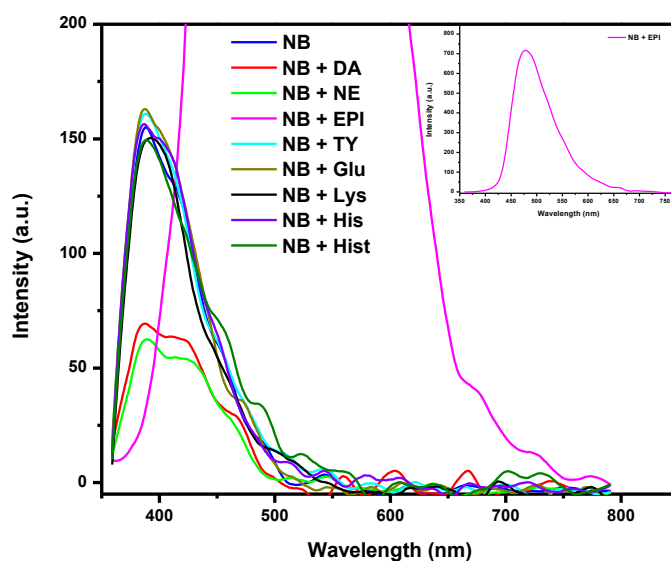
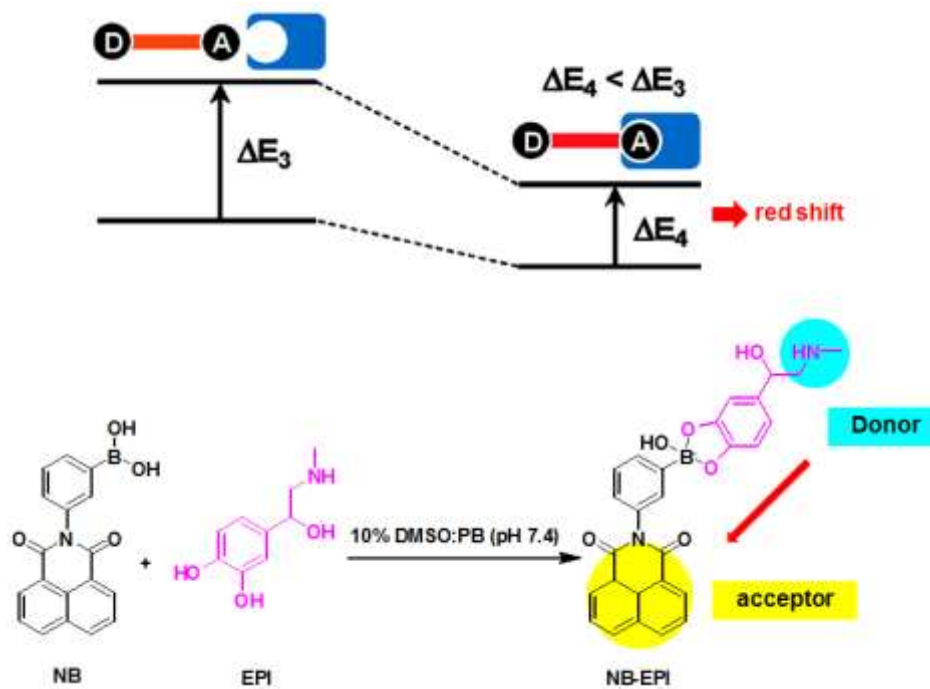


**Figure 4.15** Fluorescence spectra of sensor **NB** ( $1 \times 10^{-5}$  M) in 10% DMSO: phosphate buffer (0.01 M, pH 7.4) in the presence of various guests at 100 equivalent and inset shows the fluorescence spectra of sensor **NB** and **EPI**.



**Scheme 4.8** Principal of photoinduced charge transfer (PCT) system

To verify the visual detection of sensor **NB** toward analytes, the solution of sensor **NB** and various analytes was exposed under 356 nm UV visible light. The fluorescence color changes of sensor **NB** toward analytes were displayed in Fig. 4.16. The sensor **NB** solution in the presence of **DA** or **NE** showed a very low brightness of luminescence. On the other hand, the solution of **NB-EPI** complex exhibited a highly green luminescence. Contrastly, the sensor **NB** solution with other guests including **TY**, **Glu**, **Lys**, **His** and **Hist** did not show the luminescence.



**Figure 4.16** Fluorescence color change of sensor **NB** ( $1 \times 10^{-5}$  M) in 10% DMSO:phosphate buffer (0.01 M, pH 7.4) in the presence of the various guests 100 equiv.

Furthermore, to develop the **EPI** sensor on the solid support, the filter paper was dipped in  $5 \times 10^{-5}$  M of sensor **NB** solution. Then, this filter paper was painted in word “**EPI**” by using paintbrush. The prepared filter paper exposed under 356 nm UV light, showed the green luminescence in word “**EPI**” as shown in Fig. 4.17. As a result of fluorescence changes on solid support, sensor **NB** offers an excellent promising for **EPI** detection. Consequently, It may imply that the sensor **NB** can bind with **EPI** on solid support.

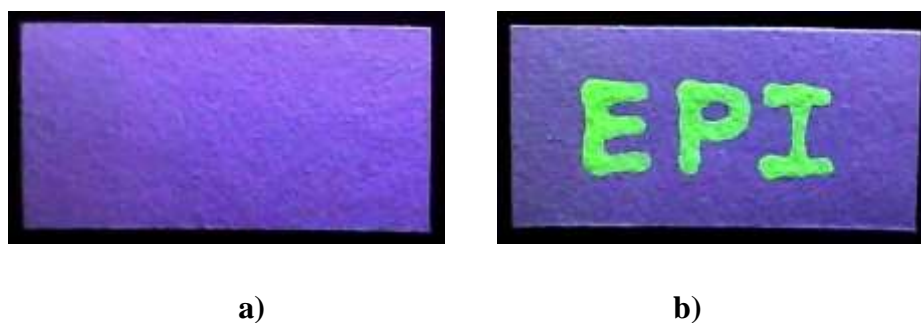
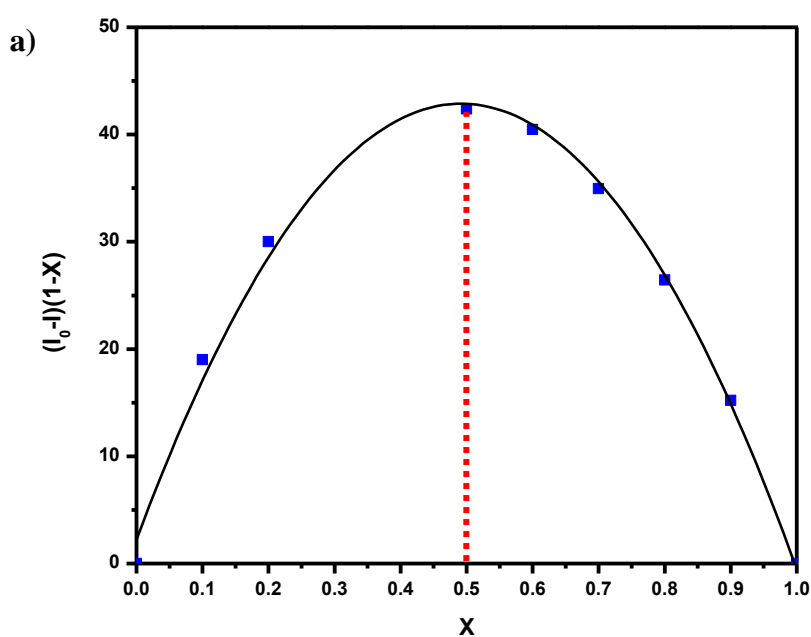


**Figure 4.17** Fluorescence images of a) sensor **NB** and b) sensor **NB** dipped with **EPI** on a filter paper in word “**EPI**” under the black light

Sensor **NB** offers considerable promises as **EPI** selective fluorescence probes. However, our purpose is to discriminate the similar structure of catecholamine derivatives. We developed the ratiometric fluorescence probe upon the intermolecular FRET mechanism by incorporation of sensor **CC** and sensor **NB**.

#### 4.3.5 Job's plot study of sensor **NB** with DA, NE and EPI

Considering the binding mode between sensor **NB** and catecholamine, the stoichiometry of complexes was validated by the continuous variation method or Job's method. The plot of  $(I_0 - I)(1 - X_{\text{guest}})$  versus  $X$  showed the stoichiometry of 1:1 binding mode for sensor **NB** and catecholamine guests ( shown in Fig. 4.18).





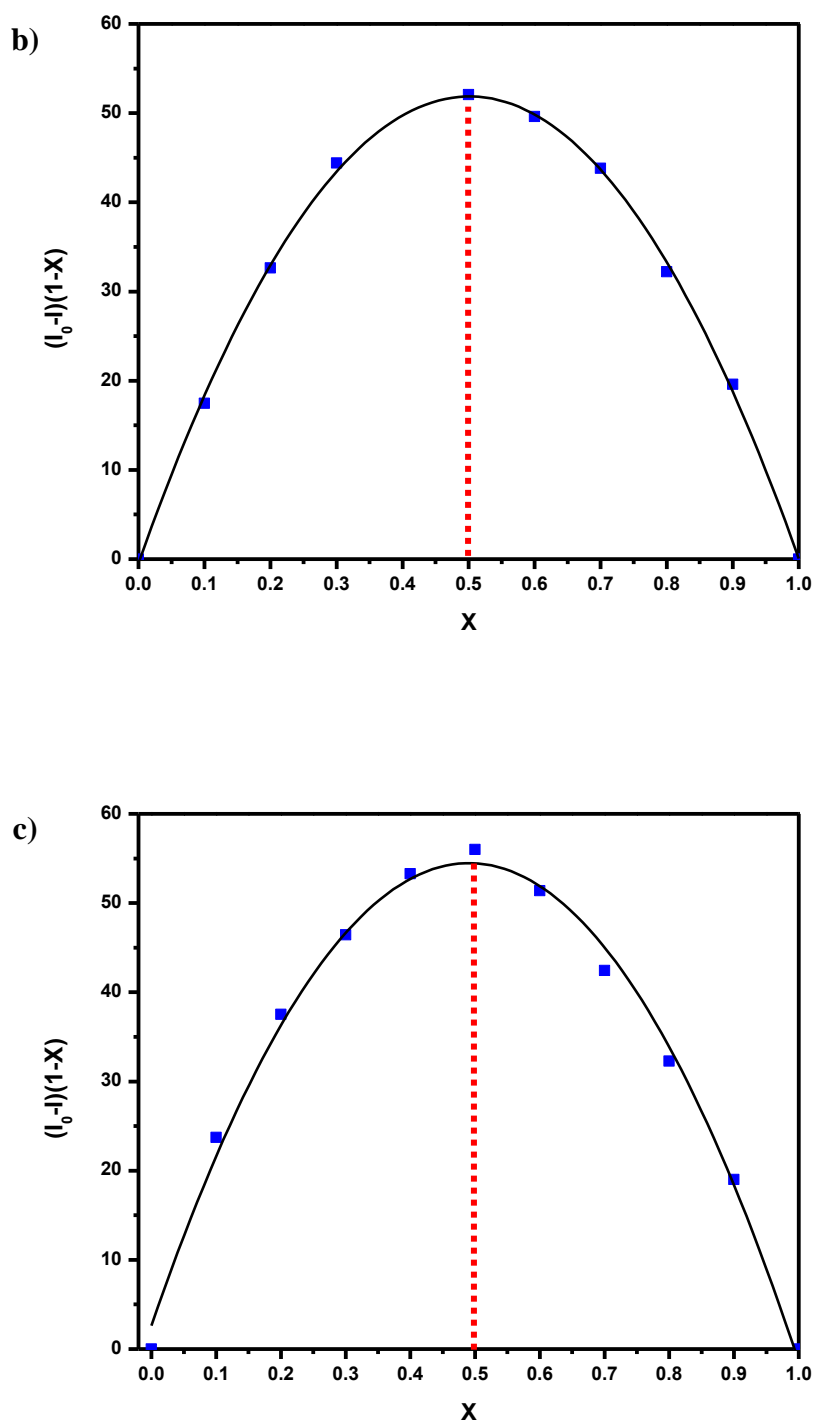


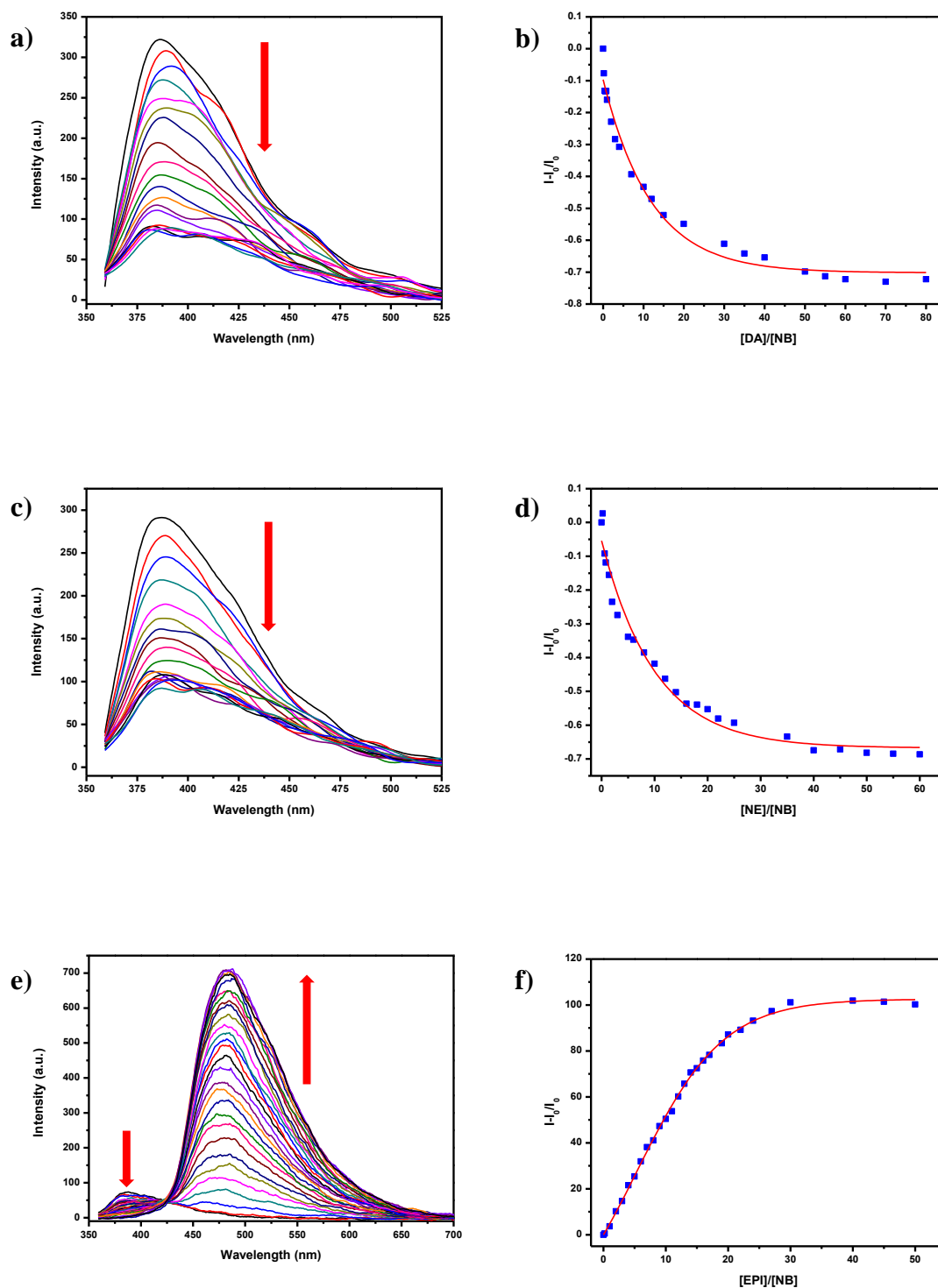
**Figure 4.18** Job's plots for 1:1 complex of sensor **NB** with a) **DA** b) **NE** and c) **EPI** at pH 7.4 ( $1 \times 10^{-5}$  M in 10% DMSO: phosphate buffer)

#### 4.3.6 Complexation studies of sensor **NB** with **DA**, **NE** and **EPI** by fluorescence spectrophotometric titration technique

To verify the binding affinity of sensor **NB**, fluorescence titration of sensor **NB** was carried out in 10% DMSO:phosphate buffer (0.01 M, pH 7.4). Prior to fluorescence measurement, the solution mixture of the sensor **NB** and catecholamine guests was stirred at room temperature for 5 min. The fluorescence intensity at 384 nm of the complexation of sensor **NB** toward **DA**, **NE** and **EPI** gradually decreased upon the increment of catecholamine guests as illustrated by Fig. 4.19a, 4.19c and 4.19e, respectively. Moreover, the new emission band at 490 nm of complexation **NB-EPI** was developed. The fluorescence titration was carried out at least twice. Fluorescence titration data were analyzed by using Benesi-Hildebrand plot (see also Fig. 4.20) from Microsoft Excel and equation 4.1.[R] According to table 4.2, the log  $K_s$  values of complex **NB** with **DA**, **NE** and **EPI** computed by equation 4.1 were 4.07, 4.08 and 3.00, respectively.

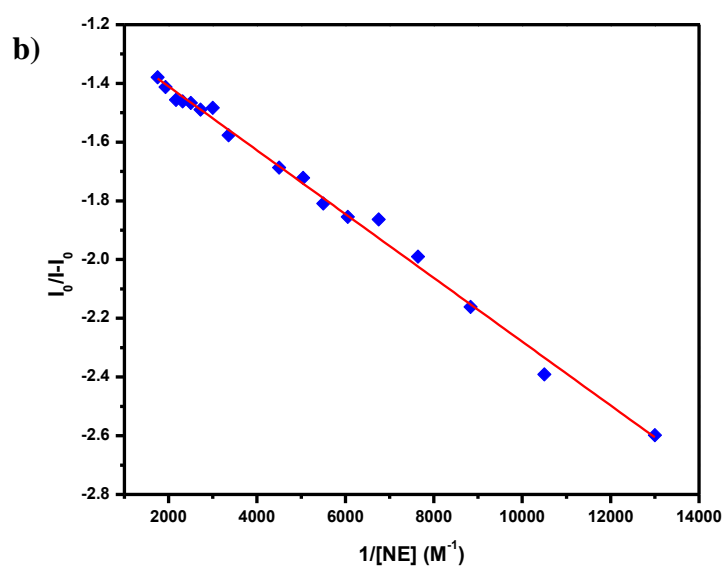
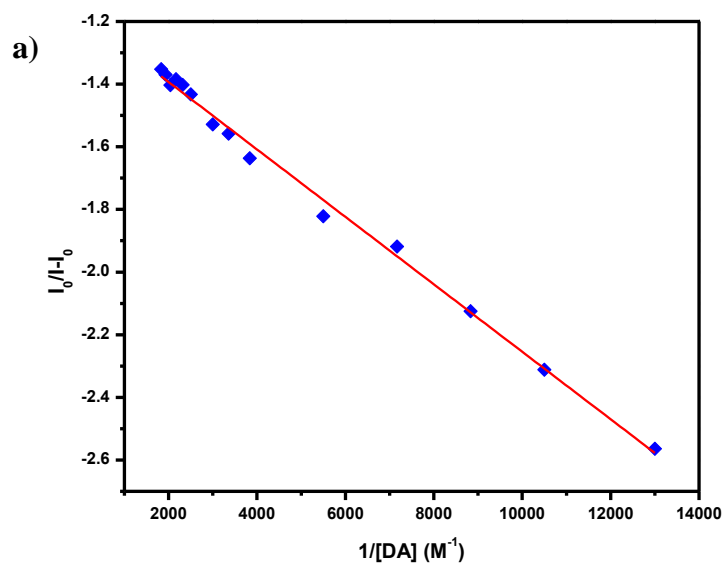
$$\frac{I_0}{I - I_0} = \frac{\alpha}{K_s[G]} + \alpha \quad 4.1$$

- $I_0$  = initial intensity
- $I$  = intensity of a particular concentration of guest
- $\alpha$  = point of intersection of Y axis
- $K_s$  = binding constant of the sensor with the guest
- $[G]$  = concentration of guest



**Figure 4.19** The fluorescence titration spectra of sensor **NB** ( $1 \times 10^{-5}$  M) upon gradual addition a) **DA**, c) **NE** and e) **EPI** and fluorescence responses ( $(I-I_0)/I_0$ ) in the presence

of 0-80 equiv. of b) **DA**, d) **NE** and f) **EPI** in 10% DMSO:phosphate buffer (0.01 M, pH 7.4)



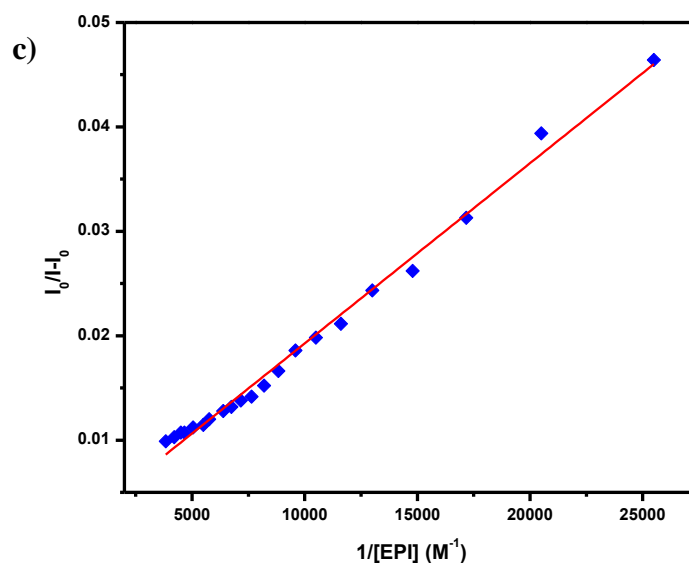


**Figure 4.20** Benesi-Hildebrand plots of sensor **NB** ( $1 \times 10^{-5}$  M) toward 0-80 equiv. of a) **DA** b) **NE** and c) **EPI** in 10% DMSO:phosphate buffer (0.01 M, pH 7.4) for calculation of binding constant ( $K_s$ )

The trend of  $\log K_s$  values of sensor **NB** toward catecholamine guests was **DA**  $\approx$  **NE** > **EPI** as summarized in table 4.2. The fluorescence changes and the  $\log K_s$  values in the case of **DA** and **NE** can be reasonably explained that the ammonium ion preferred to promote the condensation reaction of boronic acid and catechol group producing a negative boronate ester. It is rationalized that the  $\log K_s$  values of sensor **NB** with **DA** and **NE** is slightly higher than these sensor **NB** with **EPI**.

**Table 4.2** The Binding constant ( $\log K_s$ ) of sensor **NB** with **DA**, **NE** and **EPI**

Guest	Equation	R <sup>2</sup>	$\log K_s$
<b>DA</b>	$y = -1 \times 10^{-4}x - 1.1779$	0.9953	4.07
<b>NE</b>	$y = -1 \times 10^{-4}x - 1.1927$	0.9933	4.08
<b>EPI</b>	$y = 2 \times 10^{-6}x - 0.0200$	0.9930	3.00

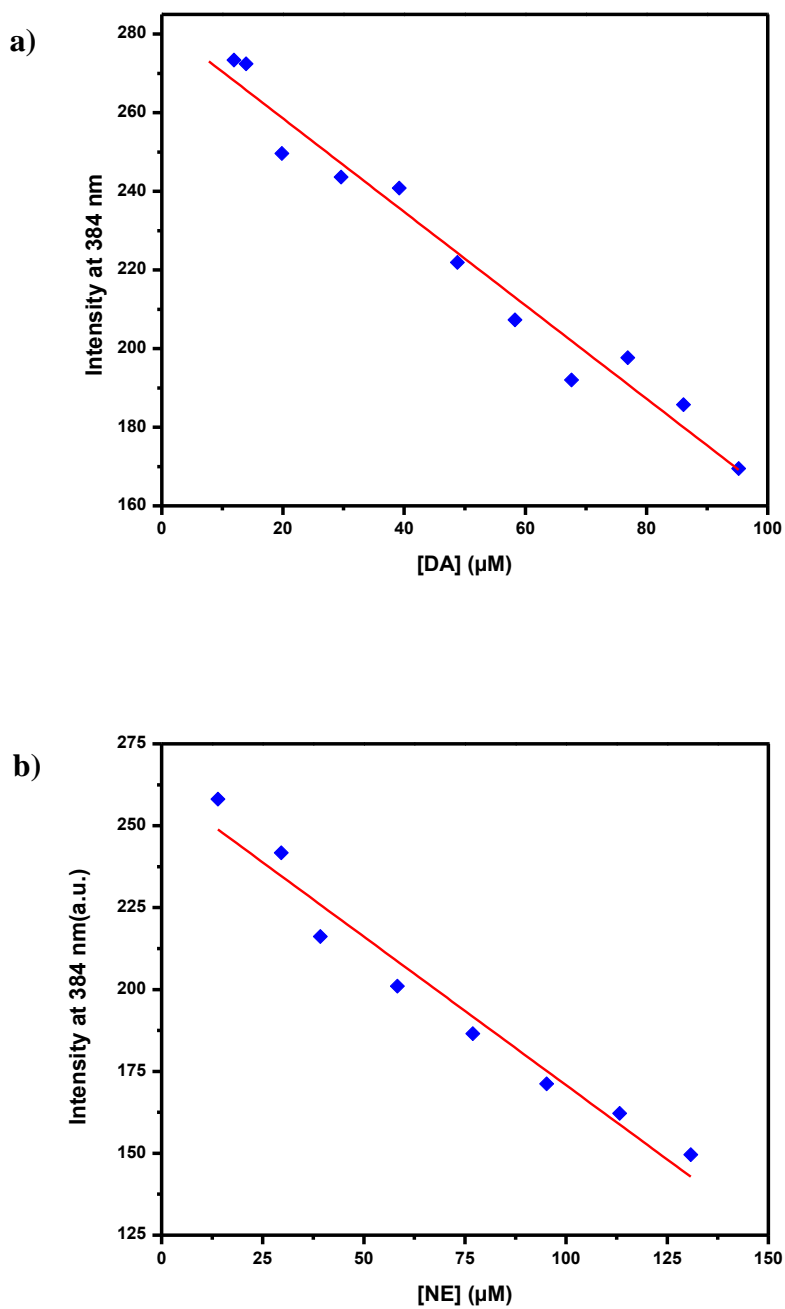
#### 4.3.7 Determination of detection limit of sensor **NB** with **DA**, **NE** and **EPI** by fluorescence spectrophotometry

The detection limits of sensor **NB** with **DA**, **NE** and **EPI** were examined by fluorescence spectrophotometry. The sensor **NB** ( $1 \times 10^{-5}$  M) was prepared in 10% DMSO:phosphate buffer (0.01 M, pH 7.4) and fluorescence intensity was recorded at 384 nm for 10 times. (As listed in Table 4.3)

**Table 4.3** The fluorescence intensity of sensor **NB** at 384 nm

Entry	Intensity
1	140.6431
2	144.6393
3	139.4108
4	145.3288
5	141.9485
6	146.5246
7	147.2602
8	143.9869
9	142.3952
10	141.8269
Standard Deviation	2.568395

Figure 4.21 illustrated the linear relationships of sensor **NB** as a function of catecholamine concentration in 10% DMSO:phosphate buffer (0.01 M, pH 7.4). In addition, the detection limits calculated by  $3SD/slope$  and linear correlation as well as the  $R^2$  values were collected in Table 4.4.



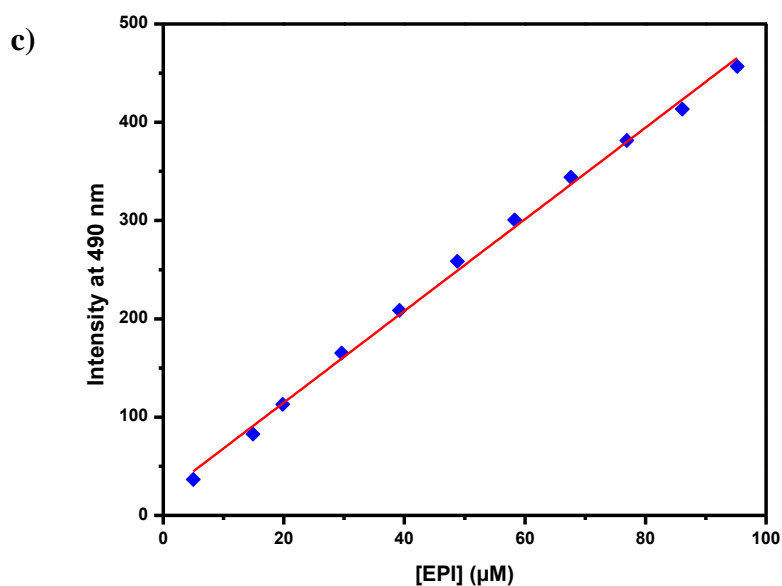


**Figure 4.21** Linear plot of fluorescence intensity between sensor **NB** with a) **DA** b) **NE** c) **EPI** complexes and concentration of catecholamine guests

**Table 4.4** The detection limits of sensor **NB** with **DA**, **NE** and **EPI**

Guest	Equation	R <sup>2</sup>	Detection Limit (LOD)
<b>DA</b>	$y = -1 \times 10^6 x + 281.98$	0.9672	7.71 (μM)
<b>NE</b>	$y = -906497x + 261.45$	0.9625	8.50 (μM)
<b>EPI</b>	$y = 5 \times 10^6 x + 26.650$	0.9972	1.54 (μM)

The detection limits of sensor **NB** toward **DA**, **NE** and **EPI** are in the normal range found in a human serum of  $10^{-2}$ - $10^{-4}$  mM [81]. Sensor **NB** can serve as an **EPI** sensing in very low concentration compared to **DA** and **NE**.



#### 4.3.8 Complexation studies of sensors **NB** and sensor **CC** with various guests by fluorescence spectrophotometry technique

To verify the discrimination of **DA** and **NE**, our concept hypothesized that the adaptively self-assembled complexation of boronic acid site based **NB** and crown ether based **CC** with catechol and ammonium unit of **DA** or **NE**, respectively, would induce the shift of the emission band at 384 nm belonging to sensor **NB** to 475 nm corresponding to sensor **CC** under fluorescence resonance energy transfer (FRET) process. As expected, the guests act as a bridging analyte between FRET donor and acceptor as depicted in Fig. 4.22. One is naphthalimide fluorophore defined as a FRET donor ( $\lambda_{\text{ex}} = 340 \text{ nm}$ ,  $\lambda_{\text{em}} = 384 \text{ nm}$ ) consisting of a boronic acid for diol binding and another one is coumarin fluorophore defined as a FRET acceptor ( $\lambda_{\text{ex}} = 420 \text{ nm}$ ,  $\lambda_{\text{em}} = 475 \text{ nm}$ ) bearing crown ether for binding with ammonium ion. Since the different structures of the **DA** and **NE** are addressed in the amine unit. It probably seems that, the classification of **DA** and **NE** stemmed from fluorescence resonance energy transfer (FRET) process.

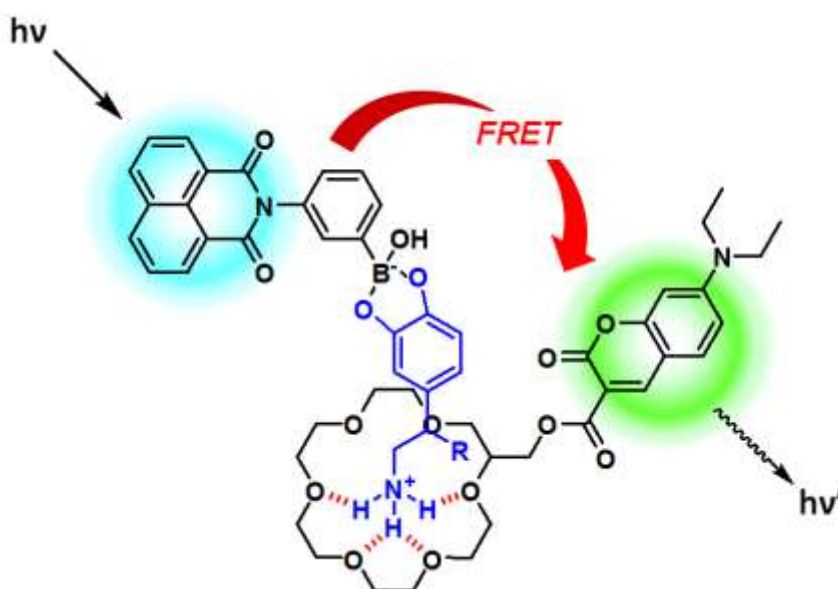


**Figure 4.22** The conceptually proposed structure and mechanism of **NB**-guest-**CC** complex under FRET mechanism

Since the solution of phosphate buffer contains sodium cation which probably interfere the cation-dipole interaction of ammonium ion with crown ether based **CC**. The addition of 15-crown-5 into the solution mixture would prevent the interference of sodium ion in buffer solution. Importantly, the binding constant of 15-crown-5 with sodium ion should higher than that of 15-crown-5 with ammonium ion [82]. As anticipated, the crown ether group based **CC** preferably forms complex with ammonium ion of catecholamine.

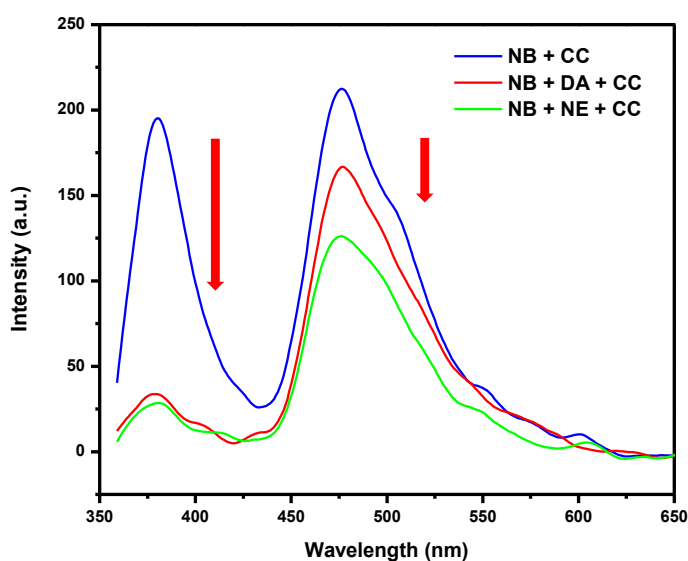


**Figure 4.23** Fluorescence spectra of sensor **NB** ( $1 \times 10^{-5}$  M) and sensor **CC** ( $5 \times 10^{-5}$  M) in 10% DMSO:phosphate buffer (0.1 M, pH 7.4) in the presence of **DA** or **NE** 100 equiv. ( $\lambda_{\text{ex}} = 340$  nm)

To differentiate the **DA** and **NE** by ratiometric FRET response, the emission band of sensor **NB** and sensor **CC** showed the different emission band at 384 nm and 490 nm, respectively. Upon the addition of **DA** or **NE**, the fluorescence intensity of both sensors was quenched possibly caused by PET process from phenyl donor group to naphthalimide and coumarin acceptor group as shown in Fig. 4.23. Considerably, the fluorescence change of the complex **NB-NE-CC** is slightly different from that of the complex **NB-DA-CC**. The fluorescence intensity at 490 nm corresponding to the complex of **NB-NE-CC** was more decreased than that of complex **NB-DA-CC**.

It implies that **NE** could bind strongly with sensors **NB** and **CC** than **DA** because the hydroxyl group of **NE** may form the hydrogen bonding with oxygen atom of coumarin.

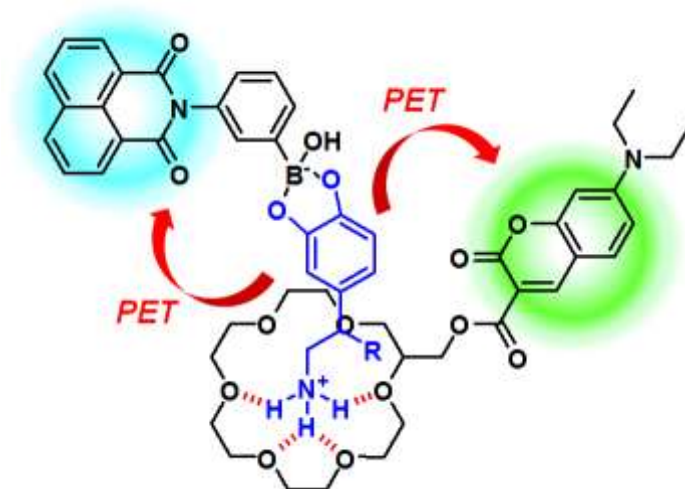


**Figure 4.24** The conceptually proposed structure and mechanism of **NB**-guest-**CC** complex under PET process

Unfortunately, the fluorescence change of these complexes did not undergo FRET mechanism. However, the self-coordination between sensor **NB** and sensor **CC** by the bridging analytes of **DA** or **NE** induced the different ratiometric fluorescence intensity of coumarin and naphthalimide ( $I_{\text{coumarin}}/I_{\text{naphthalimide}}$ ). As a result, the ratio of dual emission of complex **NB-DA-CC** of 4.84 showed a small larger than that observed for complex **NB-NE-CC** ( $R = 4.28$ ). Hence, this conceptual approach offers a differentiate-sensing purpose for **DA** and **NE**. (as shown in Fig 4.24)

To verify the selectivity of both sensors, the complexation of sensor **NB** and sensor **CC** toward 100 equiv. of various guests including **DA**, **NE**, **EPI**, **TY**, **Glu**, **Lys**, **His** and **Hist** was evaluated in 10% DMSO:phosphate buffer (0.1 M, pH 7.4). Fig. 4.25 suggested that the fluorescence spectra of sensor **NB** and sensor **CC** changed after adding **DA**, **NE**, **EPI** and **Hist**. The fluorescence changes of complex **NB-DA-CC** and **NB-NE-CC** was explained in previous mentioned above. Obviously, the emission band at 490 nm showed a small increase upon adding **Hist** because the

ammonium group of **Hist** could interact with crown ether of sensor **CC** by ion-dipole interaction.

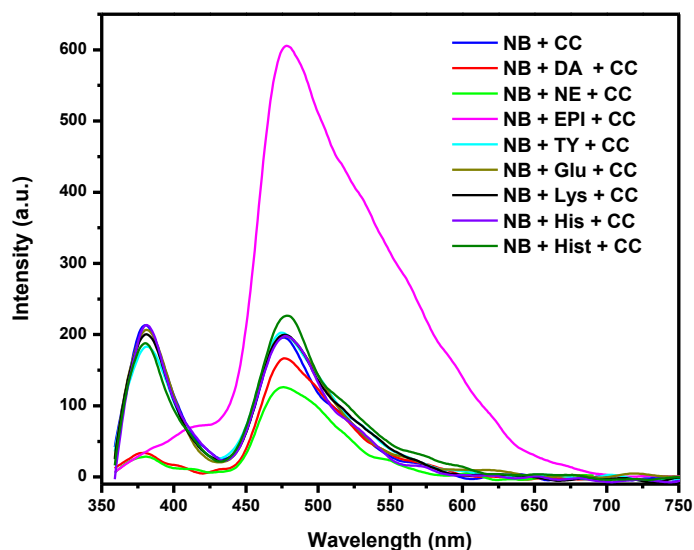


**Figure 4.25** Fluorescence spectra of sensor **NB** ( $1 \times 10^{-5}$  M) and sensor **CC** ( $5 \times 10^{-5}$  M) in 10% DMSO:phosphate buffer (0.1 M, pH 7.4) in the presence of various guest 100 equiv. ( $\lambda_{\text{ex}} = 340$  nm)

#### 4.3.9 Complexation studies of sensor **CC** with various guests by fluorescence spectrophotometry technique

To clarify the binding ability of sensor **CC** with various biogenic amines, the complex of sensor **CC** and analyte was investigated in aqueous media (10% DMSO: phosphate buffer pH 7.4). The fluorescence intensity at 475 nm was quenched in the case of **NE** possibly caused by the electron-rich aromatic ring of catecholamine in **NE** inducing PET process. Conversely, the case of **Hist** and **TY** enhanced slightly the fluorescence intensity of sensor **CC** as shown in Fig. 4.26.

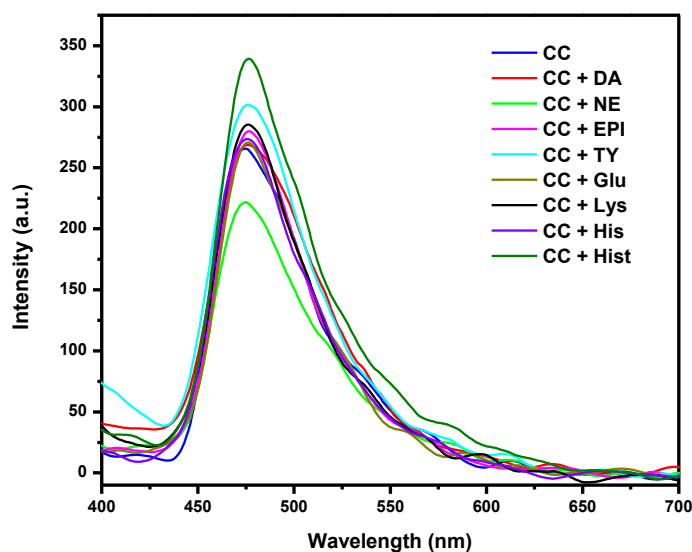


**Figure 4.26** Fluorescence spectra of sensor **CC** ( $5 \times 10^{-5}$  M) in 10% DMSO:phosphate buffer (0.1 M, pH 7.4) in the presence of various guests 100 equiv. ( $\lambda_{\text{ex}} = 340$  nm)

#### 4.3.10 Principle component analysis (PCA) method for analysis of complexation

To identify the type of catecholamine, our attempts were to clarify the fluorescence spectra of fluorescence sensor toward various catecholamines by using PCA method to reduce the dimensionality of data set for easier interpretation.

The PCA results for sensor **NB** with various biogenic amines in 10% DMSO:phosphate buffer (0.01 M, pH 7.4) presented 99.30% variance along PC1, while the vertical PC2 axis showed 0.65% variance as illustrated by Fig. 4.27a. This PCA plot exhibited a highly potential discrimination of **EPI** from other biogenic amines on the borderline between quadrant II and quadrant IV. Furthermore, the cluster of **DA** exhibited approximately the same classification as **NE** cluster. The clustering of other analytes existed an identical group of sensor **NB**. This implied that sensor **NB** cannot interact with amino acids. To determine the categorization performance, linear discriminant analysis (LDA) was used to show the classification

of the analytes. Cross-validated LDA exhibited 80% accurate classification for all 8 biogenic amines.

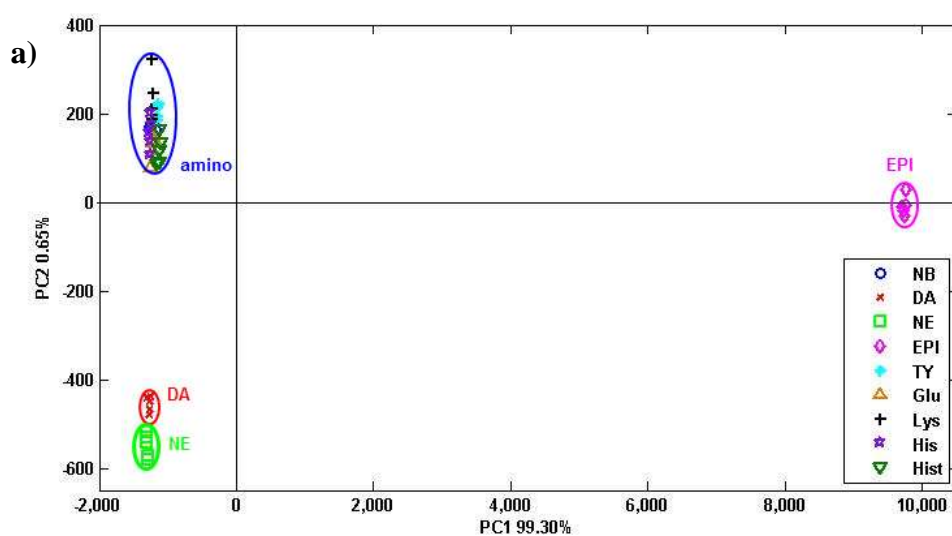
PCA score plot of sensor **CC** toward the analytes in 10% DMSO:phosphate buffer (0.1 M, pH 7.4) showed the variance along PC1 with 74.98% and vertical PC2 axis with 10.60% of variance (shown in Fig. 4.27b). This PCA score plot displayed the different discrimination from sensor **NB** with various guests pattern. Especially, the clusters of **TY** and **Lys** were separated from other guests at the same quadrant II. Moreover, the cluster of **Hist** exists at quadrant II was cross-validation LDA exhibits 62.22% precise discrimination in 45 cases.

From PCA score plot of sensor **CC** toward the analytes in Fig. 4.27b, sensor **CC** can definitely separate **NE** from **DA**. It can be explained that hydroxyl group of **NE** showed complementary binding between ammonium ions and crown ether of sensor **CC** whereas, aliphatic ammonium ion of **DA** is rather flexibility. Consequently, it seems that sensor **CC** cannot form complex with **DA**.

According to ability of sensor **NB** and sensor **CC** for discrimination of analytes, sensor **NB** is capable of binding selectivity with catecholamine because diol group of catecholamines can react with boronic acid of sensor **NB** through condensation reaction. The case of biogenic amine without diol group could not form complexes with sensor **NB**. In the case of sensor **CC**, It was capable of differentiation of biogenic amines including **NE**, **TY**, **Lys** and **Hist**. The complexation of sensor **CC** and **TY** was expected to be the ion-dipole interaction between ammonium ion and crown ether and  $\pi$ - $\pi$  stacking interaction of aromatic ring of **TY** and coumarin moiety. Although, the structure of **DA** was similar to **TY** but **DA** cannot interact with sensor **CC** possibly caused by the repulsion of electron rich on aromatic ring of **DA** and coumarin unit of sensor **CC**. For comparison between **Hist** and **His** analytes, the bulky carboxylic acid group adjacent amino group of **His** caused a decrease of binding ability of sensor **CC** with **His** while, **Hist** analyte can complex with sensor **CC**. Considering **Lys** and **Glu** amino acid, PCA score plot in Fig. 4.27b showed the separation of **Lys** in quadrant II, while **Glu** could not be separated from sensor **CC**. Due to the steric effect of aliphatic amino group on side chain of **Lys**.

From cross-validation LDA values, PCA score plot of sensor **NB** toward analytes show 80% of LDA accuracy which is higher than the cross-validation LDA of PCA score plot in case of sensor **CC** with 62% accuracy. This result implied that PCA score plot sensor **NB** is more reliably acceptable than that of sensor **CC**.

Since this work has focused on discrimination of catecholamine derivatives. To improve an efficiency of discrimination between **DA** and **NE**, the classification was developed by using two sensing elements including sensor **NB** and sensor **CC**. The PCA score plot for **NB-G-CC** showed 80.69% of variance along PC1 and the vertical PC2 axis exhibited 18.41% of the variation as illustrated in Fig. 4.27c. This LDA model showed excellent separation of the analyte with 86.67% accuracy in 45 cases. This PCA plot of two sensing elements exhibited a higher discrimination of **DA** and **NE** than that of a single sensor.



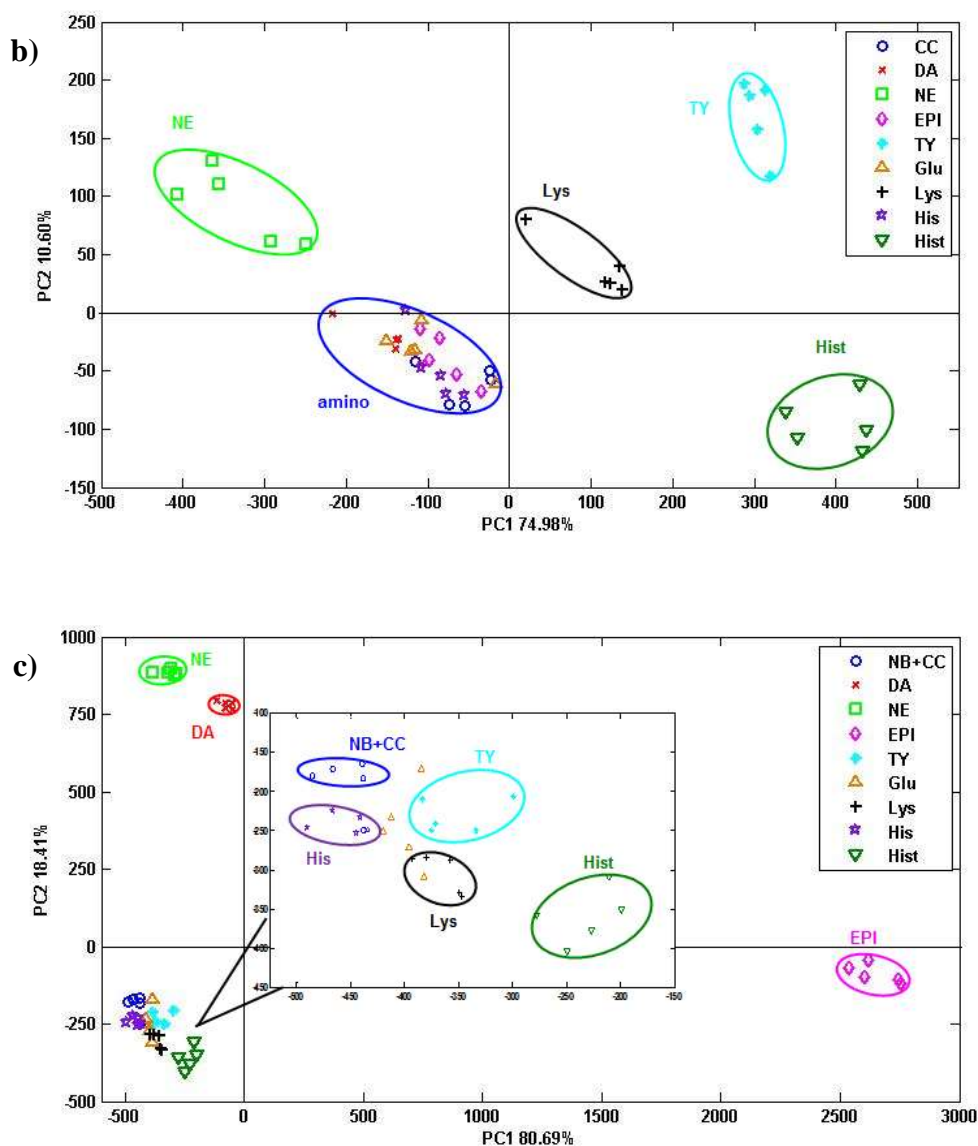


**Figure 4.27** PCA score plot of a) sensor **NB** b) sensor **CC** and c) the mixture sensors **NB** and **CC** upon addition of various guests (100 equiv.) in 10% DMSO:phosphate buffer. PCA score plot shows clustering for all 9 samples.

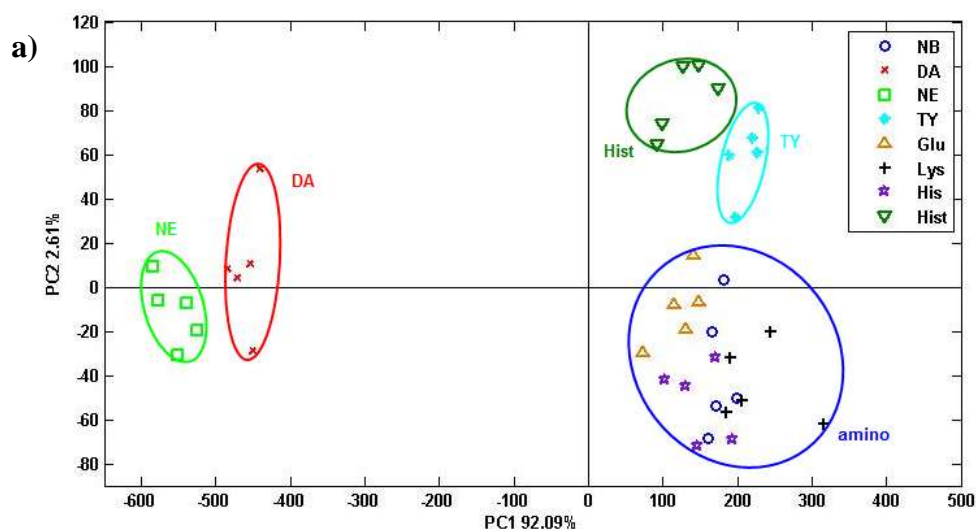
Because of the highly selective binding affinity of sensor **NB** with **EPI**, so, we have examined the clustering discrimination of other biogenic amines excluding **EPI**. Fig. 4.28a showed two dimensional score plot for two principal components (PC1 and PC2) representing 94.70% variance. The appearance of catecholamine clusters including **DA** and **NE** on the border line between quadrant I and quadrant III was separated from other biogenic amines while, the cluster of **Hist** and **TY** appeared in



quadrant II. This implied that the sensor **NB** can bind slightly with **Hist** and **TY**. Cross-validation LDA of this model showed 77.5% accurate discrimination for 7 biogenic amines.

In the case of sensor **CC**, It showed 86.67% variance for the first two PCs. This pattern can categorized **Lys** and **TY** in quadrant II and the cluster of **NE** and **Hist** appeared in quadrant I and quadrant IV, respectively, as depicted in Fig. 4.28b whereas, the sensor **CC** and amino cluster existed in quadrant III. Furthermore, this PCA pattern showed cross-validation LDA at 75% accuracy in 40 cases. However, the PCA pattern of sensor **CC** excluding **EPI** displayed a similar PCA pattern including **EPI**.

In our purposes to separate the similar structures of **DA** and **NE**, the fluorescence spectra of both sensor **NB** and sensor **CC** toward biogenic amines were classified by using PCA analysis. Two dimensional score plot for PC1 and PC2 representing 96.81% variance was illustrated in Fig. 4.28c. This PCA model demonstrated that two sensing elements of sensor **NB** and sensor **CC** could clearly differentiate the similar molecules of **DA** and **NE** in quadrant I and quadrant III, respectively. Hence, both sensors give a high performance for discrimination of **DA** and **NE** while, the **Hist** cluster appeared in quadrant II closed to the cluster of sensors and other biogenic amines. Moreover, cross-validation LDA exhibited 77.5% accuracy of discrimination for all 7 biogenic amines. Compared to the PCA score plot of two sensing elements excluding **EPI**, the values of accuracy discrimination of PCA score plot including **EPI** are higher.



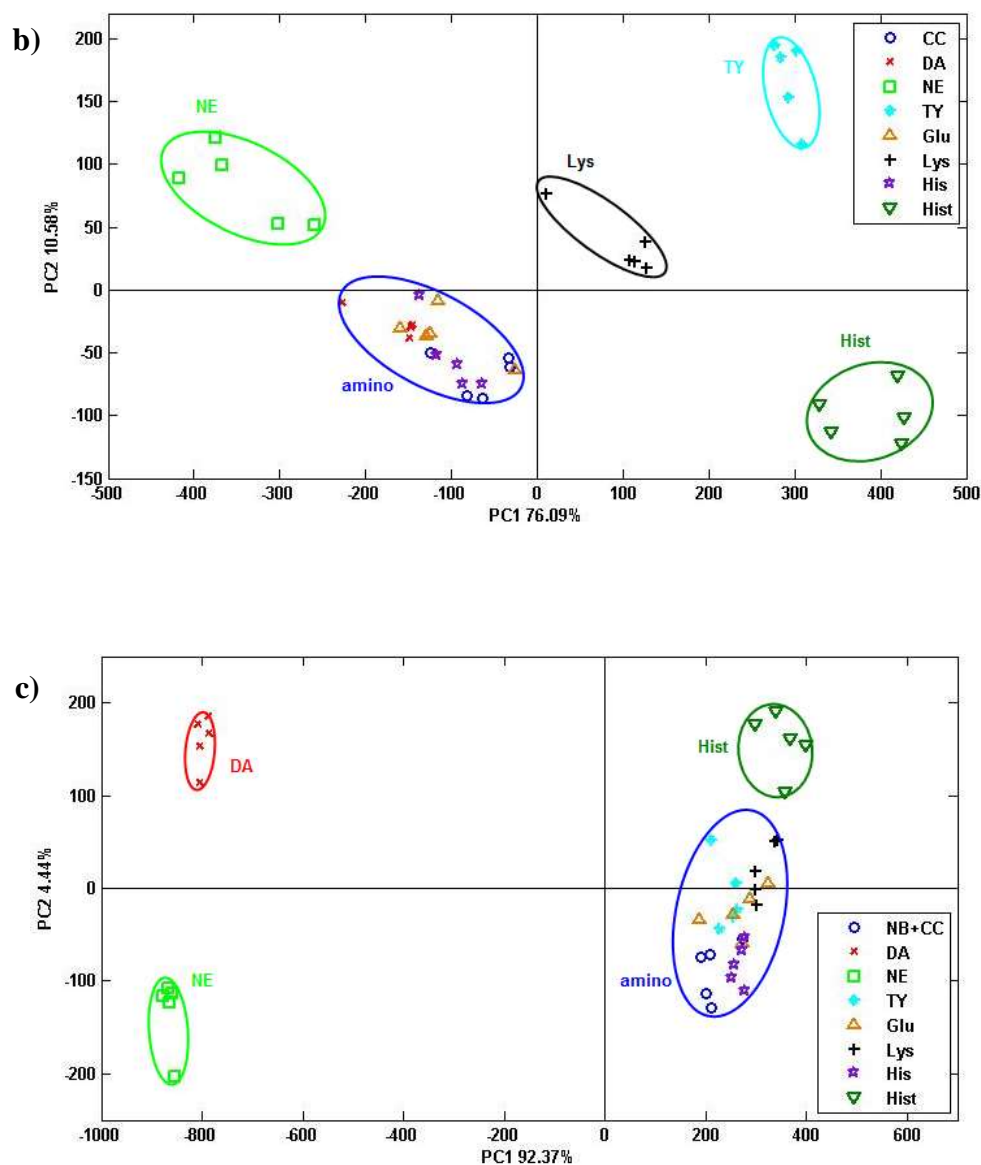


**Figure 4.28** PCA score plots of a) sensor **NB** b) sensor **CC** and c) sensors **NB** and **CC** upon addition of various guests (100 equiv.) in 10% DMSO:phosphate buffer and excluding fluorescence data of **EPI** for determining of PCA analysis

#### 4.3.11 Complexation study of sensor **NB** with **EPI** in human urine sample

To develop fluorescence sensor **NB** in the analytical application, we applied the detection of **EPI** in real biological system of human urine samples. A linear range was obtained by plotting the intensity of fluorescence at 490 nm versus the spiked various concentration of **EPI** in the synthetic urine as indicated in Fig. 4.29. The

spiked urine samples were prepared by the 100-fold diluted solution of urine by standard addition method. The % recovery for **EPI** at 40  $\mu\text{M}$  of the spiked solution is in the range of 100.14 to 101.06% which are the acceptable recovery in sensing application as displayed in Table 4.5. Therefore, the fluorescence sensor **NB** can serve as an effective sensing of **EPI** in analytical application of real samples.

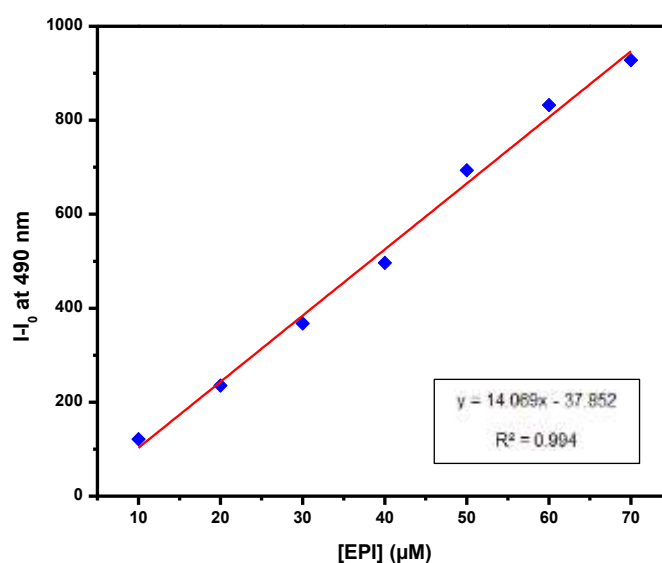


**Figure 4.29** Calibration curve of sensor **NB** with the spiked **EPI** in the synthetic urine

**Table 4.5** Results for the determination of **EPI** in human urine samples

samples	spiked amount ( $\mu\text{M}$ )	found amount <sup>a</sup> ( $\mu\text{M}$ )	recovery <sup>a</sup> (%)
human urine-1	40	40.05 $\pm$ 1.09	100.14 $\pm$ 2.74
human urine-2	40	40.42 $\pm$ 1.74	101.06 $\pm$ 4.34

<sup>a</sup> mean  $\pm$  std, n = 3

#### 4.3.12 Complexation study of sensor NB and sensor CC with NE by mass spectroscopy

To verify the complex of sensor **NB** and sensor **CC** with **NE** analyte, MALDI-TOF mass spectra in Fig. 4.30 exhibited a small peak of  $m/z$   $[\text{NB-NE-CC}+\text{CH}_3\text{OH}]^+$  at 1035.742 and the form of  $m/z$   $[\text{NB-NE-CC}+1/2\text{CH}_3\text{OH}]^+$  at 1019.797 corresponding to exact mass of **NB-NE-CC** complex at 1005.410  $m/z$ . This mass spectra result supported the complex of **NB-NE-CC** as our hypothesis.

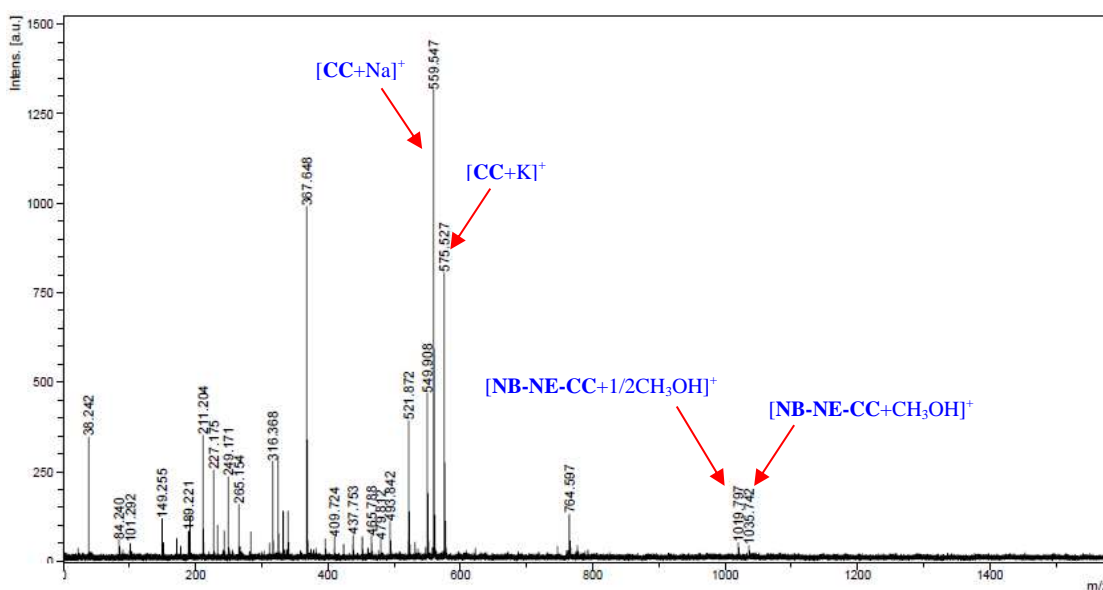


**Figure 4.30** MALDI-TOF mass spectrum of 1:1:1 complex of **NB-NE-CC** in 5%  $\text{D}_2\text{O}:\text{DMSO}$  and 5 mM NaOH

## CHAPTER V

### CONCLUSION

#### 5.1 Conclusion

As objective of the determination of catecholamine neurotransmitters, we have designed and synthesized the sensory molecules containing fluorophore as a signaling unit and binding site to bind with biogenic amines. The sensor **NB** containing a naphthalimide and boronic acid have been synthesized from 3-aminophenylboronic acid hemisulfate and 1,8 naphthalimide dicarboxylic by nucleophilic substitution reaction to give a light yellow solid with 56% yield. A novel sensor **CC** consists of coumarin and crown ether moiety that has been successfully synthesized by nucleophilic substitution reaction in the last step to obtain the brown oil with 62% yield. The chemosensory structures were characterized by spectroscopy techniques.

Initially, the complexing abilities of sensor **NB** toward several biogenic amines including **DA**, **NE**, **EPI**, **TY**, **Glu**, **Lys**, **His** and **Hist** in aqueous solution were studied by fluorescence spectrophotometry. The emission spectra of sensor **NB** exhibited the fluorescence quenching at 384 nm after addition of **DA** or **NE** possibly caused by PET mechanism. For **EPI** analyte, the fluorescence intensity at 384 nm of sensor **NB** was decreased and a new strong emission band at 490 nm was developed. This suggested that sensor **NB** showed a specific binding with catecholamine analytes. The Job's plot method for the binding mode between sensor **NB** and three catecholamine types suggests a 1:1 stoichiometry. The  $\log K_s$  values of sensor **NB** toward **DA**, **NE** and **EPI** were 4.01, 4.08 and 3.00, respectively, evaluated by fluorescence titration. The detection limit of **DA**, **NE** and **EPI** for sensor **NB** was 7.71, 8.50 and 1.54  $\mu\text{M}$ , respectively. Moreover, we have achieved to apply this sensor on solid support for **EPI** sensing purpose.

In the case of sensor **CC** expected as an acceptor part, the study of complexation between sensor **CC** and the biogenic amines showed a fluorescence quenching at 490 nm after adding **NE**, while the addition of **Hist** and **TY** caused the fluorescent enhancement at 490 nm.

Our important objective is discrimination of catecholamine types. Two sensing elements comprising **NB** and **CC** can successfully differentiate **DA** or **NE** under PET process. Ratiometric fluorescence sensor **NB** and sensor **CC** displayed the emission ratio ( $I_{490}/I_{384}$ ) of **NB-DA-CC** and **NB-NE-CC** complexes as 4.84 and 4.28, respectively. The complexation structure of **NB-NE-CC** was confirmed by mass spectroscopy showing a small peak of  $m/z$  [**NB-NE-CC+CH<sub>3</sub>OH**]<sup>+</sup> at 1035.742 and the form of  $m/z$  [**NB-NE-CC+1/2CH<sub>3</sub>OH**]<sup>+</sup> at 1019.797.

Moreover, the PCA analysis was utilized for increasing an ability of classification by the combinatorial data of fluorescence spectra obtained from one or two sensors in aqueous media with 8 biogenic amines. For discrimination of biogenic amines including **EPI**, the cross-validation LDA of sensor **NB** and sensor **CC** with analytes displayed 86.67% accuracy more than a single sensor **NB** or **CC** toward biogenic amines showing 62% and 62.22% precision, respectively. In the case of excluding **EPI** study, PCA score plot of both sensors **NB** and **CC** toward analytes obviously separated **DA** and **NE** in the different quadrant, whereas the single sensor **NB** differentiated **DA** and **NE** in the same quadrant. Therefore, the cooperative function of sensor **NB** and sensor **CC** can discriminate **DA** and **NE** better than a single sensing element.

For analytical application of human urine sample, chemosensor **NB** offers a good result for detection of **EPI**. The % recovery for **EPI** exhibited the range of 100.14% to 101.06% that are acceptable recovery in sensing application.

## 5.2 Future work

The study of interactive position of sensors **NB** and **CC** with catecholamine analytes will be verified by computational method.

## REFERENCES

- [1] Lehn, J. M. Supramolecular chemistry concepts and perspective. Weinheim : Wiley-VCH, 1995.
- [2] Steed, J. W., Turner, D.R., and Wallace, K.J. Core concepts in supramolecular chemistry and nanochemistry. New York : John Wiley & Sons, 2007.
- [3] Ariga, K., and Kunitake, T. Supramolecular chemistry fundamentals and application. New York : Springer-Verlag Heidelberg, 2006.
- [4] Steed, J. W., and Atwood, J. L. Supramolecular chemistry. London : Wiley & sons, 2000.
- [5] James, T. D. Saccharide-selective boronic acid based photoinduced electron transfer (PET) fluorescent sensors. Topics in Current Chemistry 277 (2007) : 107-152.
- [6] Lakowicz, J. R. Principle of fluorescence spectroscopy. New York : Springer, 2006.
- [7] Value, B. Molecular fluorescence principle and application. New York : Wiley-VCH, 2001.
- [8] Anslyn, E. V. Supramolecular analytical chemistry. The Journal of Organic Chemistry 72 (2007) : 687-699.
- [9] Beer, P. D. Transition-metal receptor systems for the selective recognition and sensing of anionic guest species. Accounts of Chemical Research 31 (1988) : 71-80.
- [10] Ellis, A. B., and Walt, D. R. Guest editorial. Chemical Reviews 100 (2000) : 2477-2478.
- [11] De Silva, A. P., Gunaratne, H. Q. N., Gunnlauugsson, T., Huxley, A. J. M., McCoy, C. P., Rademacher, J. T., and Rice, T. E. Signaling recognition events with fluorescent sensors and switches. Chemical Reviews 97 (1997) : 1515-1566.
- [12] Prodi, L., Bolletta, F., Montalti, M., and Zaccheroni, N. Luminescent chemosensors for transition metal ions. Coordination Chemistry Reviews 205 (2000) : 59-83.

- [13] Bargossi, C., Fiorini, M. C., Montalti, M., Prodi, L., and Zaccheroni, N. Recent developments in transition metal ion detection by luminescent chemosensors. Coordination Chemistry Reviews 208 (2000) : 17-32.
- [14] Kaur, N., and Kumar, S. Colorimetric metal ion sensors. Tetrahedron 67 (2001) : 9233-9264.
- [15] Lakowicz, J. R. Principle of fluorescence spectroscopy. 3<sup>rd</sup> ed. New York : Springer Science, 2006.
- [16] McCarrick, M., Wu, B., Harris, S. J., Diamond, D., Barrett, G., and McKervey, M. A. Novel chromogenic ligands for lithium and sodium based on calix[4]arene tetraesters. Journal of the Chemical Society, Chemical Communications (1992) : 1287-1289.
- [17] Kim, J. S., and Quang, D. T. Calixarene-derived fluorescent probes. Chemical Reviews 107 (2007) : 3780-3799.
- [18] Aoki, I., Kawabata, H., Nakashima, K., and Shinkai, S. Fluorescent calix[4]arene which responds to solvent polarity and metal ions. Journal of the Chemical Society, Chemical Communications (1991) : 1771-1773.
- [19] Ji, H.-F., Dabestani, R., Brown, G. M., and Sachleben, R. A. A new highly selective calix[4]crown-6 fluorescent caesium probe. Chemical Communications (2000) : 833-834.
- [20] Ji, H.-F., Brown, G. M., and Dabestani, R. Calix[4]arene-based Cs<sup>+</sup> selective optical sensor. Chemical Communications (1999) : 609-610.
- [21] Martínez-Mañez, R., and Sancenón, F. Fluorogenic and chromogenic chemosensors and reagents for anions. Chemical Reviews 103 (2003) : 4419-4476.
- [22] The Photochemistry portal, Luminescent PET Sensors [Online]. 2009. Available from <http://photochemistryportal.net/home/index.php/2009/08/22/luminescent-pet-sensors/> [2009, August 22].
- [23] Valeur, B., and Leray, I. Design principles of fluorescent molecular sensors for cation recognition. Coordination Chemistry Reviews 205 (2000) : 3-40.
- [24] Valeur, B., Bourson, J., Pouget, J., and Czarnik, A. W. Fluorescent chemosensors for ion and molecule recognition. Washington, DC : American Chemical Society, 1993.



- [25] Rettig, W., and Lapouyade, R. In probe design and chemical sensing. New York : Plenum, 1994.
- [26] Loehr, H. G., and Voegtle, F. Chromo- and fluoroionophores. A new class of dye reagents. Accounts of Chemical Research 18 (1985) : 65-72.
- [26] Lakowicz, J. R. Principles of fluorescence spectroscopy. New York : Plenum Publishers Corp, 1999.
- [27] Stryer, L., and Haugland, R. P. Energy Transfer: a spectroscopic ruler. Proceedings of The National Academy of Sciences of The United States of America 58 (1967) : 719-726
- [28] Chemwiki, Fluorescence Resonance Energy Transfer [Online]. 2013. Available from [http://chemwiki.ucdavis.edu/Theoretical\\_Chemistry/Fundamentals/Fluorescence\\_Resonance\\_Energy\\_Transfer](http://chemwiki.ucdavis.edu/Theoretical_Chemistry/Fundamentals/Fluorescence_Resonance_Energy_Transfer) [2013, March]
- [29] Connors, K. A. Binding constant: The measurement of molecular complex stability. Canada : John Wiley & Sons, 1987.
- [30] Bourson, J., and Valeur, B. Ion-responsive fluorescent compounds. 2. Cation-steered intramolecular charge transfer in a crowned merocyanine. The Journal of Physical Chemistry 93 (1989) : 3871-3876.
- [31] Miller, J. N., and Miller, J. C. Statistic and chemometric for analytical chemistry. Harrow : Prentice Hall, 2000.
- [32] Brereton, G. K. Chemometrics data analysis for the laboratory and chemical plant. England : John Wiley & Sons, 2003.
- [33] Böhm, K., Smidt, E., and Tintner, J. Application of multivariate data analyses in waste management. 2013.
- [34] Castro-Suarez, J. R., Ortiz-Rivera, W., Galan-Freyte, N., Figueroa-Navedo, A., Pacheco-Londoño, L. C. and Hernández-Rivera, S. P. Multivariate analysis in vibrational spectroscopy of highly energetic materials and chemical warfare agents simulants. 2013.
- [35] Matthias Scholz. Approaches to analyse and interpret biological profile data. Doctoral dissertation, Potsdam University, Germany, 2006.
- [36] Jackson, D. M., and Westlind-Danielsson, A. Dopamine receptors: Molecular biology, biochemistry and behavioural aspects. Pharmacology & Therapeutics 64 (1994) : 291-370.

- [37] Strange, P. G. Dopamine receptors: Studies on structure and function. In T. Bernard and A. M. Urs (ed.), Advances in Drug Research, pp. 313-351. : Academic Press, 1996.
- [38] Kar, A. Principles of medicinal chemistry. 3<sup>rd</sup> ed, New Delhi : New Age International (P) Ltd, 2005.
- [39] Simpkins, J. W., Bodor, N., and Enz, A. Direct evidence for brain-specific release of dopamine from a redox delivery system. Journal of Pharmaceutical Sciences 74 (1985) : 1033-1036.
- [40] Wu, H.-P., Cheng, T.-L., and Tseng, W.-L. Phosphate-modified TiO<sub>2</sub> nanoparticles for selective detection of dopamine, levodopa, adrenaline, and catechol based on fluorescence quenching. Langmuir 23 (2007) : 7880-7885.
- [41] Nishiyabu, R., Kubo, Y., James, T. D., and Fossey, J. S. Boronic acid building blocks: Tools for sensing and separation. Chemical Communications 47 (2011) : 1106-1123.
- [42] Liew, F. F., Hasegawa, T., Fukuda, M., Nakata, E., and Morii, T. Construction of dopamine sensors by using fluorescent ribonucleopeptide complexes. Bioorganic & Medicinal Chemistry 19 (2011) : 4473-4481.
- [43] Liu, C.-H., Yu, C.-J., and Tseng, W.-L. Fluorescence assay of catecholamines based on the inhibition of peroxidase-like activity of magnetite nanoparticles. Analytica Chimica Acta 745 (2012) : 143-148.
- [44] Guo, Z., Shin, I., and Yoon, J. Recognition and sensing of various species using boronic acid derivatives. Chemical Communications 48 (2012) : 5956-5967.
- [45] dos Santos, M. P., Rahim, A., Fattori, N., Kubota, L. T., and Gushikem, Y. Novel amperometric sensor based on mesoporous silica chemically modified with ensal copper complexes for selective and sensitive dopamine determination. Sensors and Actuators B: Chemical 171-172 (2012) : 712-718.
- [46] Abbaspour, A., and Noori, A. A cyclodextrin host-guest recognition approach to an electrochemical sensor for simultaneous quantification of serotonin and dopamine. Biosensors and Bioelectronics 26 (2011) : 4674-4680.

- [47] Goldstein, D. S., Eisenhofer, G., and McCarty, R. Catecholamines: Bridging basic science with clinical medicine. San Diego : Academic Press, 1998.
- [48] Kimura, E., Watanabe, A., and Kodama, M. A catechol receptor model by macrocyclic polyamines. Journal of the American Chemical Society 105 (1983) : 2063-2066.
- [49] Young, T. E., and Babbitt, B. W. Electrochemical study of the oxidation of  $\alpha$ -methyldopamine,  $\alpha$ -methylnoradrenaline, and dopamine. The Journal of Organic Chemistry 48 (1983) : 562-566.
- [50] Strawbridge, S. M., Green, S. J., and Tucker, J. H. R. Electrochemical detection of catechol and dopamine as their phenylboronate ester derivatives. Chemical Communications (2000) : 2393-2394.
- [51] Paugam, M.-F., Valencia, L. S., Boggess, B., and Smith, B. D. Selective dopamine transport using a crown boronic acid. Journal of the American Chemical Society 116 (1994) : 11203-11204.
- [52] Kim, J., Raman, B., and Ahn, K. H. Artificial receptors that provides a preorganized hydrophobic environment: A biomimetic approach to dopamine recognition in water. The Journal of Organic Chemistry 71 (2005) : 38-45.
- [53] Secor, K. E., and Glass, T. E. Selective Amine recognition: Development of a chemosensor for dopamine and norepinephrine. Organic Letters 6 (2004), 3727-3730.
- [54] Wu, Z., Li, M., Fang, H., and Wang, B., A new boronic acid based fluorescent reporter for catechol. Bioorganic & Medicinal Chemistry Letters 22 (2012) : 7179-7182
- [55] Jang, Y. J., Jun, J. H., Swamy, K. M. K., Nakamura, K., Koh, H. S., Yoon, Y. J., and Yoon, J. Fluorescence sensing of dopamine. Bulletin of the Korean Chemical Society 26 (2005) : 2041-2043.
- [56] Coskun, A., and Akkaya, E. U. Three-point recognition and selective fluorescence sensing of L-DOPA. Organic Letters 6 (2004) : 3107-3109.
- [57] Raymo, F. M., and Cejas, M. A. Supramolecular association of dopamine with immobilized fluorescent probes. Organic Letters 4 (2002) : 3183-3185.

- [58] Kolusheva, S., Molt, O., Herm, M., Schrader, T., and Jelinek, R. Selective detection of catecholamines by synthetic receptors embedded in chromatic polydiacetylene vesicles. Journal of the American Chemical Society 127 (2005) : 10000-10001.
- [60] Tao, Y., Lin, Y., Ren, J., and Qu, X. A dual fluorometric and colorimetric sensor for dopamine based on BSA-stabilized Au nanoclusters. Biosensors and Bioelectronics 42 (2013) : 41-46.
- [61] Tsien, R. Y., and Poenie, M. Fluorescence ratio imaging: a new window into intracellular ionic signaling. Trends in Biochemical Sciences 11 (1986) : 450-455.
- [62] He, G., Zhang, X., He, C., Zhao, X., and Duan, C. Ratiometric fluorescence chemosensors for copper(II) and mercury(II) based on FRET systems. Tetrahedron 66 (2010) : 9762-9768.
- [63] Royzen, M., Dai, Z., and Canary, J. W. Ratiometric displacement approach to Cu(II) sensing by fluorescence. Journal of the American Chemical Society 127 (2005) : 1612-1613.
- [64] Guliyev, R., Coskun, A., and Akkaya, E. U. Design strategies for ratiometric chemosensors: Modulation of excitation energy transfer at the energy donor site. Journal of the American Chemical Society 131 (2009) : 9007-9013.
- [65] Lee, S. Y., Kim, H. J., Wu, J. S., No, K., and Kim, J. S. Metal ion-induced FRET modulation in a bifluorophore system. Tetrahedron Letters 49 (2008) : 6141-6144.
- [66] Xu, Z., Qian, X., and Cui, J. Colorimetric and ratiometric fluorescent chemosensor with a large red-shift in emission: Cu(II)-only sensing by deprotonation of secondary amines as receptor conjugated to naphthalimide fluorophore. Organic Letters 7 (2005) : 3029-3032.
- [67] Guo, Z., Zhu, W., Shen, L., and Tian, H. A fluorophore capable of crossword puzzles and logic memory. Angewandte Chemie - International Edition 46 (2007) : 5549-5553.

- [68] Yu, H., Fu, M., and Xiao, Y. Switching off FRET by analyte-induced decomposition of squaraine energy acceptor: A concept to transform ‘turn off’ chemodosimeter into ratiometric sensors. Physical Chemistry Chemical Physics 12 (2010) : 7386-7391.
- [69] Adams, S. R., Harootunian, A. T., Buechler, Y. J., Taylor, S. S., and Tsien, R. Y. Fluorescence ratio imaging of cyclic AMP in single cells. Nature 349 (1991) : 694-697.
- [70] Lee, M. H., Quang, D. T., Jung, H. S., Yoon, J., Lee, C.-H., and Kim, J. S. Ion-induced FRET on-off in fluorescent calix[4]arene. The Journal of Organic Chemistry 72 (2007) : 4242-4245.
- [71] Zhang, X., Xiao, Y., and Qian, X. A ratiometric fluorescent probe based on FRET for imaging  $\text{Hg}^{2+}$  ions in living cells. Angewandte Chemie - International Edition 47 (2008) : 8025-8029.
- [72] Zhou, Z., Yu, M., Yang, H., Huang, K., Li, F., Yi, T., and Huang, C. FRET-based sensor for imaging chromium(III) in living cells. Chemical Communications (2008) : 3387-3389.
- [73] Jisha, V. S., Thomas, A. J., and Ramaiah, D. Fluorescence ratiometric selective recognition of  $\text{Cu}^{2+}$  ions by dansyl–naphthalimide dyads. The Journal of Organic Chemistry 74 (2009) : 6667-6673.
- [74] Lee, K. R., and Kang, I.-J. Effects of dopamine concentration on energy transfer between dendrimer–QD and dye-labeled antibody. Ultramicroscopy 109 (2009) : 894-898.
- [75] Kuhar, M. J., Couceyro, P. R., and Lambert, P. D. Biosynthesis of Catecholamines. In G. J. Siegel, B. W. Agranoff, R. W. Albers, et al. (ed.), Basic neurochemistry: Molecular, cellular and medical aspects, 6<sup>th</sup> ed. Philadelphia : Lippincott-Raven, 1999.
- [76] Sornkrit Marbumrung. BF<sub>2</sub>-Curcumin-based and Anthraquinone Imidazole-based Sensors for Detection of Nucleotides. Doctoral dissertation, Department of Chemistry, Faculty of Science, Chulalongkorn University, 2011.
- [77] Tilley, E., Atwater, J., and Mavinic, D. Effects of storage on phosphorus recovery from urine. Environmental Technology 29 (2007) : 807-816.

- [78] James, T.D., and Phillips M. D. and Shinkai, S. Boronic acid in saccharide recognition. London : The Royal Society of Chemistry, 2006.
- [79] Steed, J. W., and Atwood, J. L. Supramolecular chemistry. 2<sup>nd</sup> ed. Wilshire : Anthony Rowe Ltd, 2009.
- [75] Kuhar, M. J., Couceyro, P. R., and Lambert, P. D. Biosynthesis of Catecholamines. In G. J. Siegel, B. W. Agranoff, R. W Albers, et al. (ed.), Basic neurochemistry: Molecular, cellular and medical aspects, 6th ed. Philadelphia : Lippincott-Raven, 1999.
- [80] Bosch, L. I., Mahon, M. F., and James, T. D. The B–N bond controls the balance between locally excited (LE) and twisted internal charge transfer (TICT) states observed for aniline based fluorescent saccharide sensors. Tetrahedron Letters 45 (2004) : 2859-2862.
- [81] de Champlain, J., Farley, L., Cousineau, D., and van Ameringen, M. R. Circulating catecholamine levels in human and experimental hypertension. Circulation Research 38 (1976) : 109-114.
- [82] Wang, Z., Chang, S. H., and Kang, T. J. Cation complexation behavior of pyrene- and anthracene-appended new crown ether derivatives. Spectrochimica Acta Part A: Molecular and Biomolecular Spectroscopy 70 (2008) : 313-317.

## **APPENDIX**

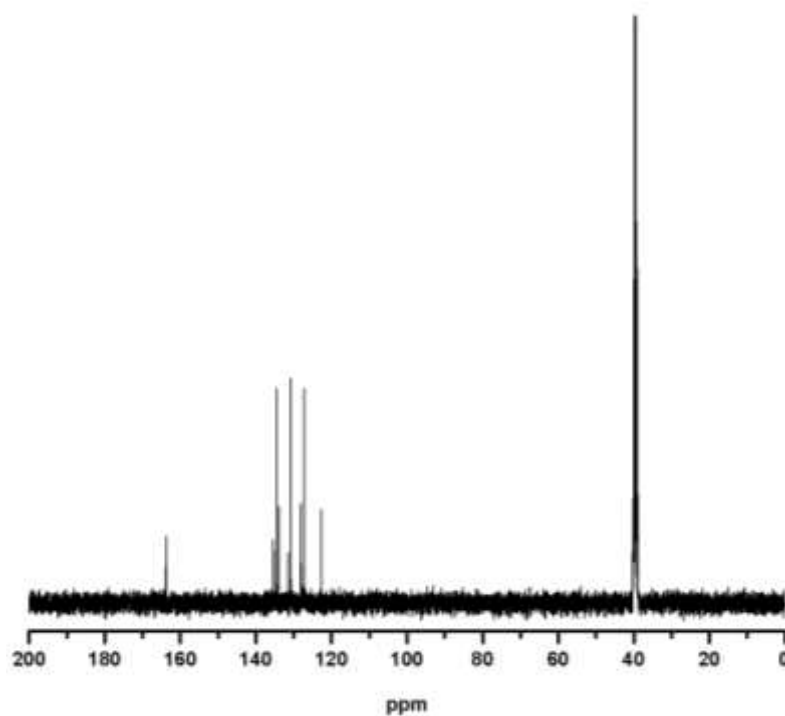


**Figure A1** The  $^{13}\text{C}$ -NMR spectrum of sensor **NB** in  $\text{DMSO-}d_6$  at 400 MHz

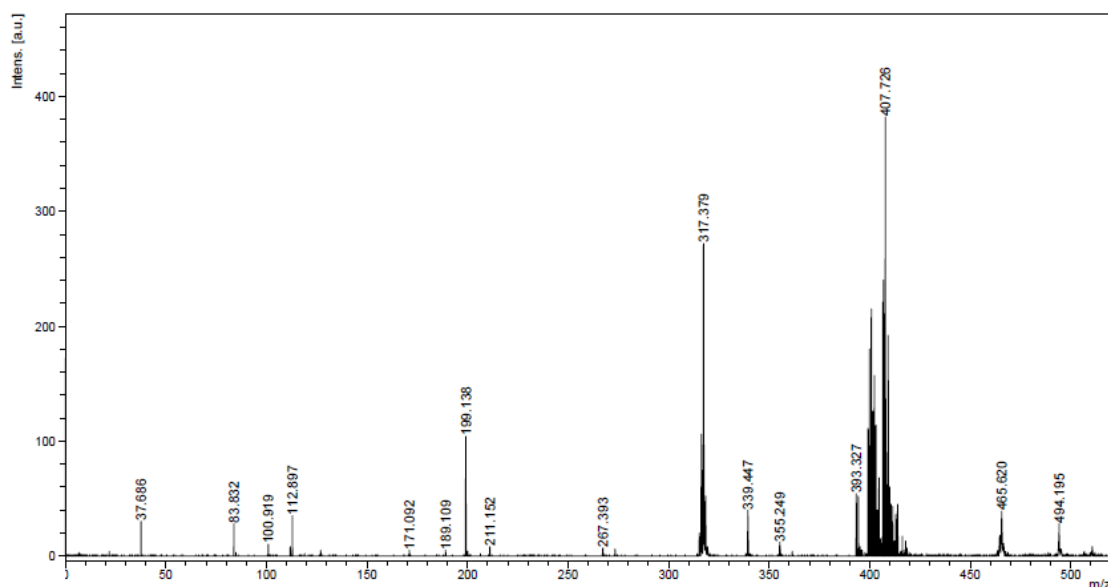


**Figure A2** MALDI-TOF mass spectrum of sensor **NB** shown at 317.379 m/z



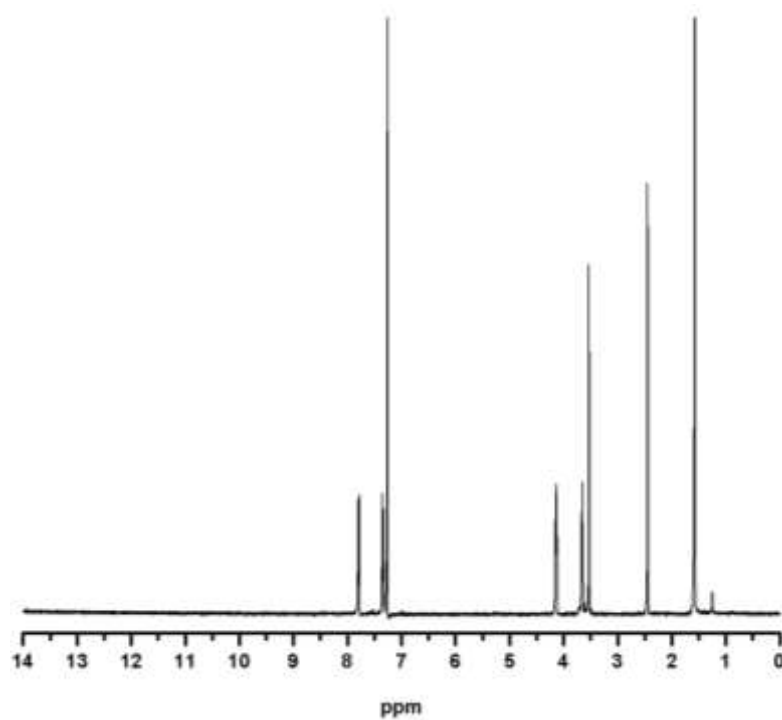


**Figure A3** The  $^1\text{H-NMR}$  spectrum of **1** in  $\text{CDCl}_3$  at 400 MHz

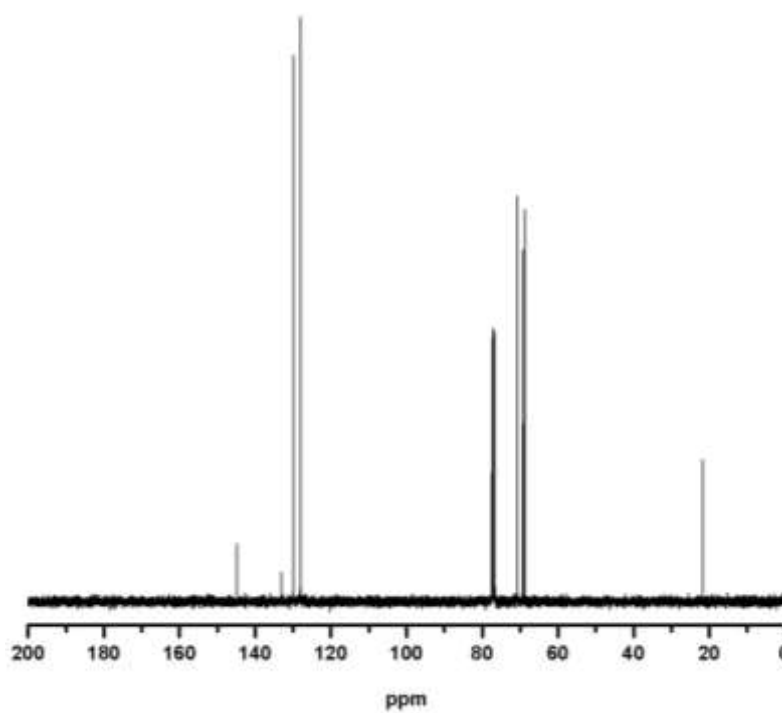


**Figure A4** The  $^{13}\text{C-NMR}$  spectrum of **1** in  $\text{CDCl}_3$  at 400 MHz

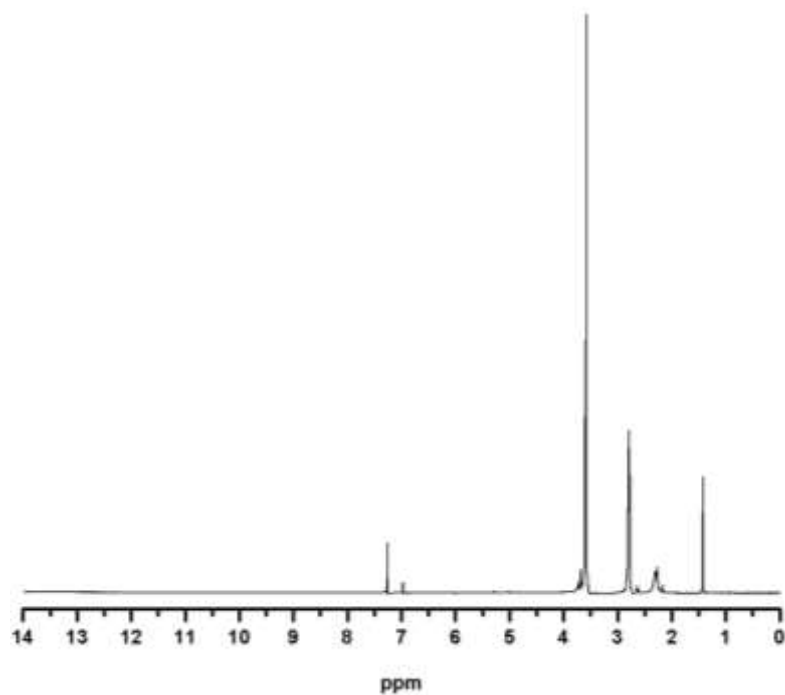


**Figure A5** The  $^1\text{H-NMR}$  spectrum of **2** in  $\text{CDCl}_3$  at 400 MHz

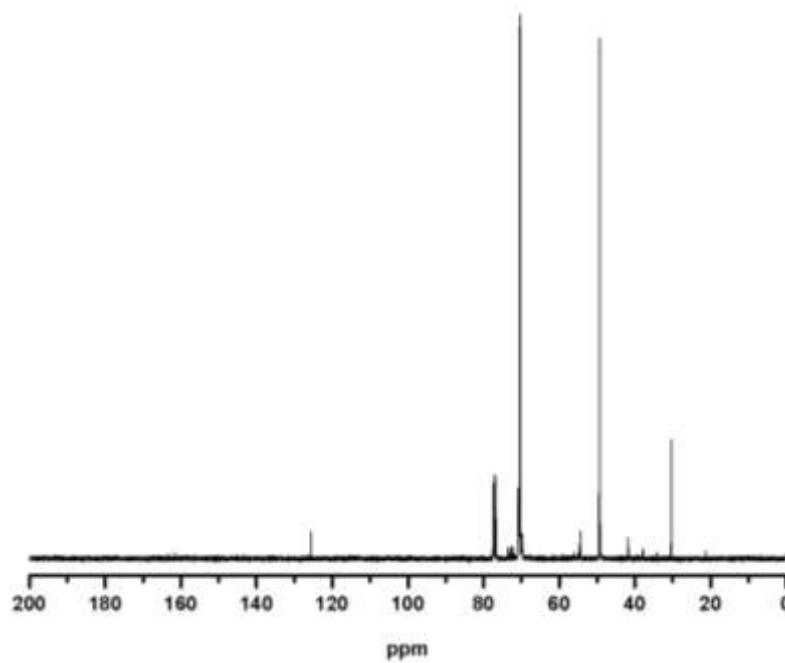


**Figure A6** The  $^{13}\text{C-NMR}$  spectrum of **2** in  $\text{CDCl}_3$  at 400 MHz

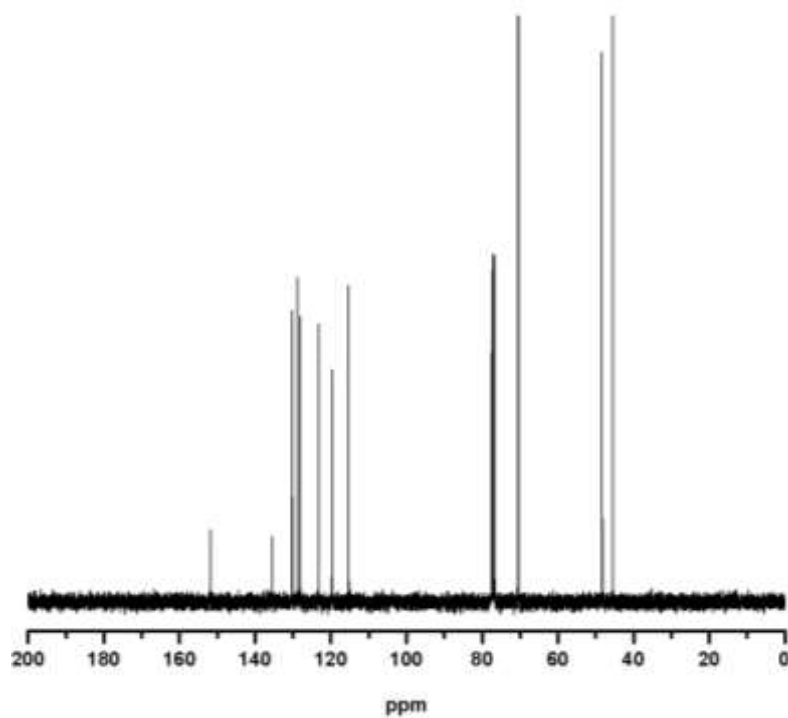


**Figure A7** The  $^{13}\text{C}$ -NMR spectrum of sensor **DC** in  $\text{CDCl}_3$  at 400 MHz

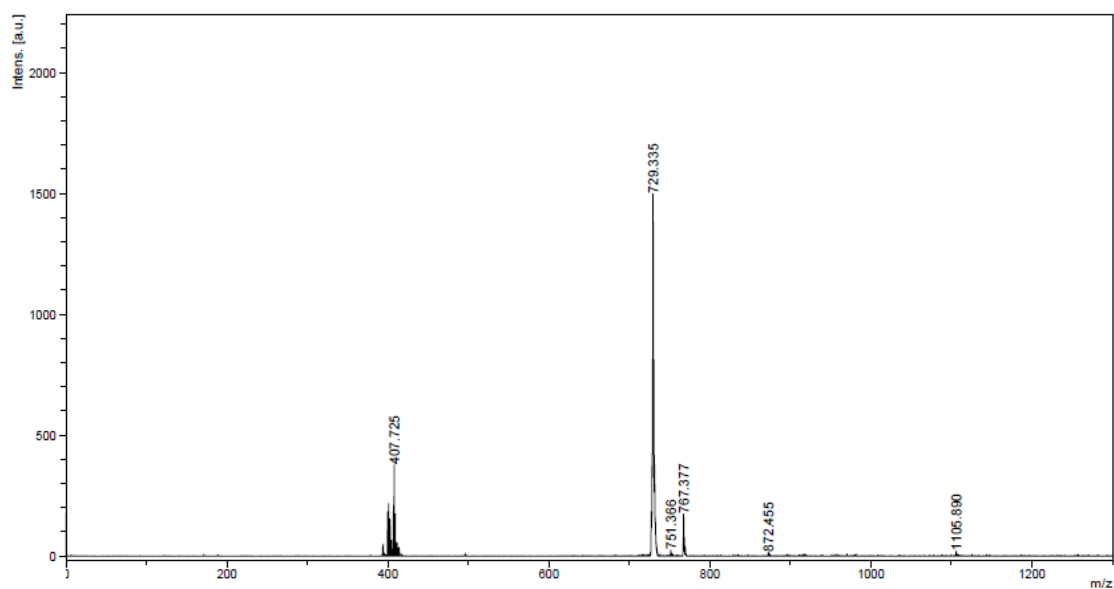


**Figure A8** MALDI-TOF mass spectrum of sensor **DC** shown at 729.335 m/z

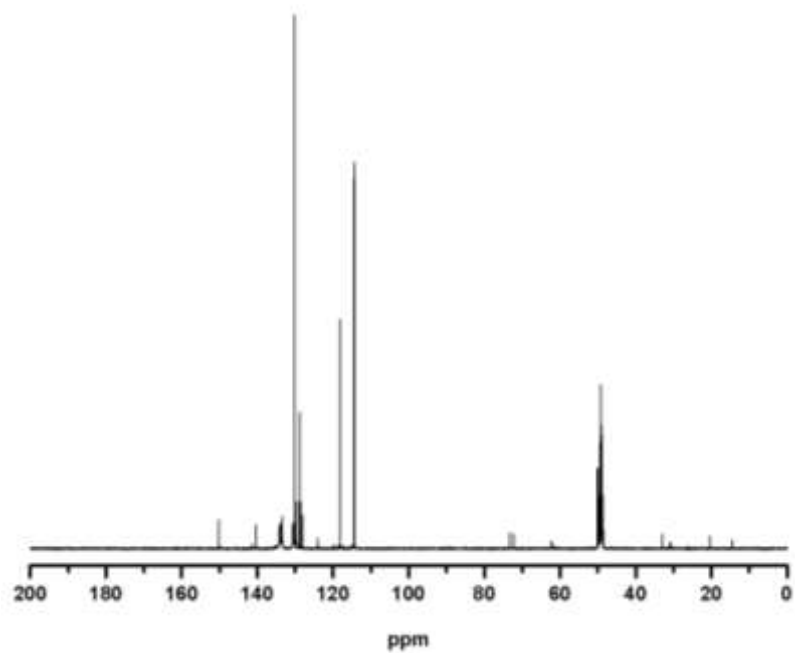


**Figure A9** The  $^{13}\text{C}$ -NMR spectrum of sensor *m*-BA in  $\text{CD}_3\text{OD}$  at 400 MHz

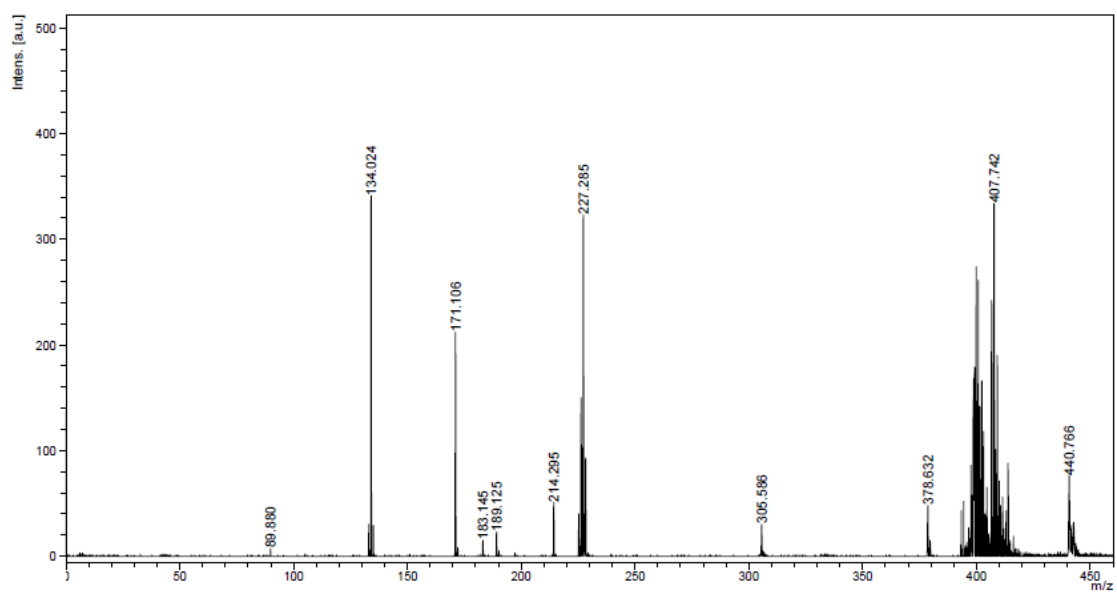


**Figure A10** MALDI-TOF mass spectrum of sensor *m*-BA shown at 227.285 m/z

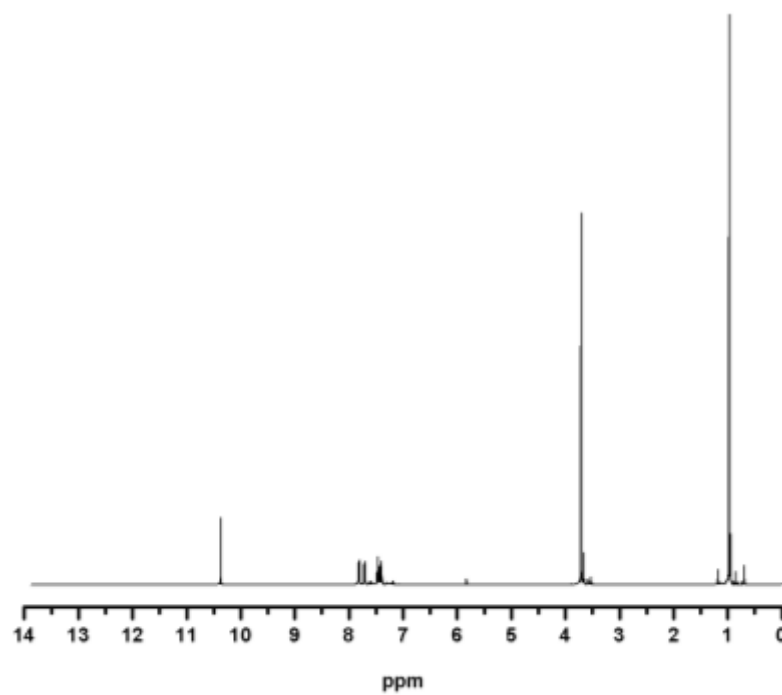


**Figure A11** The  $^1\text{H-NMR}$  spectrum of **3** in  $\text{CDCl}_3$  at 400 MHz

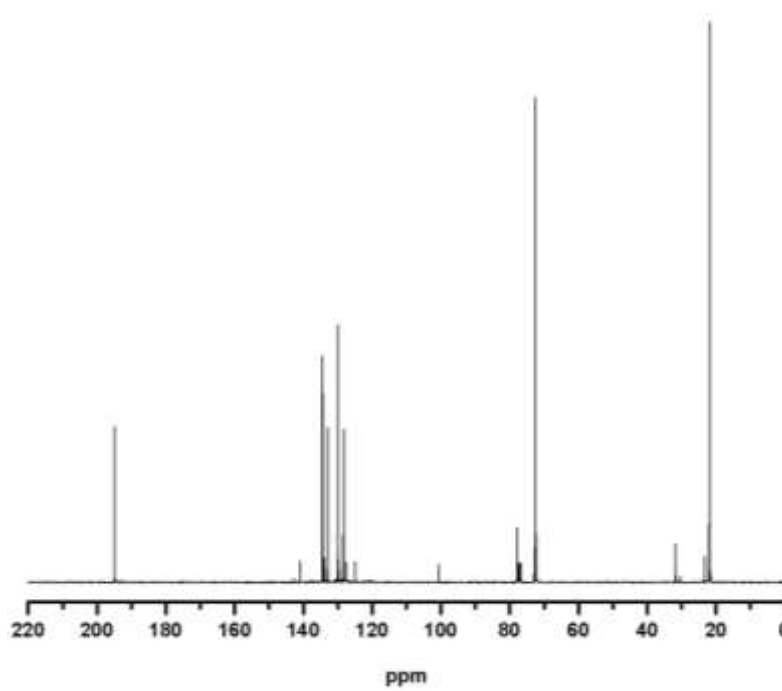


**Figure A12** The  $^{13}\text{C-NMR}$  spectrum of **3** in  $\text{CDCl}_3$  at 400 MHz

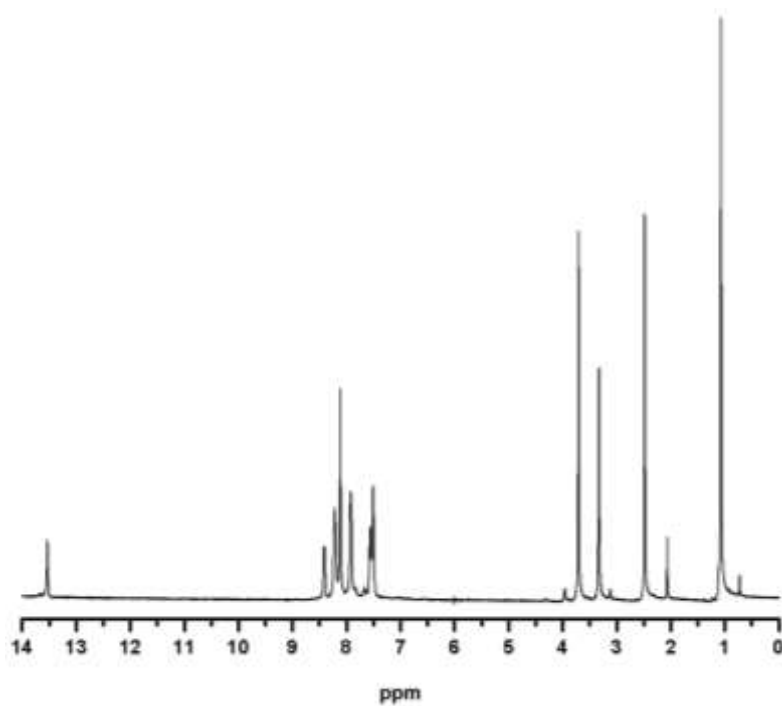


**Figure A13** The  $^1\text{H-NMR}$  spectrum of **4** in  $\text{DMSO-}d_6$  at 400 MHz

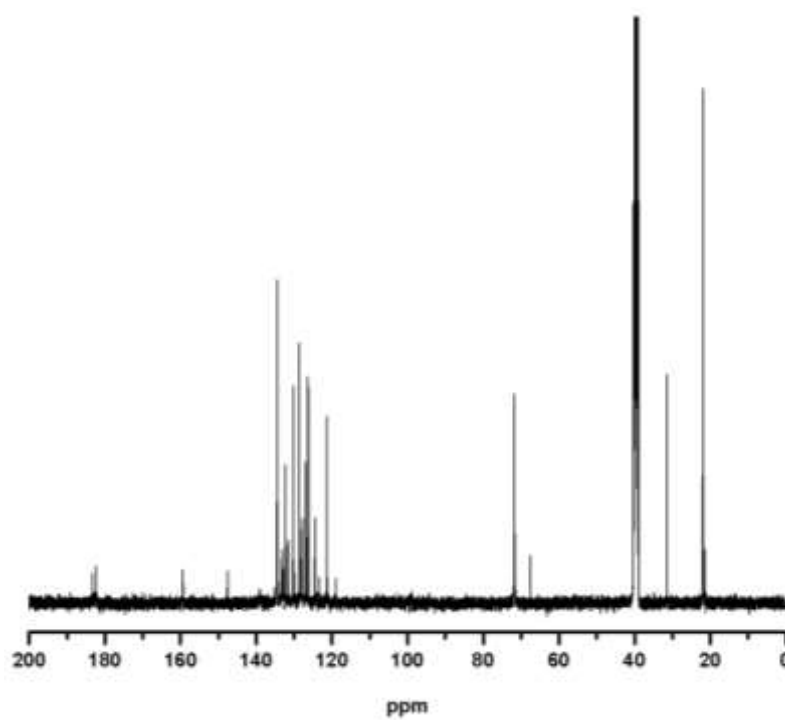


**Figure A14** The  $^{13}\text{C-NMR}$  spectrum of **4** in  $\text{DMSO-}d_6$  at 400 MHz

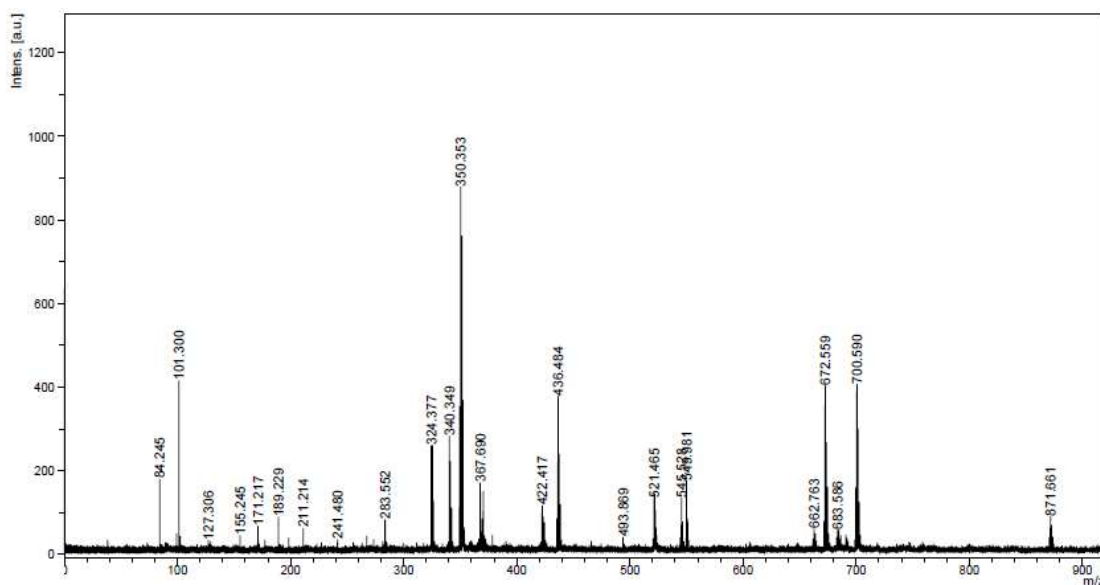


Figure A15 MALDI-TOF mass spectrum of **4** shown at 436.48 m/z

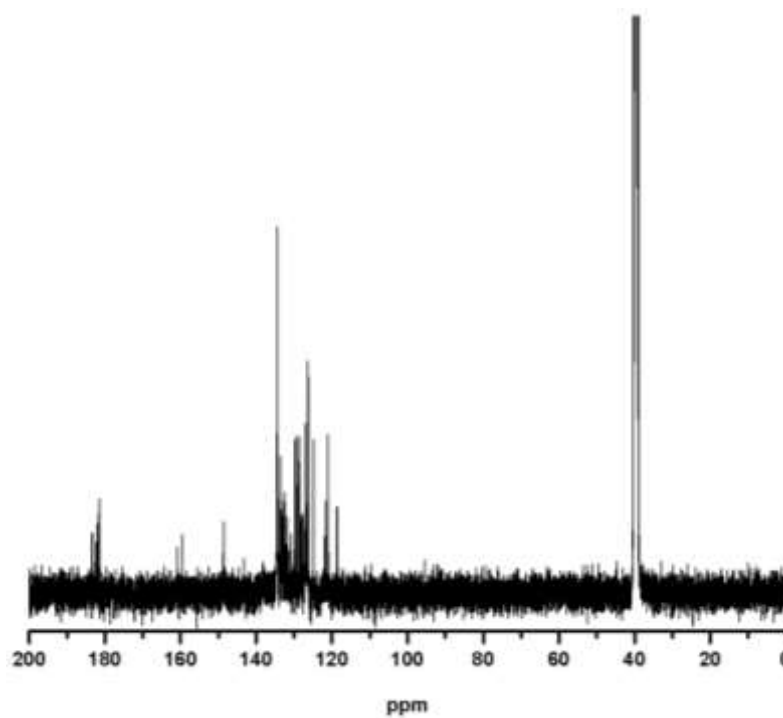


Figure A16 The  $^{13}\text{C}$ -NMR spectrum of sensor *o*-AB in  $\text{DMSO-}d_6$  at 400 MHz

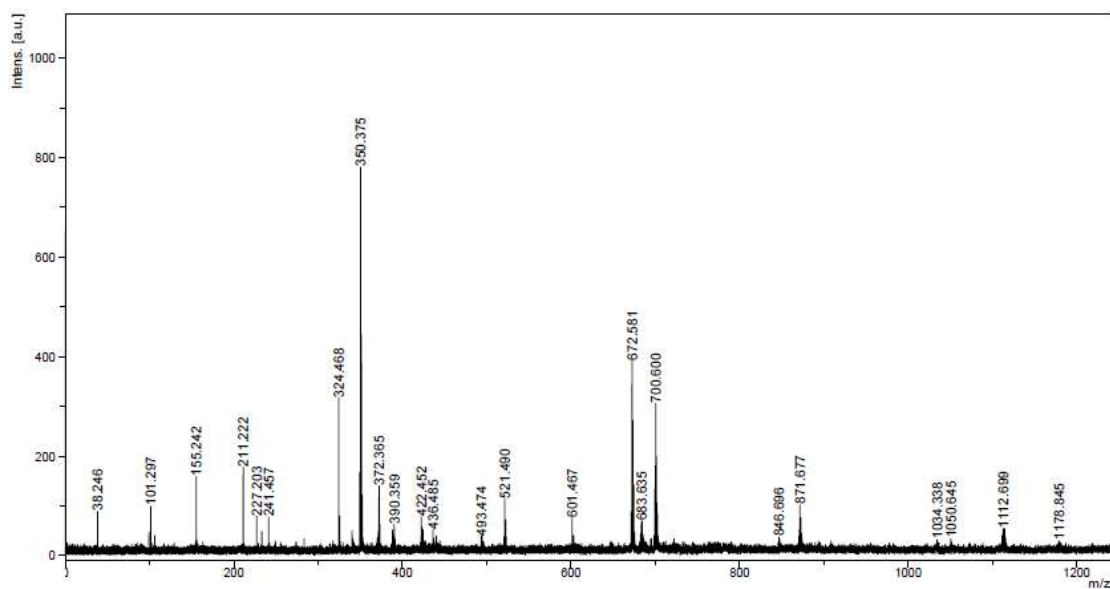


Figure A17 MALDI-TOF mass spectrum of sensor *o*-AB shown at 493.47 m/z

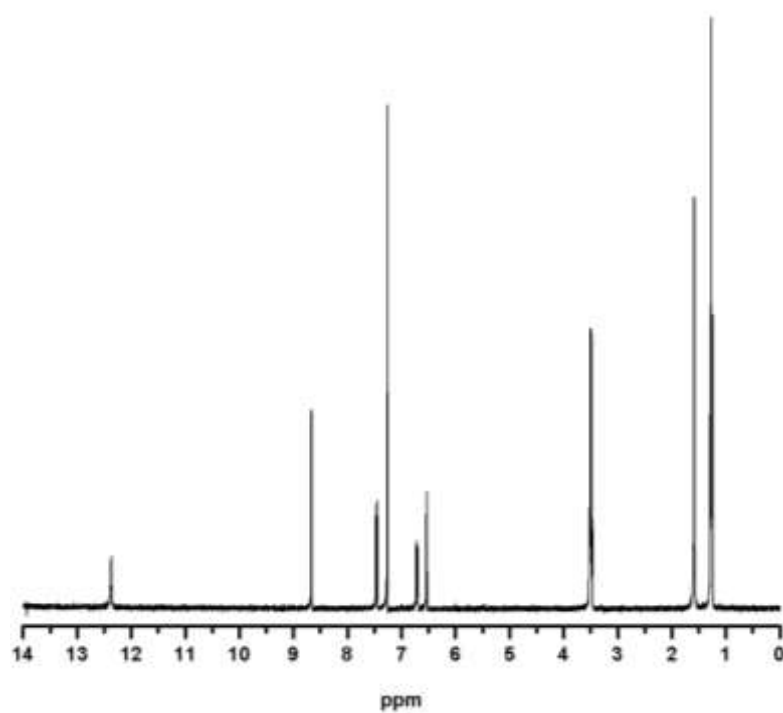
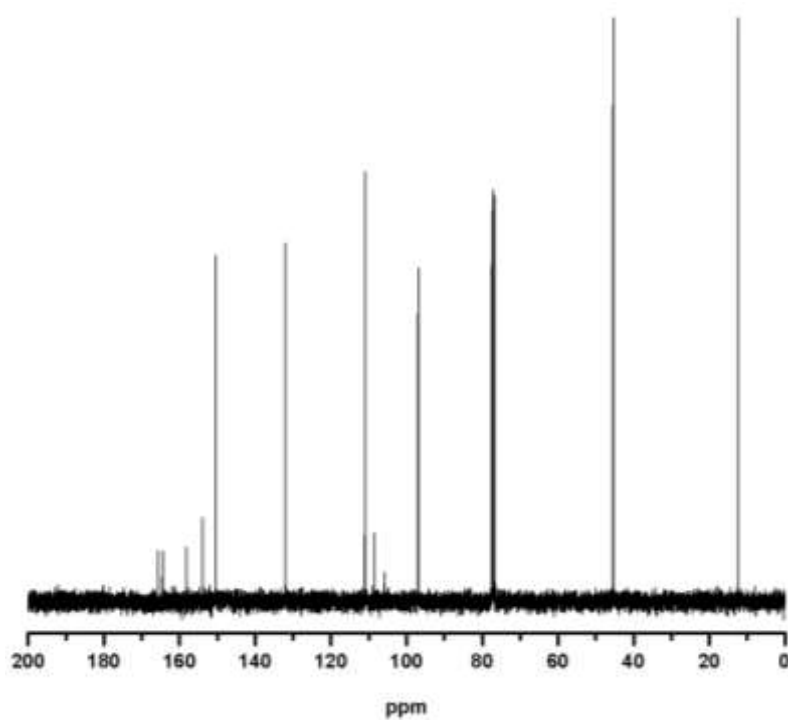
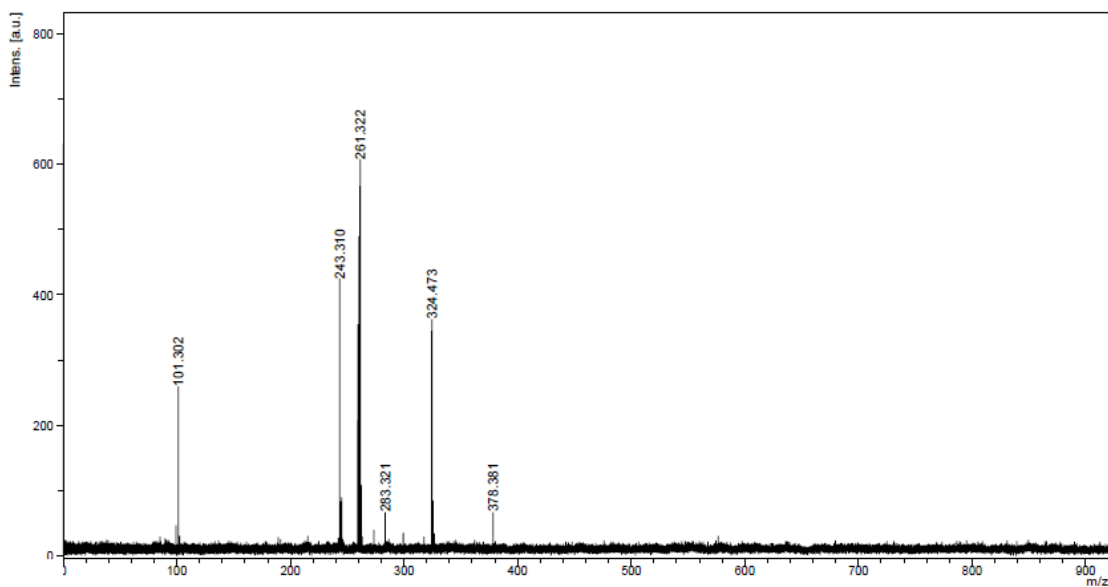


Figure A18 The  $^1\text{H}$ -NMR spectrum of **5** in  $\text{CDCl}_3$  at 400 MHz





**Figure A19** The  $^{13}\text{C}$ -NMR spectrum of **5** in  $\text{CDCl}_3$  at 400 MHz



**Figure A20** MALDI-TOF mass spectrum of **5** shown at 261.322 m/z

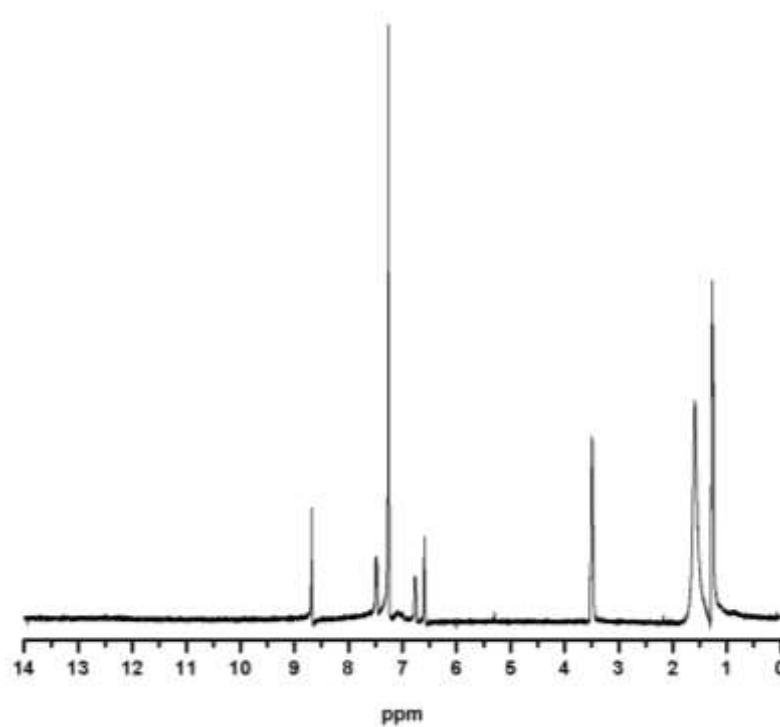


**Figure A21** The  $^1\text{H-NMR}$  spectrum of **6** in  $\text{CDCl}_3$  at 400 MHz

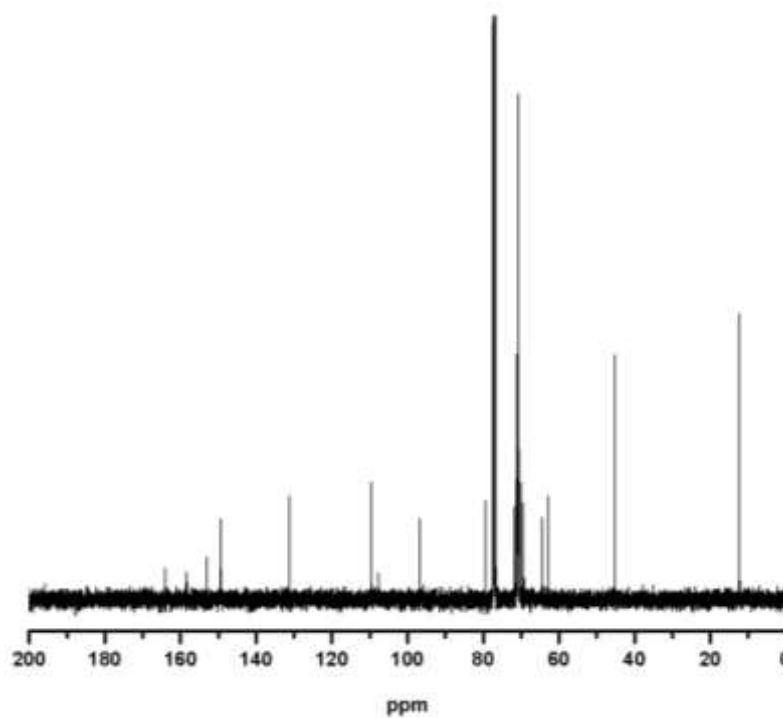


**Figure A22** The  $^{13}\text{C-NMR}$  spectrum of sensor **CC** in  $\text{CDCl}_3$  at 400 MHz

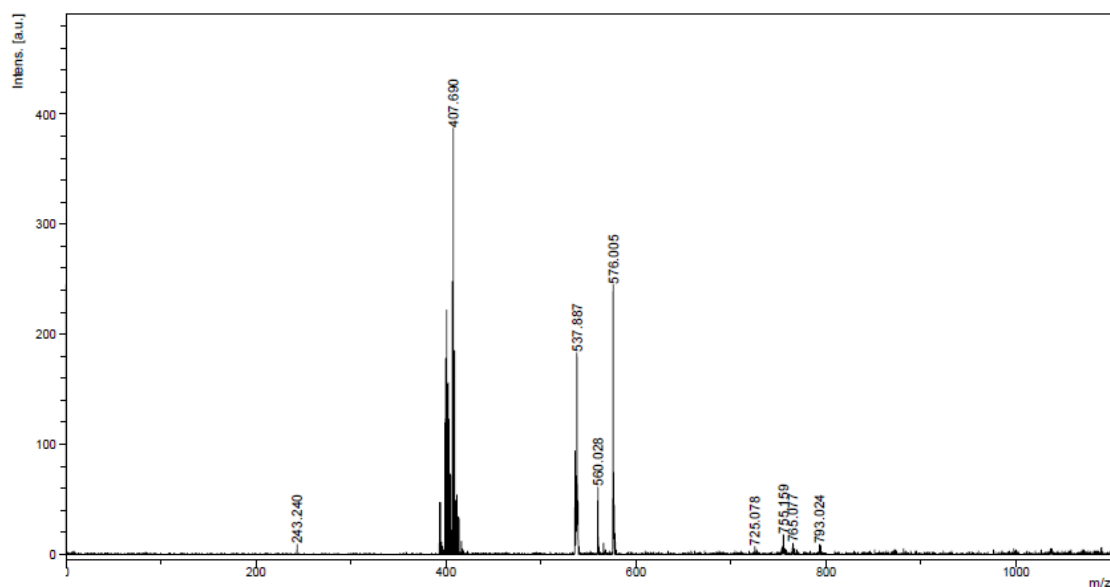


**Figure A23** MALDI-TOF mass spectrum of sensor **CC** shown at 537.887 m/z

### Mass Spectrum List Report

Analysis Info		Acquisition Date	
Analysis Name	D:\Data\Data Service\Year 2013\Small molecule\03152013\CC_pos.d	3/15/2013 2:22:02 PM	
Method	tune_low.m	Operator	BDAL@DE
Sample Name	CC_pos	Instrument / Ser#	microTOF-Q II 10335
Comment			

Acquisition Parameter			
Source Type	ESI	Ion Polarity	Positive
Focus	Not active	Set Capillary	4500 V
Scan Begin	50 m/z	Set End Plate Offset	-500 V
Scan End	1000 m/z	Set Collision Cell RF	150.0 Vpp
		Set Nebulizer	0.3 Bar
		Set Dry Heater	180 °C
		Set Dry Gas	4.0 l/min
		Set Divert Valve	Waste

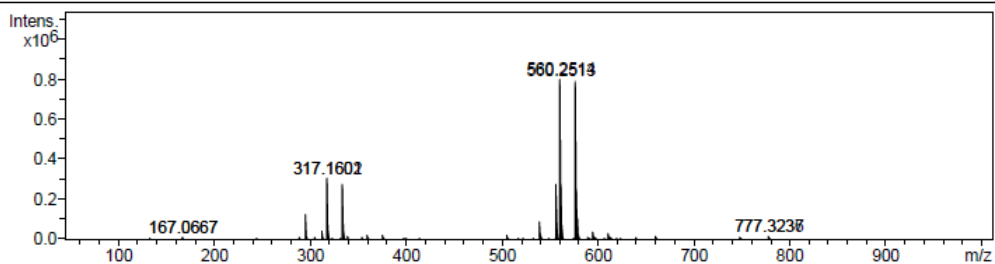


**Figure A24** The ESI-High Resolution Mass spectrum of sensor **CC**

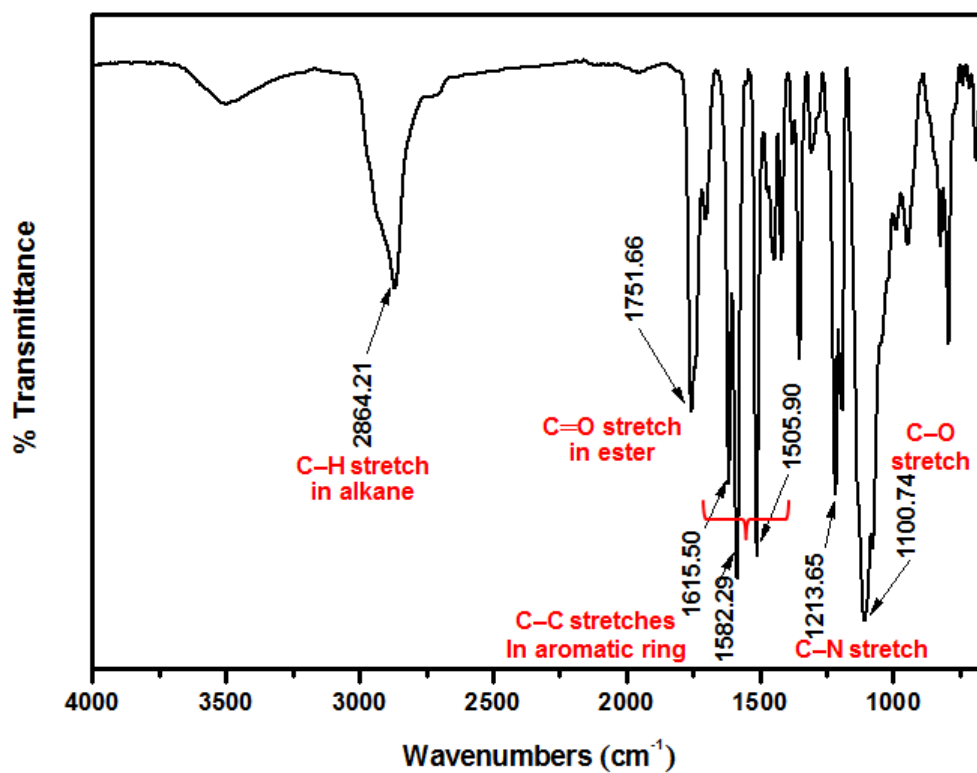


Figure A25 IR spectrum of sensor CC

**VITAE**

Name: Miss Yanisa Sanguansap

Date of birth: May 27, 1988

Nationality: Thai

Address: 51/9 Phetgasam Road, Krasom, Taguatong, Phangnga,  
82130

Education: 2012 M.Sc. (Chemistry), Chulalongkorn University,  
Bangkok, Thailand  
2010 B.Sc. (Chemistry), Chulalongkorn University,  
Bangkok, Thailand

Conference attendance: Poster presentation “Catecholamine sensing by artificial  
sensor under fluorescence spectrophotometry” at The  
38<sup>th</sup> Congress On Science and Technology of Thailand  
(STT38) in Chiang Mai, Thailand, October 17-19, 2012  
  
Poster presentation “Catecholamine sensing by artificial  
sensor under fluorescence spectrophotometry” at  
Sokendai Asian Winter School "Frontiers in Photo-  
Molecular Science" in Okazaki, Japan, January 14-17,  
2013